博士論文

DNA-Guided Anisotropic Self-Organization of Spherical Nanoparticles

（DNAが誘導する球状ナノ粒子の構造異方的な自己組織化）

余　力

DNA-Guided Anisotropic Self-Organization of Spherical Nanoparticles

（DNA が誘導する球状ナノ粒子の構造異方的な自己組織化）

余　力

Department of Advanced Materials Science

Graduate School of Frontier Sciences

The University of Tokyo

July 2019

Preface

The present dissertation is the collection of the studies, which have been accomplished at the Department of Advanced Materials Science, Graduate School of Frontier Sciences, The University of Tokyo and Bioengineering Laboratory, RIKEN Cluster for Pioneering Research under the direction of Professor Mizuo Maeda from September 2016 to July 2019. I would like to express my deep appreciation and respect to Professor Mizuo Maeda for his continuous guidance, encouragement, and heartwarming support throughout my work.

I would also like to express my great gratitude to Professor Katsuhiko Ariga, Professor Kozo Ito, Professor Yukio Nagasaki (University of Tsukuba), and Professor Takashi Uemura for their careful reviewing and helpful suggestions on the manuscript.

During the past three years' work, I really appreciated to have a chance to collaborate with excellent scientists. I am indebted to Dr. Tohru Takarada (Senior Research Scientist, RIKEN) for his guidance, assistance, and concern in detail. He has imparted to me so much valuable knowledge through his insightful guidance that will benefit me a whole lifetime. I would like to express my sincere gratitude to Associate Professor Yoshitsugu Akiyama (Tokyo University of Science), Professor Guoqing Wang (Ocean University of China), and Mr. Shota Shiraishi (Tokyo University of Science) for their valuable contribution to this work. I am also grateful to Associate Professor Naoki Kanayama (Shinshu University), Assistant Professor Yuji Tsuchido (Waseda University), and Ms. Tomoka Kikitsu (RIKEN Center for Emergent Matter Science) for their technical

supports and insightful comments. Furthermore, I would like to thank Ms. Masumi Furumoto, Ms. Kumiko Matsumoto, Ms. Satomi Yanaba, Ms. Surachada Chuaychob, Mr. Takafumi Sako, Mr. Tzung-Ying Yang, Mr. Michitsuna Tsutsumi and all the other members of Bioengineering Laboratory for their great help in my work and daily life. I also thank secretaries in The University of Tokyo Ms. Yukiko Tan, Ms. Sachie Iimura and Ms. Kiwa Ito for the paper work.

In addition, I am greatly indebted to the following scholarships and research funding programs for their generous support of my research: the International Program Associate (IPA) Foundation provided by RIKEN, the Monbukagakusho Honors Scholarship for Privately-Financed International Students provided by JASSO (MEXT), and the Academic Research Grant for GSFS Doctor Course Students provided by The University of Tokyo.

Finally, I would like to express my devoted appreciation to my wife, Cui Xu for her sacrificial help, affectionate encouragement and loving care. I must say sorry to my lovely son because I have not taken care of him since he was born 15 months ago. I also deeply thank my parents and parents-in-law, for their selfless and heartwarming love.

Li Yu

July 2019

Contents

Chapter 1

General Introduction

1.1 Deoxyribonucleic Acid (DNA)

1.1.1 General

DNA carries genetic information, which makes it standout among various biomolecules in organisms. Over recent decades, researchers have accomplished huge amounts of work on the elucidation of its structure and function.[1–4] The structure of DNA is illustrated in Figure 1.1. DNA is composed of deoxyribose, phosphoric acid, and nucleobase.[5] The phosphoric acid forms a phosphate diester with the 5'-OH and 3'-OH groups of deoxyribose. The phosphate group is negatively charged at neutral pH. There are four kinds of nucleobases in DNA: adenine (A) and guanine (G) with a purine skeleton and cytosine (C) and thymine (T) with a pyrimidine skeleton.

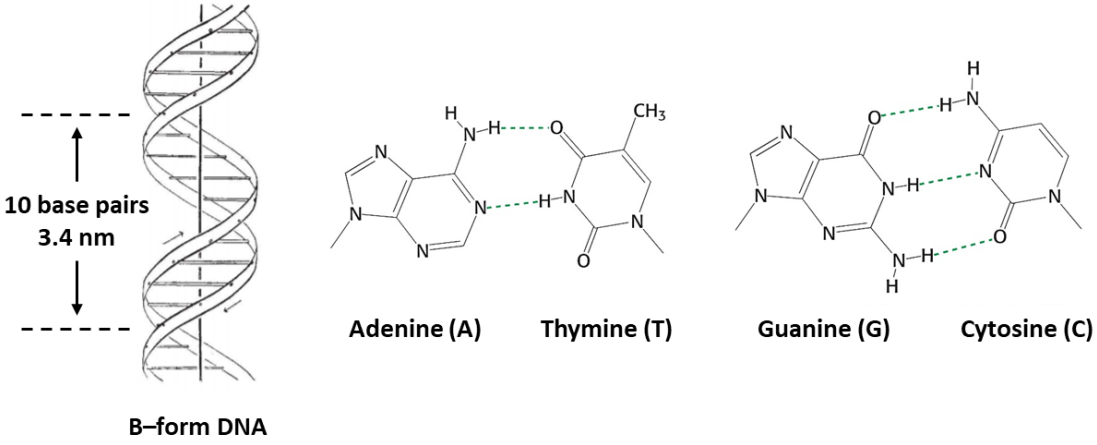

Figure 1.1 Structure of B-form DNA duplex and Watson–Crick base pairing.

The double helix structure of DNA was revealed by Watson and Click. The most common B-form is right-handed. In this thesis, it is presumed that all DNA duplexes exhibit B-form. The formation of the double helix structure is due to the Watson–Crick base pairing; two hydrogen bonds are formed between A and T, while three hydrogen

bonds are produced between G and C.[6] The double helix wraps around 10 base pairs per turn with a height of 3.4 nm and a diameter of 2 nm.[7] Raising temperature induces dissociation of double strands, whereas increasing ionic strength reinforces the helical structure.[8]

1.1.2 Synthesis

In the past few decades, DNA *in vitro* synthesis has developed rapidly. Even though current synthesis methods still have some limitations and imperfections, artificially synthesized DNA has promoted the development of bioscience and nanoscience with its low cost and high efficiency. The following is an overview of DNA synthesis methods.

The *in vitro* synthesis methods of DNA can be divided into two categories: chemical synthesis and enzymatic synthesis. As for chemical methods, oligo DNA synthesis generally uses a solid phase phosphoramidite method.[9] This method has the advantages of high efficiency and high accuracy, as well as facile modification with functional groups. In general, a microliter volume of solution is used for synthesis on a small column or a microreactor chip. The synthesis involves the addition of mononucleotide at the end of the synthetic strand. The procedure is composed of four steps: deprotection, coupling, capping, and oxidation. The elongating direction is from 3'-end to 5'-end. However, the integrity of the sequence and the efficiency of the synthesis prevent the product from being longer than approximately 250 nucleotides (nt). All oligo DNAs used in this thesis are chemically synthesized, except for long template DNAs in Chapter 3.

Among enzymatic syntheses, polymerase chain reaction (PCR) is the most conventional technique to amplify specific double-stranded (ds) DNA fragments.[10] The most significant feature of PCR is the ability to dramatically increase the amount of the

specific dsDNA fragments from a tiny quantity of long dsDNA samples. First, the long dsDNA samples are denatured at a high temperature (ex. 95 °C) to give the corresponding single-stranded (ss) DNAs. Then, the solutions are cooled down to a lower temperature (ex. 60 °C) so that primers are hybridized to the ssDNA sample. Finally, the DNA polymerase synthesizes a complementary strand by elongating the primer in the 5' to 3' direction at the optimal reaction temperature (ex. 72 °C). Through multiple cycles of this procedure, the specific dsDNA fragments are amplified exponentially.

Rolling circle amplification (RCA, Figure 1.2) is another enzymatic DNA synthesis method that mimics the replication of cyclic ssDNA genome of viruses.[11] Due to its high sensitivity and specificity, RCA is widely used in fundamental research, practical testing, medical diagnosis, as well as material fabrication. The DNA polymerase elongates the primer that is hybridized to the circular template ssDNA like PCR. The DNA synthesis takes place from 3' end of the primer along the circular template. When the DNA polymerase returns to meet the 5' end of the primer, the polymerase continues the DNA synthesis with tearing off the tail of the primer strand. Therefore, RCA is a method to prepare a long ssDNA with a repeat unit. Since the reaction temperature cycle is not necessary, all reaction steps can be performed isothermally. In Chapter 3, all template ssDNAs with a repeat unit are prepared by using the RCA method.

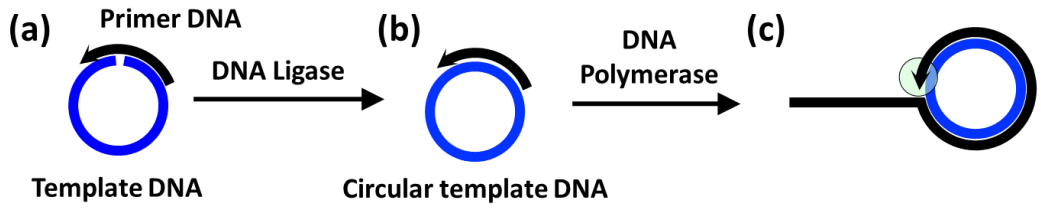

Figure 1.2 Schematic illustrations of RCA. (a) Linear template ssDNA is circularized with the assist of primer ssDNA. (b) Termini of template DNA are linked by DNA ligase to produce a circular form. (c) Long ssDNA with a repeat sequence is synthesized by DNA polymerase.

1.1.3 Immobilization of DNA to Nanoparticles

The progress of nanotechnology helps the advancement of biosciences. Biomolecule–modified nanoparticles (NPs) have been employed in biochemical and biomedical sensing since they can improve signal transduction, signal intensity, and signal readout.[12–14] Among surface-grafted biomolecules, DNA has intrigued many researchers due to the following reasons: (i) precise molecular recognition by complementary base pairing, (ii) facile and flexible sequence design, and (iii) high physical and biochemical stability. At present, DNA has been successfully immobilized on the surface of core NPs such as gold, silver, quantum dots, and polymer assemblies through covalent or coordination bonds.

1.2 Gold Nanoparticles

1.2.1 General

NPs have at least one dimension between 1 and 100 nm, and exhibit unique physical and chemical properties by virtue of the extremely high ratio between surface area and volume.[15] As such, NPs have successfully been applied to electronic,[16] magnetic,[17,18] and optical devices.[19,20] Among a variety of NPs, gold NPs (AuNPs) have widely been used because of the following reasons: (i) well-established surface modification methods, (ii) highly controllable sizes and shapes, and (iii) strong plasmon absorption in the visible light region.[12,13,21] Especially, the plasmon absorption property makes possible the application to various optical devices.

1.2.2 Localized Surface Plasmon Resonance

Some electrons in metal NPs exist in a freely movable state. Under specific conditions, light can cause collective oscillations of the free electrons in metal NPs. This phenomenon is called plasmon. Some metal NPs can absorb visible and infrared light in a specific range of wavelength, due to localized surface plasmon resonance (LSPR) (Figure 1.3).[22] For example, AuNPs exhibit strong absorption of visible light due to their LSPR effect. The light of resonant wavelength is absorbed or scattered so that aqueous AuNP dispersions show a bright red color.

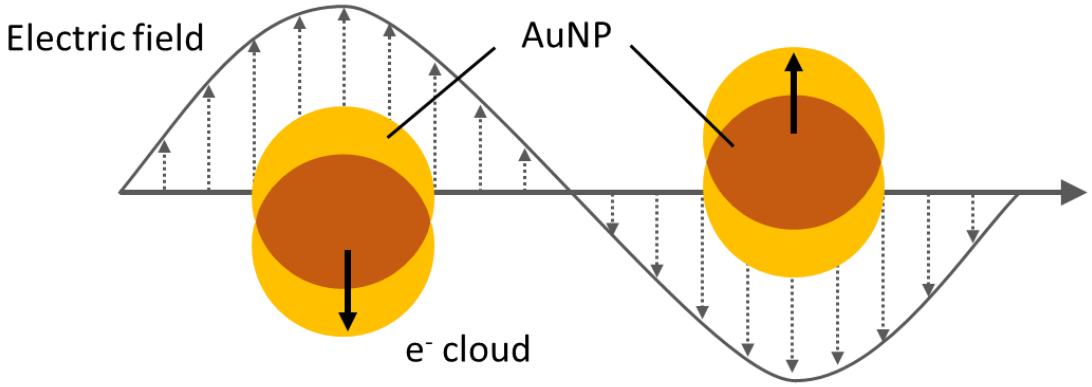

Figure 1.3 Plasmon oscillation for AuNP.

The absorption cross section of AuNPs is proportional to the cube of the radius of the AuNP, and the scattering cross section is proportional to the sixth power. Therefore, as the particle size increases, both absorption and scattering enhance. It is possible to perform optical observation of a single AuNP by a dark field microscope with very strong scattered light. The detail will be introduced later in **1.6**. In addition, the localized electric field intensity at the AuNP surface attenuates as it gets farther from the surface.

The LSPR wavelength and the light absorption/scattering intensity thereof change dramatically depending on the particle size and shape (anisotropy and surface unevenness), the dielectric constant of the surrounding, the interparticle distance and the ordering. In general, the resonant wavelength shifts to a longer value when the particle size, the degree of anisotropy, the surface irregularity and the surrounding refractive index increase or when the distance between particles decreases. Here, the author focuses the following three aspects: size,[23] anisotropy,[24] and arrangement.[25]

i) Size: In general, LSPR characteristics are related to the size of plasmonic NPs. Adjusting the NP size can improve various LSPR effects, such as catalysis. AuNPs with a diameter larger than 5 nm have a strong LSPR band in the visible region. When the

AuNP diameter increases from 10 nm to 80 nm, the absorption peak is red-shifted from 520 nm to 540 nm. As the size of AuNPs increases, the free electron collective oscillation frequency decreases due to the electromagnetic field shielding effect, and therefore the LSPR peak is red-shifted.

ii) Anisotropy: Gold nanorods (AuNRs) exhibit two LSPR bands derived from the short and long axes. The LSPR band derived from the long axis is red-shifted with the increase of the aspect ratio of AuNR. In addition, polyhedral structures, plate-like structures, and hollow structures with unique optical properties have also been reported. For example, the hollow structures are known to change in LSPR with altering shell thickness.

iii) Arrangement: A general category of plasmonic nanomaterials includes AuNP arrays. A strong near-field coupling relies on interparticle gaps smaller than 2 nm, which are usually fabricated through top-down manners such as photolithography. However, the gap size can hardly reach 2 nm and the strict reliance to facilities is required. On the other hand, far-field coupling depends on periodic arrays over long-ranged areas. Therefore, a new methodology to arrange NPs in a highly ordered manner is necessary. If strong enhancement of the near-field and far-field coupling effects by tuning the lattice parameter, an obvious LSPR signal can be generated.

1.2.3 Functionalization with Biomolecules

AuNPs are able to be functionalized with various biomolecules and organic molecules (Figure 1.4). In addition to removing and protecting the toxic protective agent from the particle surface, another functional molecule can be immobilized on the AuNP surface to bring about new functions. This makes it possible to impart chemical and

biological properties in addition to the inherent physicochemical properties of AuNPs. For functionalizing AuNPs, formation of a self-assembled monolayer (SAM) of alkyl thiols on the particle surface is the most widely used method. The alkyl thiols are attached onto the Au surface through a gold–sulfur (Au–S) bond.[26] The bond strength of Au–S is estimated to be 40–50 kcal/mol.[27] Besides covalent bonding, there are other methods such as electrostatic interaction, which has been used to immobilize proteins, lipids, and nucleic acids on the Au surface.

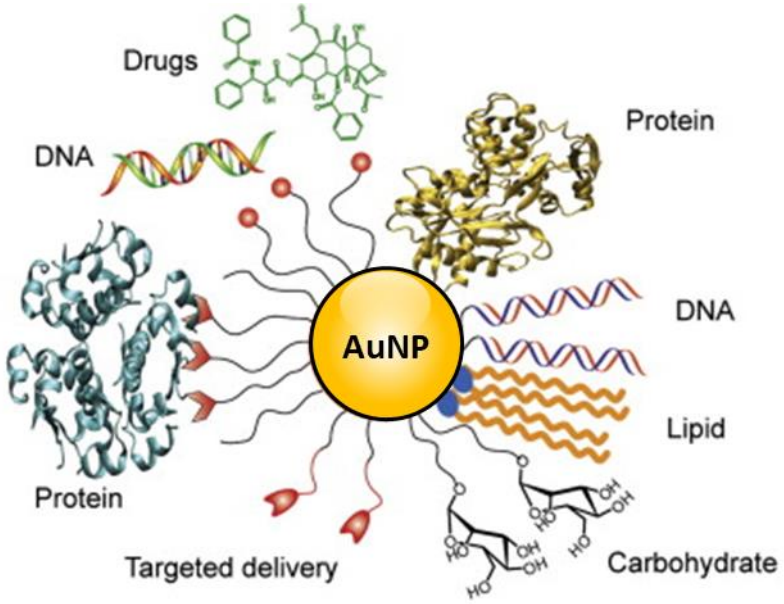

Figure 1.4 Surface modification of AuNP with various biomolecules.

Biomolecule-functionalized AuNPs have a wide range of applications. For example, detection methods based on the interaction of AuNPs with proteins have been employed in medical diagnosis,[21] food safety monitoring, and environmental assessment.[28] They can also be used for the treatment of bacterial infections or diseases such as Alzheimer's disease.[29] In addition, DNA-modified AuNPs (DNA–AuNPs) can be used in a variety of biosensors.

1.3 Hybridization-Based Assemblies of DNA–AuNPs

Current attention to AuNP assemblies is attracted by their collective properties, which can be utilized in various nanodevices. For example, AuNP assemblies exhibit optical and electronic properties based on LSPR coupling of individual AuNPs.[30,31] These outstanding properties are further enhanced when the AuNP assemblies are fabricated in a long-ranged, highly ordered manner.[32–34] Self-assembly is a straightforward strategy to produce AuNP assemblies in a highly controllable and designable way. Among them, two-dimensional (2D) AuNP arrays have witnessed tremendous progress in synthesis and characterization.[35–37]

To fabricate the 2D AuNP arrays, various approaches have been developed. For example, Langmuir‑Blodgett (LB) methodology is based on the transfer process of a monolayer adsorbed at the air–water interface onto solids by vertically dipping the substrate. However, it is difficult to precisely control the configuration by using this process.[38,39] Photolithography can produce 2D AuNP arrays with various shapes and patterns by irradiating light on a substrate, although sophisticated instruments are required to fabricate these arrays.[40]

As a new methodology, the base-pairing specificity of DNA sequences has been effectively exploited as a useful tool to direct the self-assembling process of AuNPs. Specifically, ssDNA–AuNPs were crosslinked through DNA hybridization to produce discrete assemblies, including 1D chains, 2D arrays, and 3D superlattices (Figure 1.5).[41–44] The interparticle distance can be changed simply by designing DNA length. A few examples of the discrete assembly consisting of AuNPs and AuNRs are shown in Figure 1.5a, which was manufactured with over 85% yield and high selectivity. Another example

of 1D AuNP assembly is shown in Figure 1.5b. AuNPs with diameters of 25 and 10 nm were selectively capped with two different DNA strands. Using the PCR reaction, alternately extended linear heterogeneous chains were fabricated. The assembly of nanoarrays can also be arranged through surface functionalization with DNA and the use of linkers. Figure 1.5c introduces an example of nanoarray constructed from "nanoflower" building blocks, which was formed by using DNA origami technology. These "nanoflowers" were organized into 2D AuNP array with high regulation controlled via auxiliary DNA linker strands. As for 3D assemblies, Mirkin and coworkers provided a strategy for constructing DNA-guided AuNP 3D long-ranged crystals with various lattice parameters (Figure 1.5d). The limitation of NP superlattice engineering is that the structures are determined by the features of particles. However, AuNPs modified with DNA strands portray a kind of general building block, which can self-assemble to form superlattices with designed lattice parameter. It should be noted that all these researches employed the hybridization of complementary ssDNAs.

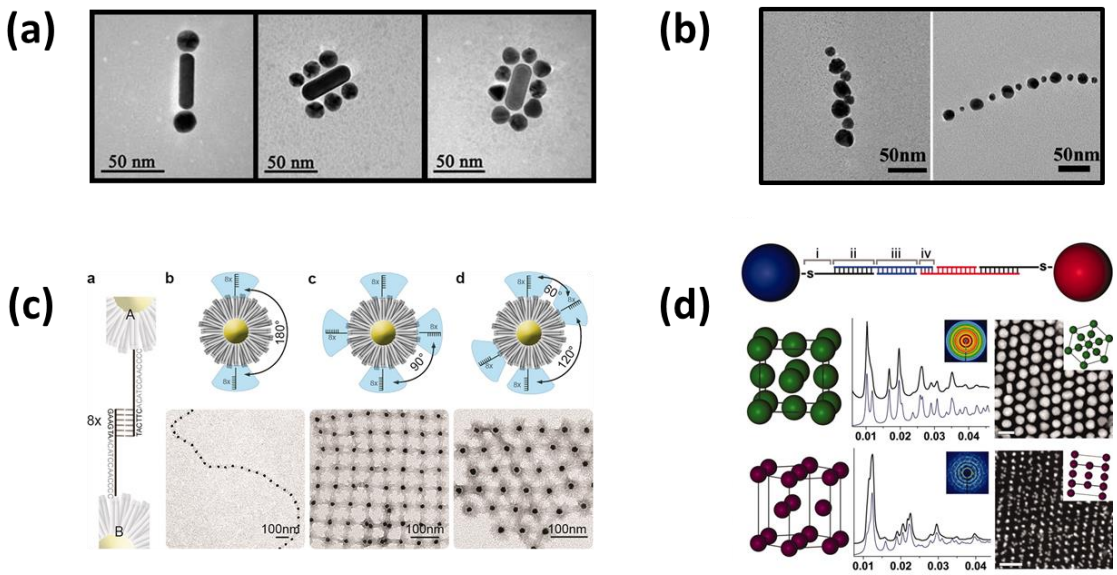

Figure 1.5 Various crosslinked assemblies of DNA–AuNPs: (a) Discrete assembly of DNA–AuNPs and DNA–AuNR,[41] Copyright 2012 American Chemical Society, (b) 1D chain of two types of DNA–AuNP,[42] Copyright 2013 American Chemical Society, (c) 2D array of DNA–AuNPs,[43] Copyright 2016 American Chemical Society, (d) 3D superlattice of DNA–AuNPs,[44] Copyright 2011 AAAS.

1.4 Non-Crosslinking Aggregation of DNA–AuNPs

To induce the self-assembly of the DNA–AuNPs in the current work, the author takes advantage of local-structure-sensitive colloidal behaviors of dsDNA–AuNPs. In 2003, Maeda and coworkers found that ssDNA–AuNPs dispersed stably in solution at high ionic strength due to steric and electrostatic repulsion, whereas the fully matched dsDNA–AuNPs aggregated spontaneously within a few minutes under the same conditions (Figure 1.6).[45] Concomitantly, the solution color was rapidly changed from red to purple, which was attributable to the red-shifting of its LSPR band. Notably, this aggregation was strongly inhibited when the surface-grafted dsDNA had a single-base mismatch or protrusion at the distal end. Further investigations uncovered that the non-crosslinking aggregation took place regardless of composition (gold and vinyl polymer),[46,47] shape (sphere, rod, and plate),[48] and size (5–300 nm)[47,49] of the particle core. The unique features of the non-crosslinking aggregation are summarized as follows: (i)

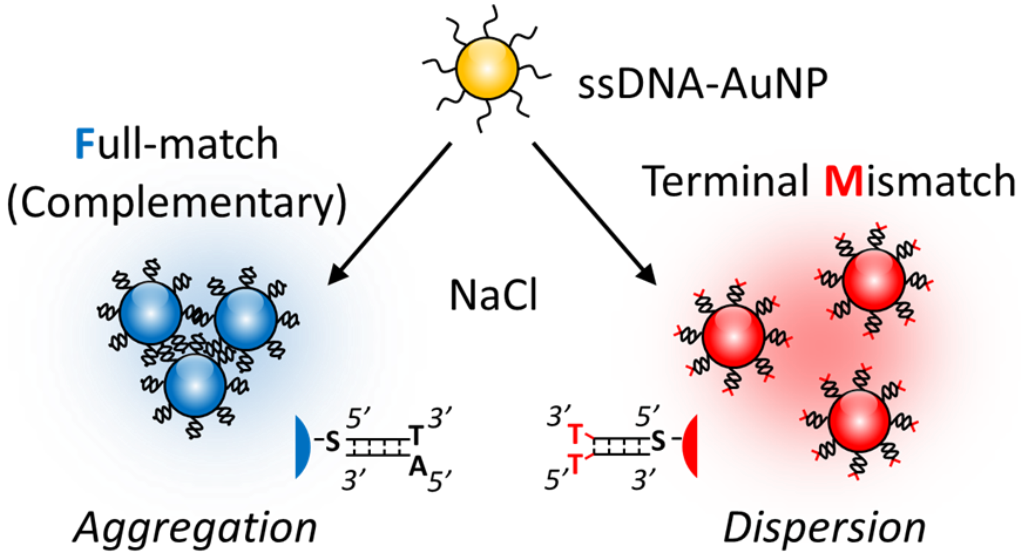

Figure 1.6 Non-crosslinking aggregation of DNA–AuNPs.

high sensitivity to terminal base pairing/unpairing, (ii) no limitation in the design of DNA sequence, and (iii) high reversibility regulated by temperature and ionic strength. The non-crosslinking aggregation of DNA-modified particles has successfully been applied in visible chemical/biochemical sensing of heavy metal ions (Hg^{2+} and Ag^{+}),[50] small organic molecules (ATP),[51] proteins,[52] and DNA (single-nucleotide polymorphism).[47]

Nucleobase stacking is considered an origin of drastic reduction of colloidal stability of the fully matched dsDNA–AuNPs (Figure 1.7). Enhancement of ionic strength could make the outermost DNA base pairs dehydrated, thereby accelerating their π–π stacking interaction between different particles. An investigation using colloidal probe atomic force microscopy strongly suggested the generation of the interparticle attractive forces between the terminal base pairs of the surface–grafted dsDNA.[53] In contrast, the single-base mismatched or protruded terminal structure could diminish the blunt-end stacking and also enhance steric and entropic repulsion due to the fraying motion of unpaired nucleobases.

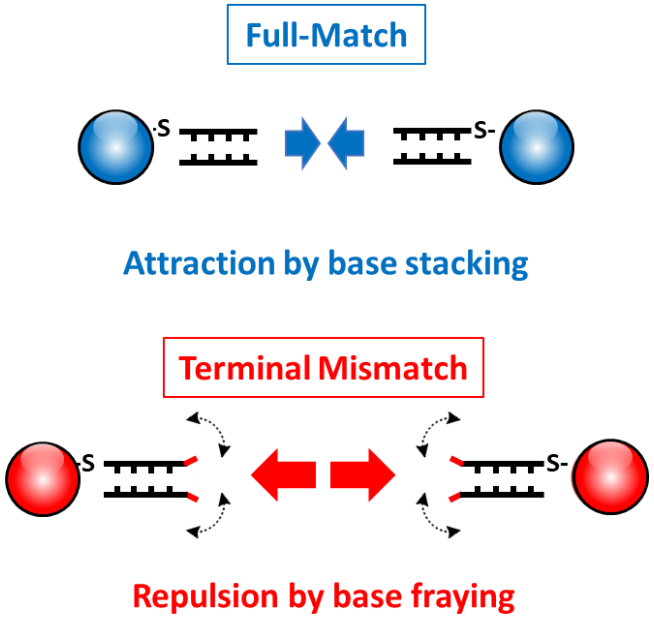

Figure 1.7 Proposed mechanism for non-crosslinking aggregation of DNA–

1.5 Transmission Electron Microscopy

This and next subsections provide essential fundamentals of analytical methods mainly used in the current study. Transmission electron microscope (TEM) is an electron microscope which illumines an electron beam to a sample to form an image of the transmitted electron (Figure 1.9).[54] Depending on the structure and composition of the sample, the density of transmitted electrons changes. Electrons are emitted from an electron gun and accelerated in an accelerating tube. The accelerated electrons pass through the focusing lens, hit the sample, reach the objective lens, the intermediate lens, the projection lens, and the fluorescent plate, and finally form the TEM image or electron beam diffraction. The main reason for using an electron beam is the resolution. The resolution of the microscope is less than or equal to the wavelength of the source;

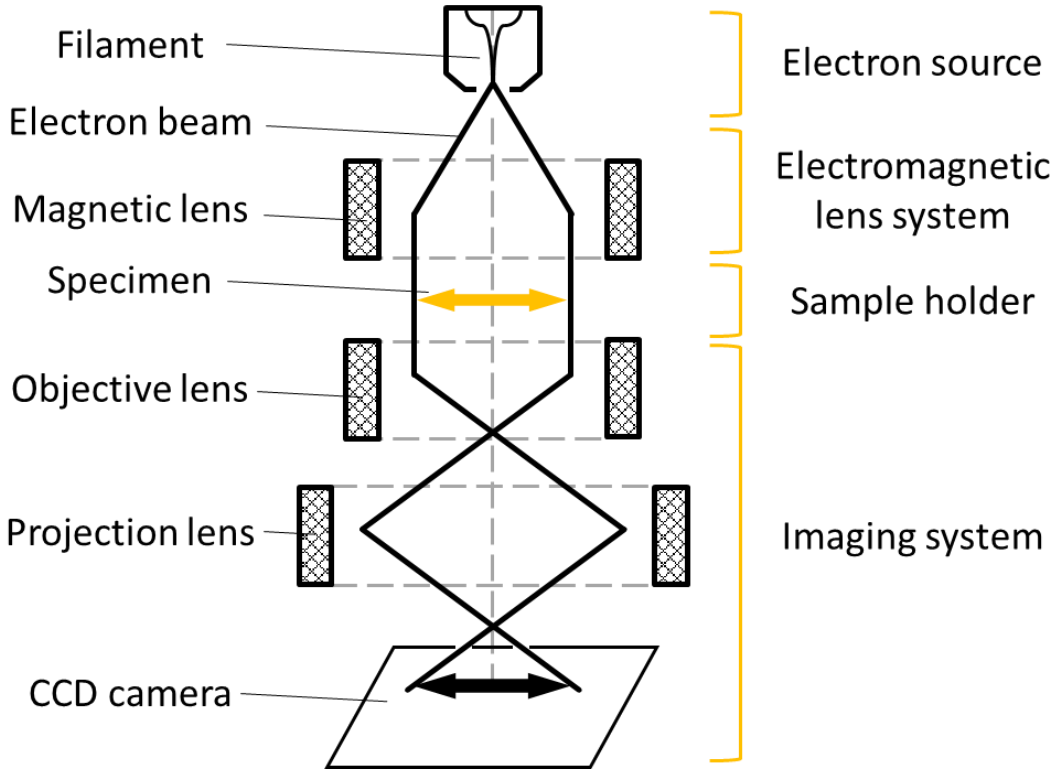

Figure 1.8 Principle of transmission electron microscopy.

therefore, it cannot be distinguished if the distance between two different points is shorter than the wavelength. The voltage that accelerates the electron beam is called "acceleration voltage". The wavelength of the electron beam at an acceleration voltage of 300 kV is 0.002 nm. In contrast, the wavelength of visible light in optical microscopes system is 380 to 780 nm. Therefore, the image is clearly observed even at very high magnification.

The sample is irradiated with the electron beam. Therefore, in addition to the shape and the surface structure of the sample, the degree of aggregation and the crystal pattern are also able to be investigated. It is necessary to use a very thin sample in order for the electrons to be easily interacted. Transmission electrons are observed to form a bright-field image. On the other hand, when scattered electrons are used, a dark-field image is obtained. Samples are loaded on a metal grid with carbon membrane. The sample must be solid since a high vacuum is produced inside the tube. Metallic samples are measurable, but samples that do not conduct electricity such as DNA need a pretreatment such as electron staining. Also, they may be broken by electron beams. These are the reasons why only AuNPs are observed in TEM images of DNA–AuNPs.

1.6 Dark-Field Microscopy

Dark-field microscopy (DFM) is an observation using scattered light from the sample (Figure 1.10). In the case of a general light microscope (bright field illumination), a darker image is obtained for a sample than the background of illumination light. On the contrary, the dark-field observation uses incident light obliquely from the source through a condenser so that the light does not enter the objective lens, and the light scattered by the sample is observed. In this case, a bright sample floats up on a dark background. It is common to use an optical microscope with a dedicated dark-field condenser attached.

In an optical microscope using visible light, the resolution is theoretically limited to about 200 nm by the wavelength of light. However, it is possible to detect the presence or motion of colloid particles with a few nm in diameter without any pre-treatment, because DFM is easy to obtain high-contrast images. Furthermore, the scattered light spectrum can be measured by introducing the scattered light incident on the objective lens into the spectroscope. Since this scattered light is generated by the LSPR property, the spectrum changes depending on the sample size and the degree of anisotropy and alignment regularity.[55]

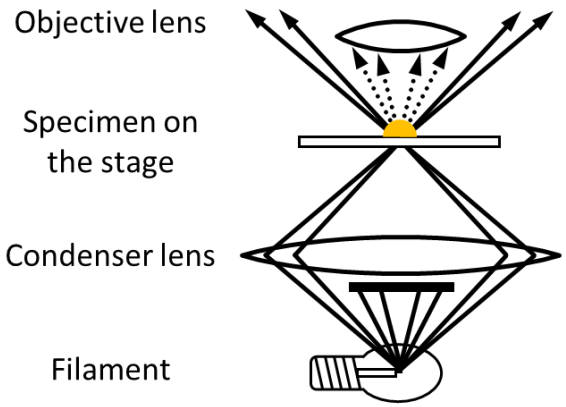

Figure 1.9 Principle of dark-field microscopy.

1.7 Purpose of the Present Study

To construct DNA–AuNP assemblies that undergo structural changes with high sensitivity to single-base difference, the author tried to establish a hierarchical self-organization strategy with two steps; First, the DNA–AuNPs were immobilized onto a long ssDNA template by using the DNA hybridization to precisely produce a linear precursor. Next, the non-crosslinking aggregation was implemented in order to program the self-organization performance. By this methodology, the author succeeded in constructing an anisotropic structure from isotropic AuNPs. Besides, 2D AuNP arrays with highly regulated arrangement have also been created through the self-organization of the long AuNP chains. Emphasis is placed on the fact that the structural changes exhibited high sensitivity to single-base difference.

The main body of this thesis consists of Chapters 2 and 3. In Chapter 2, the author describes a method to produce an anisotropic assembly by using isotropic particles. Spherical AuNPs almost uniformly modified with ssDNA are employed as isotropic particles to construct their linear trimers. Anisotropic AuNP assemblies are obtained by orienting the trimers in a non-crosslinking manner. To prove its generality, a series of trimers consisting of the fully matched and terminal-mismatched dsDNA–AuNPs in a strictly defined order are designed. Chapter 3 describes a method of constructing 2D AuNP arrays through self-organization. A key technology is to prepare precursory 1D ssDNA–AuNP chains by using RCA. The drastic structure transformation from 1D to 2D is achieved by using the non-crosslinking aggregation. When complementary ssDNA is added, dsDNA–AuNP chains are rapidly folded to provide 2D arrays. Finally, the author discusses the prospective use of this methodology to fabricate functional nanodevices in Chapter 4 (General Conclusions).

1.8 References

1) Rothemund, P. W. Folding DNA to Create Nanoscale Shapes and Patterns. *Nature* **2006**, *440*, 297–302.

2) Britten, R. J.; Kohne, D. E. Repeated Sequences in DNA. *Science* **1968**, *161*, 529–540.

3) Lindahl, T. Instability and Decay of the Primary Structure of DNA. *Nature* **1993**, *362*, 709–715.

4) Seeman, N. C. DNA Replication and Recombination. *Nature* **2003**, *421*, 427–431.

5) Ghosh, A.; Bansal, M. A Glossary of DNA Structures from A to Z. *Acta Cryst. D* **2003**, *59*, 620–626.

6) Yakovchuk, P.; Protozanova, E.; Frank-Kamenetskii, M. D. Base-Stacking and Base-Pairing Contributions into Thermal Stability of the DNA Double Helix. *Nucleic Acids Res.* **2006**, *34*, 564–574.

7) Watson, J. D.; Crick, F. H. C. Molecular Structure of Nucleic Acids; A Structure for Deoxyribose Nucleic Acid. *Nature* **1953**, *171*, 737–738.

8) Clausen-Schaumann, H.; Rief, M.; Tolksdorf, C.; Gaub, H. E. Mechanical Stability of Single DNA Molecules. *Biophys. J.* **2000**, *78*, 1997–2007.

9) Hayakawa, Y.; Wakabayashi, S.; Kato, H.; Noyori, R. The Allylic Protection Method in Solid-Phase Oligonucleotide Synthesis. An Efficient Preparation of Solid-Anchored DNA Oligomers. *J. Am. Chem. Soc.* **1990**, *112*, 1691–1696.

10) Pfaffl, M. W. A New Mathematical Model for Relative Quantification in Real-Time RT-PCR. *Nucleic Acids Res.* **2001**, *29*, 2002–2007.

11) Lizardi, P. M.; Huang, X.; Zhu, Z.; Bray-Ward, P.; Thomas, D. C.; Ward, D. C. Mutation Detection and Single-Molecule Counting using Isothermal Rolling-Circle Amplification. *Nature Genet.* **1998**, *19*, 225–232.

12) Rao, C. N. R.; Kulkarni, G. U.; Thomas, P. J.; Edwards, P. P. Metal Nanoparticles and Their

Assemblies. *Chem. Soc. Rev* **2000**, *29*, 27–35.

13) Yang, X.; Yang, M.; Pang, B.; Vara, M.; Xia, Y. Gold Nanomaterials at Work in Biomedicine. *Chem. Rev.* **2015**, *115*, 10410–10488.

14) Sapsford, K. E.; Algar, W. R.; Berti, L.; Gemmill, K. B.; Casey, B. J.; Oh, E.; Stewart, M. H.; Medintz, I. L. Functionalizing Nanoparticles with Biological Molecules: Developing Chemistries That Facilitate Nanotechnology. *Chem. Rev.* **2013**, *113*, 1904–2074.

15) Lu, H. M.; Jiang, Q. Size-Dependent Surface Energies of Nanocrystals. *J. Phys. Chem. B* **2004**, *108*, 5617–5619.

16) Tseng, R. J.; Tsai, C.; Ma, L.; Ouyang, J.; Ozkan, C. S.; Yang, Y. Digital Memory Device Based on Tobacco Mosaic Virus Conjugated with Nanoparticles. *Nat. Nanotechnol.* **2006**, *1*, 72–77.

17) Roller, E. M.; Khorashad, L. K.; Fedoruk, M.; Schreiber, R.; Govorov, A. O.; Liedl, T. DNA-Assembled Nanoparticle Rings Exhibit Electric and Magnetic Resonances at Visible Frequencies. *Nano Lett.* **2015**, *15*, 1368–1373.

18) Sun, S., Murray, C. B.; Weller, D.; Folks, L.; Moser, A. Monodisperse FePt Nanoparticles and Ferromagnetic FePt Nanocrystal Superlattices. *Science* **2000**, *287*, 1989–1992.

19) Sonnichsen, C.; Reinhard, B. M.; Liphardt, J.; Alivisatos, A. P. A Molecular Ruler Based on Plasmon Coupling of Single Gold and Silver Nanoparticles. *Nat. Biotechnol.* **2005**, *23*, 741–745.

20) Yan, B.; Thubagere, A.; Premasiri, W. R.; Ziegler, L. D.; Negro, L. D.; Reinhard, B. M. Engineered SERS Substrates with Multiscale Signal Enhancement: Nanoparticle Cluster Arrays. *ACS Nano* **2009**, *3*, 1190–1202.

21) Dreaden, E. C.; Alkilany, A. M.; Huang, X.; Murphy, C. J.; El-Sayed, M. A. The Golden Age: Gold Nanoparticles for Biomedicine. *Chem. Soc. Rev*. **2012**, *41*, 2740–2779.

22) Anker, J. N.; Hall, W. P.; Lyanders, O.; Shah, N. C.; Zhao, J.; Van Duyne, R. P. Biosensing with Plasmonic Nanosensors. *Nat. Mater.* **2008**, *7*, 442–453.

23) Ringe, E.; McMahon, J. M.; Sohn, K.; Cobley, C.; Xia, Y.; Huang, J.; Schatz, G. C.; Marks, L. D.; Van Duyne, R. P. Unraveling the Effects of Size, Composition, and Substrate on the Localized Surface Plasmon Resonance Frequencies of Gold and Silver Nanocubes: A Systematic Single-Particle Approach. *J. Phys. Chem. C.* **2010**, *114*, 12511–12516.

24) Cao, J.; Sun, T.; Grattan, K. T. V. Gold Nanorod-Based Localized Surface Plasmon Resonance Biosensors: A Review. *Sensors and Actuators B.* **2014**, *195*, 332–351.

25) Hanske, C.; Hill, E. H.; Vila-Liarte, D.; Gonzalez-Rubio, G.; Matricardi, C.; Mihi, A.; Liz-Marzan, M. Solvent-Assisted Self-Assembly of Gold Nanorods into Hierarchically Organized Plasmonic Mesostructures. *ACS Appl. Mater. Interfaces* **2019**, *11*, 11763–11771.

26) Mirkin, C. A.; Letsinger, R. L.; Mucic, R. C.; Storhoff, J. J. A DNA-Based Method for Rationally Assembling Nanoparticles into Macroscopic Materials. *Nature* **1996**, *382*, 607–609.

27) Whitesides, G. M.; Laibinis, P. E. Wet Chemical Approaches to the Characterization of Organic Surfaces: Self-Assembled Monolayers, Wetting, and the Physical-Organic Chemistry. *Langmuir* **1990**, *6*, 87–96.

28) Huang, X.; Aguilar, Z. P.; Xu, H.; Lai, W.; Xiong, Y. Membrane-Based Lateral Flow Immunochromatographic Strip with Nanoparticles as Reporters for Detection: A Review. *Biosens. Bioelectron.* **2016**, *75*, 166–180.

29) Haes, A. J.; Chang, L.; Klein, W. L.; Van Duyne, R. P. Detection of a Biomarker for Alzheimer's Disease from Synthetic and Clinical Samples Using a Nanoscale Optical Biosensor. *J. Am. Chem. Soc.* **2005**, *127*, 2264–2271.

30) Liu, N.; Liedl, T. DNA-Assembled Advanced Plasmonic Architectures. *Chem. Rev.* **2018**, *118*, 3032–3053.

31) Shipway, A. N.; Katz, E.; Willner, I. Nanoparticle Arrays on Surfaces for Electronic, Optical, and Sensor Applications. *ChemPhysChem* **2000**, *1*, 18–52.

32) Stewart, M. E.; Anderton, C. R.; Thompson, L. B.; Maria, J.; Gray, S. K.; Rogers, J. A.; Nuzzo, R. G. Nanostructured Plasmonic Sensors. *Chem. Rev.* **2008**, *108*, 494–521.

33) Ko, H.; Singamaneni, S.; Tsukruk, V. V. Nanostructured Surfaces and Assemblies as SERS Media. *Small* **2008**, *4*, 1576–1599.

34) Auguie, B.; Barnes, W. L. Collective Resonances in Gold Nanoparticle Arrays. *Phys. Rev. Lett.* **2008**, *101*, 143902.

35) Fan, M.; Andrade, G. F.; Brolo, A. G. A Review on the Fabrication of Substrates for Surface Enhanced Raman Spectroscopy and Their Applications in Analytical Chemistry. *Anal. Chim. Acta* **2011**, *693*, 7–25.

36) McMillan, R. A.; Paavola, C. D.; Howard, J.; Chan, S. L.; Zaluzec, N. J.; Trent, J. D. Ordered Nanoparticle Arrays Formed on Engineered Chaperonin Protein Templates. *Nat. Mater.* **2002**, *1*, 247–252.

37) Raj, C. R.; Okajima, T.; Ohsaka, T. Gold Nanoparticle Arrays for the Voltammetric Sensing of Dopamine. *J. Electroanal. Chem.* **2003**, *543*, 127–133.

38) Hsu, C.-M.; Connor, S. T.; Tang, M. X.; Cui, Y. Wafer-Scale Silicon Nanopillars and Nanocones by Langmuir–Blodgett Assembly and Etching. *Appl. Phys. Lett.* **2008**, *93*, 133109.

39) Kim, F.; Kwan, S.; Akana, J.; Yang, P. Langmuir−Blodgett Nanorod Assembly. *J. Am. Chem. Soc.* **2001**, *123*, 4360–4361.

40) Li, J.; Kamata, K.; Iyoda, T. Tailored Ag Nanoparticle Array Fabricated by Block Copolymer Photolithography. *Thin Solid Films* **2008**, *516*, 2577–2581.

41) Xu, L.; Kuang, H.; Xu, C.; Ma, W.; Wang, L.; Kotov, N. A. Regiospecific Plasmonic Assemblies for *in Situ* Raman Spectroscopy in Live Cells. *J. Am. Chem. Soc.* **2012**, *134*, 1699–1709.

42) Zhao, Y.; Xu, L.; Liz-Marzan, L. M.; Kuang, H.; Ma, W.; Asenjo-Garcia, A.; Garcia de Abajo, F. J.; Kotov, N. A.; Wang, L.; Xu, C. Alternating Plasmonic Nanoparticle Heterochains Made by

Polymerase Chain Reaction and Their Optical Properties. *J. Phys. Chem. Lett.* **2013**, *4*, 641–647.

43) Schreiber, R.; Santiago, I.; Ardavan, A.; Turberfield, A. J. Ordering Gold Nanoparticles with DNA Origami Nanoflowers. *ACS Nano* **2016**, *10*, 7303–7306.

44) Macfarlane, R. J.; Lee, B.; Jones, M. R.; Harris, N.; Schatz, G. C.; Mirkin, C. A. Nanoparticle Superlattice Engineering with DNA. *Science* **2011**, *334*, 204–208.

45) Sato, K.; Hosokawa, K.; Maeda, M. Rapid Aggregation of Gold Nanoparticles Induced by Non-Cross-Linking DNA Hybridization. *J. Am. Chem. Soc.* **2003**, *125*, 8102–8103.

46) Mori, T.; Maeda, M. Stability Change of DNA-Carrying Colloidal Particle Induced by Hybridization with Target DNA. *Polym. J.* **2002**, *34*, 624–628.

47) Fujita, M.; Hiramine, H.; Pan, P.; Hikima, T.; Maeda, M. Effects of Complementary DNA and Salt on the Thermoresponsiveness of Poly(*N*-isopropylacrylamide)-*b*-DNA. *Langmuir* **2016**, *32*, 1148–1154.

48) Wang, G.; Akiyama, Y.; Kanayama, N.; Takarada, T.; Maeda, M. Directed Assembly of Gold Nanorods by Terminal-Base Pairing of Surface-Grafted DNA. *Small* **2017**, *13*, 1702137.

49) Isoda, K.; Kanayama, N.; Fujita, M.; Takarada, T.; Maeda, M. DNA Terminal Mismatch-Induced Stabilization of Polymer Micelles from Raft-Generated Poly(*N*-isopropylacrylamide)-DNA Block Copolymers. *Chem. - Asian J.* **2013**, *8*, 3079–3084.

50) Kanayama, N.; Takarada, T.; Maeda, M. Rapid Naked-Eye Detection of Mercury Ions Based on Non-Crosslinking Aggregation of Double-Stranded DNA-Carrying Gold Nanoparticles. *Chem. Commun.* **2011**, *47*, 2077–2079.

51) Miyamoto, D.; Tang, Z.; Takarada, T.; Maeda, M. Turbidimetric Detection of ATP Using Polymeric Micelles and DNA Aptamers. *Chem. Commun.* **2007**, 4743–4745.

52) Chang, C. C.; Wang, G.; Takarada, T.; Maeda, M. Target-Recycling-Amplified Colorimetric Detection of Pollen Allergen Using Non-Cross-Linking Aggregation of DNA-Modified Gold

Nanoparticles. *ACS Sens.* **2019**, *4*, 363–369.

53) Kanayama, N.; Sekine, T.; Ozasa, K.; Kishi, S.; Nyu, T.; Hayashi, T.; Maeda, M. Terminal-Specific Interaction between Double-Stranded DNA Layers: Colloidal Dispersion Behavior and Surface Force. *Langmuir* **2016**, *32*, 13296–13304.

54) Ellegaard, C.; Hanson, A. E.; Haaning, A.; Hansen, K.; Marcussen, A.; Bohr, T.; Hansen, J. L.; Watanabe, S. Electron Microscopy Image Enhanced. *Nature* **1998**, *392*, 768–769.

55) Sherry, L. J.; Jin, R.; Mirkin, C. A.; Schatz, G. C.; Van Duyne, R. P. Localized Surface Plasmon Resonance Spectroscopy of Single Silver Triangular Nanoprisms. *Nano Lett.* **2006**, *6*, 2060–2065.

Chapter 2

DNA-Guided Anisotropic Self-Organization of AuNPs

2.1 Abstract

A strategy was described to produce an anisotropic assembly from isotropic particles.[1] To generate the anisotropy, local-structure-sensitive colloidal stability of double-stranded DNA-modified gold nanoparticles was exploited; fully matched particles were spontaneously aggregated at high ionic strength, whereas terminal-mismatched particles continued to stably disperse. Linear trimers prepared by aligning both the fully matched and terminal-mismatched particles on a DNA template in a strictly defined order underwent highly directed assembly. The identity of the central particle determined the structural anisotropy. The trimers containing the terminal-mismatched or fully matched particle at the center selectively assembled in an end-to-end or side-by-side manner, respectively. Further, similar trimers having a central terminal-mismatched particle larger than the peripheral fully matched particles formed assemblies that had small particles between the large particles. By contrast, the trimers with a central fully matched particle larger than the peripheral terminal-mismatched particles formed an assembled structure in which the large particles were surrounded by the small particles. The anisotropy was programmable by the rule that an attractive force emerged only between the fully matched particles. This methodology could be useful to fabricate nanodevices.

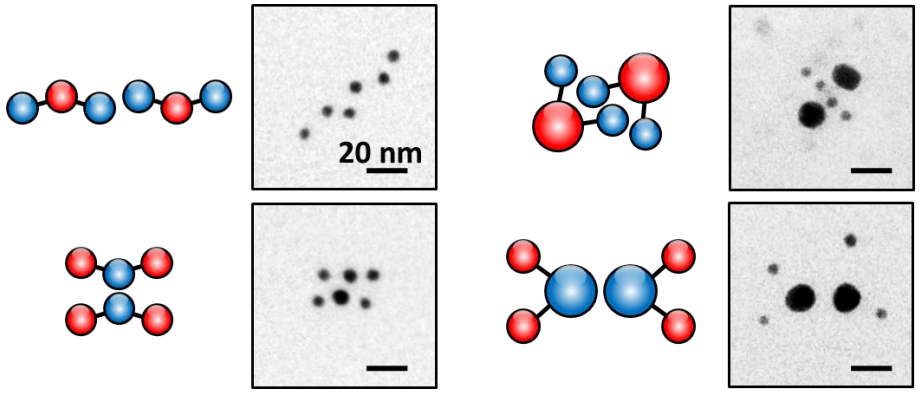

2.2 Introduction

In Chapter 1, the author described the importance of studying nanoparticle assemblies with an ordered structure. However, facile methods to construct highly directed assemblies have not yet been well established. Anisotropic particles are of growing interest in fundamental researches and industrial applications, including multiplexed biosensing,[2,3] electronic devices,[4] and colloidal stabilizers.[5] In general, anisotropic particles readily self-assemble into an anisotropic structure by virtue of an entropic advantage;[6] however, the creation of anisotropic structures from isotropic building blocks is still a technical challenge. For this purpose, Janus and patchy particles with an isotropic core surrounded by different compositional corona have been developed.[7–10] This strategy was successfully applied to asymmetric DNA modification of AuNP surfaces to construct highly directed assemblies.[11–19]

Chapter 2 describes an alternative method to produce an anisotropic assembly of isotropic particles. Specifically, spherical AuNPs almost uniformly modified with ssDNA were used as an isotropic particle to construct their linear trimers. Then, various anisotropic AuNP assemblies were prepared by orienting the trimers. To induce the self-assembly of the trimers, the author used local-structure-sensitive colloidal behaviors of double-stranded (ds) DNA–AuNPs; fully matched dsDNA–AuNPs aggregated spontaneously at high ionic strength, whereas the particles having a single-base mismatch[20] or a single-nucleotide protrusion[21] at the outermost surface dispersed stably under the same conditions (Chapter 1, **1.6**). An investigation using colloidal probe atomic force microscopy has suggested that the interparticle attractive forces were dominated by π-π stacking interaction between the terminal base pairs of the surface-grafted

dsDNA.[22,23] The interparticle attraction has been employed to induce structural changes of the AuNP assemblies. Previous researches demonstrated that fully matched dsDNA–AuNP dimers and trimers were spontaneously shrunk in a non-cross-linking manner.[24,25] The folding of fully matched dsDNA–AuNP chains into an island-like 2D array structure was also identified (Chapter 3).[26] Notably, terminal-mismatched dsDNA–AuNP dimers, trimers, and chains exhibited no structural changes. These results have prompted the author to design a series of trimers consisting of the fully matched and terminal-mismatched dsDNA–AuNPs in a strictly defined order. In this chapter, the non-crosslinked assembly of these trimers was described.

2.3 Experimental Section

2.3.1 General

All reagents were purchased from Wako Pure Chemical unless otherwise specified. Citric acid-coated AuNPs with a nominal diameter of 5 nm and 15 nm were obtained from BBI Solutions. Bis(*p*-sulfonatophenyl)phenylphosphine (BSPP) dehydrate dipotassium salt was purchased from Strem Chemicals. Tris-borate-EDTA (TBE) buffer was obtained from Nippon Gene. Ultra-pure water (>18 MΩ cm) was prepared using a Milli-Q pure water purification system (Millipore) and was sterilized for all experiments. Agarose (L03) was obtained from Takara Bio. All chemically synthesized DNA strands were purchased from Tsukuba Oligo Service and Eurofins Genomics. The DNA sequences used in this study are provided below.

Anchor DNA-t (59 nt):

5′-ACACCGTTCTACATCACTTTCTCGTATAACATTTACACCTTTTCGC

AACAATAACTGA-3′-DTT

Anchor DNA-a (59 nt):

5′-CACGCACACTAAGGGAAGTAGCCGCACATCTGAGTATCTTTTTCG

CAACAATAACTGA-3′-DTT

Extender DNA-t (70 nt):

5′-CCCTTAGTGTGCGTGA-T_{54}-3′

Extender DNA-a (70 nt):

5′-GATGTAGAACGGTGTA-T_{54}-3′

Remover DNA-t (70 nt):

5′-A_{54}-TCACGCACACTAAGGG-3′

Remover DNA-a (70 nt):

5′-A_{54}-TACACCGTTCTACATC-3′

Cover DNA-t (16 nt):

5′-TGACACTGCCTCCTAA-3′-SH

Cover DNA-a (16 nt):

5′-AGACACTGCCTCCTAA-3′-SH

Complementary DNA-t (16 nt):

5′-TTAGGAGGCAGTGTCT-3′

Complementary DNA-a (16 nt):

5′-TTAGGAGGCAGTGTCA-3′

Template DNA for *T-T-T* (174 nt):

5′-AGATACTCAGATGTGCGGCTACTTCCCTTAGTGTGCGTGA-T_{27}-AGATACTCAGATGTGCGGCTACTTCCCTTAGTGTGCGTGA-T_{27}-AGATACTCAGATGTGCGGCTACTTCCCTTAGTGTGCGTGA-3′

Template DNA for *T-A-A* (174 nt):

5′-AGATACTCAGATGTGCGGCTACTTCCCTTAGTGTGCGTGA-T_{27}-GGTGTAAATGTTATACGAGAAAGTGATGTAGAACGGTGTA-T_{27}-GGTGTAAATGTTATACGAGAAAGTGATGTAGAACGGTGTA-3′

Template DNA for *T-A-T* (174 nt):

5′-AGATACTCAGATGTGCGGCTACTTCCCTTAGTGTGCGTGA-T_{27}

GGTGTAAATGTTATACGAGAAAGTGATGTAGAACGGTGTA-T_{27}-AGATACTCAGATGTGCGGCTACTTCCCTTAGTGTGCGTGA-3′

2.3.2 Synthesis of ssDNA–AuNP Monomers

The AuNPs were functionalized with anchor DNA-t with cover DNA-t or anchor DNA-a with cover DNA-a by following the reported procedure with some minor modifications (Figure 2.1).[24,27,28] The 5 nm or 15 nm AuNP was stabilized with BSPP by heating at 50 ºC for 1 h. Anchor DNA was treated with TCEP to form a dithiol group at the 3′-end. Then, this mixture was directly added to a 0.5 × TBE dispersion of BSPP–AuNP at a 1:1 (for 5 nm AuNP) or 2:1 (for 15 nm AuNP) molar ratio, followed by incubation at 50 ºC for 1 h. To this dispersion, four equivalents (relative to the AuNP) of

extender DNA were added, and then the mixture was incubated at 60 ºC for 5 min. Subsequently, the mixture was allowed to stand at room temperature for 1 h.

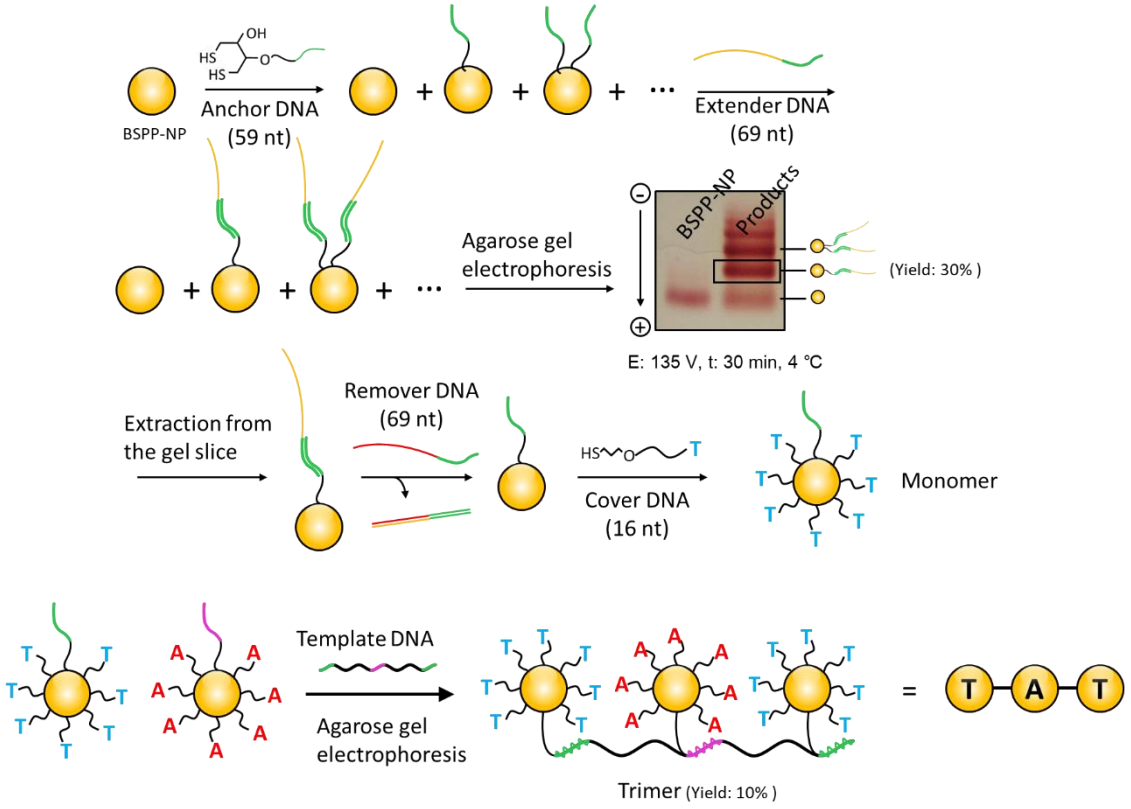

Figure 2.1 Schematics for preparation of AuNP trimers having fully matched dsDNA and terminal-mismatched dsDNA on the surface. This ssDNA–AuNP trimer is referred to as *T-A-T*.

To purify the anchor-DNA–AuNP, the above mixture supplemented with 5% v/v glycerol (final concentration) was subjected to 3% agarose gel electrophoresis (135 V, 30 min, and 4 ºC). After the subjacent area of the corresponding band was cut out, an additional electrophoresis was performed. The anchor-DNA–AuNP hybridized with the extender DNA was electrophoretically permeated into the hole and extracted. To a 0.5 × TBE dispersion of the anchor-DNA–AuNP hybridized with the extender DNA, 25 mM NaCl (final concentration) and 0.33 mg/mL BSPP dehydrate dipotassium salt (final

concentration) was added. After concentrating to 1 μM (for 5 nm AuNP) or 250 nM (for 15 nm AuNP) via centrifugation at 21900 × *g* for 90 min (for 5 nm AuNP) or 20 min (for 15 nm AuNP), four equivalents (relative to the AuNP) of remover DNA were added to the AuNP dispersion to release the extender DNA from the AuNP surface via the strand exchange. The obtained dispersion was incubated at 60 ºC for 5 min, and then allowed to stand at room temperature for 1 h. The resulting dispersion was centrifuged, followed by resuspension of the sediment in 0.5 × TBE containing 25 mM NaCl and 0.33 mg/mL BSPP dehydrate dipotassium salt. This step was repeated three times to remove the excess ssDNA. The anchor-DNA–AuNP was further modified with cover DNA by the salt-aging method; 500 equivalents (relative to the 5 nm AuNP) or 2000 equivalents (relative to the 15 nm AuNP) of cover DNA were added before incubation at room temperature for 3 h. Subsequently, the NaCl concentration was gradually increased at intervals of 45 mM, and finally brought to 300 mM over 3 h. The excess cover DNA was removed by centrifugation for three times, and the obtained ssDNA–AuNP monomers were resuspended in the same buffer to 2 μM (for 5 nm AuNP) or 500 nM (for 15 nm AuNP). The average number of cover DNAs on the AuNP surface was determined using the method reported elsewhere.[29]

Figure 2.2 shows the calibration curves to estimate the number of cover DNA-t and cover DNA-a using an OliGreen ssDNA quantitation kit (Molecular Probes). The fluorescence was measured using a fluorescence microplate reader (ARVO X One, Perkin Elmer) with excitation at 485 nm and recording emission at 535 nm. The fluorescence intensities observed with the *T5* particle were 51216, 52764, and 49630, which provided the average cover DNA-t graft number of 9 ± 0.30 per particle. Hereafter, ± denotes the standard deviation. The fluorescence intensities observed with the *A5* particle were 55260,

57209, and 54359, which provided the average cover DNA-a graft number of 10 ± 0.28 per particle. The fluorescence intensities observed with the *A15* particle were 66687, 65105, and 64680, which provided the average cover DNA-a graft number of 180 ± 2.9 per particle.

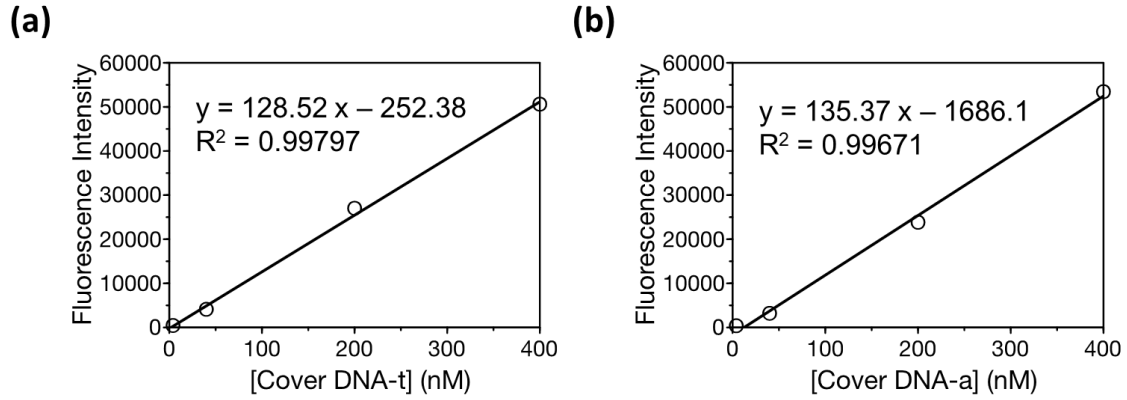

Figure 2.2 Calibration curves of (a) cover DNA-t and (b) cover DNA-a.

2.3.3 Preparation of ssDNA–AuNP Trimers

A mixture (10 μL) of ssDNA–AuNPs, 174 nt ssDNA (template DNA), and NaCl was allowed to stand at room temperature overnight after incubation at 60 ºC for 5 min. The ratio of each ssDNA–AuNP to its corresponding binding site on template DNA was 2:1 and the concentration of NaCl was 150 mM. For 5 nm and 15 nm ssDNA–AuNPs, the stock concentrations were 2 μM and 0.5 μM, respectively, in 0.5 × TBE containing 25 mM NaCl and 0.33 mg/mL BSPP dehydrate dipotassium salt. To purify the trimers, the mixture was subjected to 3% agarose gel electrophoresis (135 V, 30 min, and 4 °C). Representative images of the gels showing the separation of the trimers from the monomers, the monomers with the template DNAs, and the dimers are provided in Figure 2.3. A similar extraction process described above was subsequently applied to gather the

purified trimers from the gel band. To the obtained solution, 20 mM NaCl was immediately added to avoid the dehybridization of the trimer.

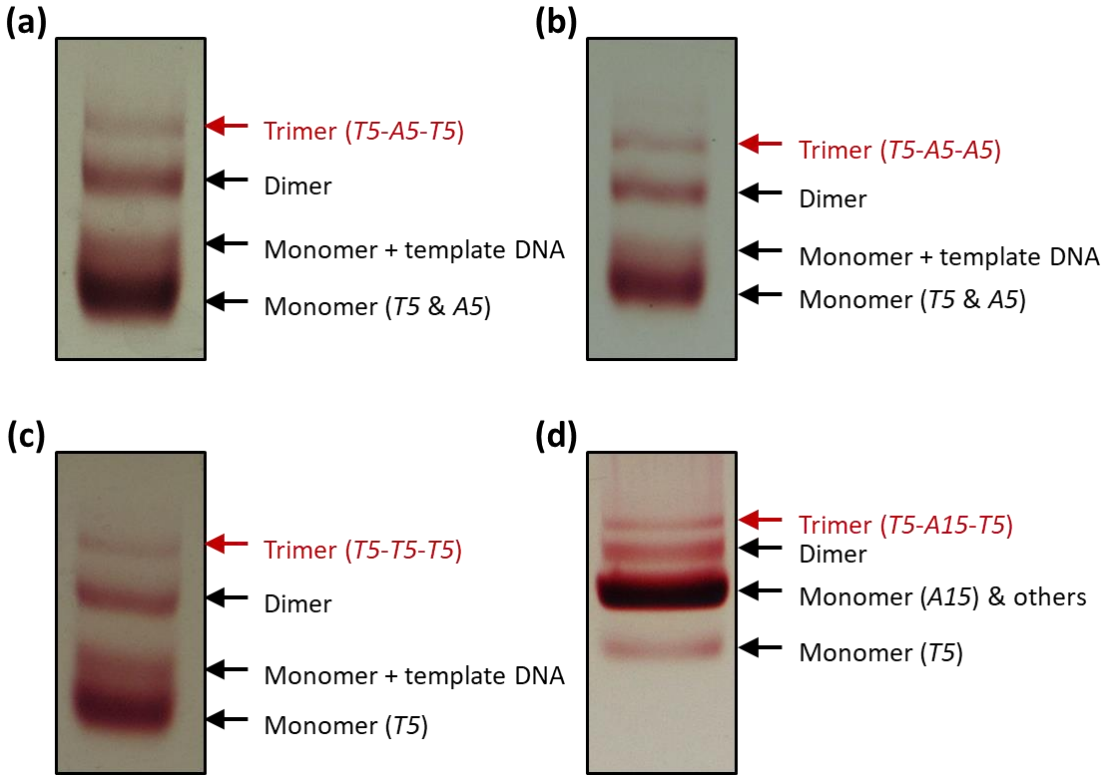

Figure 2.3 Electrophoretic purification of (a) *T5-A5-T5*, (b) *T5-A5-A5*, (c) *T5-T5-T5*, and (d) *T5-A15-T5* constructed from the monomer and the template DNA. Conditions: 3% agarose, 135 V, 30 min, and 4 °C.

2.3.4 UV-vis Spectroscopy

The concentrations of ssDNA, AuNPs, ssDNA–AuNPs, and ssDNA–AuNP trimers were measured by UV-vis spectroscopy. As an example, an aliquot of the dispersion of ssDNA–AuNP trimers in TBE buffer containing 20 mM NaCl (198 μL) was added to a 1 mL-tube containing 1% w/v Tween 20 (2 μL). Background spectrum and extinction

spectra were scanned with a Cary 50 UV-vis spectrophotometer (Varian). The concentration was calculated by Lambert-Beer′s Law.

2.3.5 Transmission Electron Microscopy (TEM)

An elastic-carbon-coated copper grid (ELS-C10) from Okenshoji was previously hydrophilized under UV/ozone treatment. A dispersion of the precursory ssDNA–AuNP trimer was mixed with 16 nt ssDNA (complementary DNA), whose sequence was complementary to cover DNA (8 equivalents of the total amount of the surface-grafted ssDNA in the ssDNA–AuNP trimer), followed by incubation at room temperature for 10 min to allow DNA hybridization. The resulting mixture (2 μL) was dropped onto the grid. After incubation at room temperature for 1.5 min, the excess solution was removed by using a capillary tube. Then, the sample was dried under a vacuum for 3 min. The measurements were performed on a JEM 1230 TEM (JEOL) operated at an accelerating voltage of 80 kV. The interparticle center-to-center distance and the circularity analysis were conducted using an image analysis software (Particle Analyzer ver. 3.5, NSST).

2.3.6 Dark-Field Microscopic Imaging and Scattering Spectroscopy

An aliquot (1 μL) of the mixture of the ssDNA–AuNP trimer, the complementary DNA, and NaCl was dropped on an aminosilane-coated slide glass (Matsunami) and held by a coverslip (Figure 2.4). The sample was excited using the halogen white light source to generate plasmon resonance scattering light. An oil immersion objective lens (100x/1.30 Oil Iris, Zeiss) was used to collect the scattering light. A 5-megapixel color camera (AxioCam ICc5, Zeiss) was employed to capture the dark-field color images. The scattering light by the AuNP alone or by the assemblies adsorbed on the surface of the

slide glass was split by a spectrometer (Solid Lambda CCD UV-NIR, Spectra Coop) equipped with a back-thinned-type CCD (Hamamatsu). The scattering spectra were corrected by subtracting the background spectra taken from the adjacent dark regions.

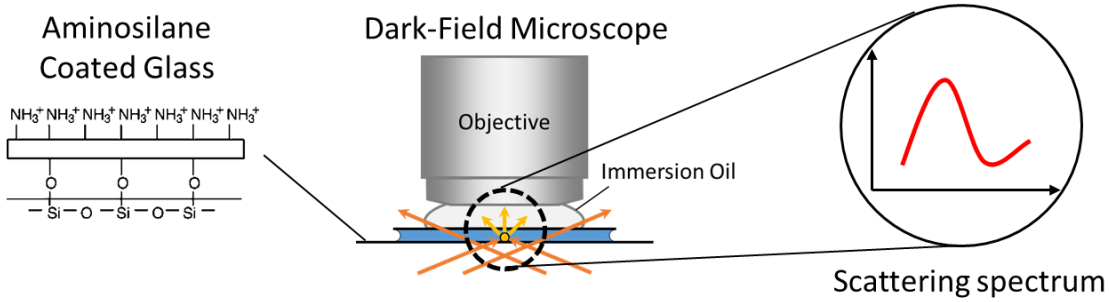

Figure 2.4 Diagram of dark-field microscopic imaging and scattering spectroscopy.

2.4 Results and Discussion

2.4.1 Design and Preparation of AuNP Trimers

Figure 2.1 shows the method used to prepare dsDNA–AuNP trimers. First, ssDNA–AuNP monomers were synthesized according to the previously reported method.[24] All DNA sequences used in this study are provided in **2.3.1**. Both 5 nm and 15 nm AuNPs were functionalized with thiol-modified ssDNA through Au–S bond formation. The 3′-dithiol-modified 59-nucleotide (nt)-long ssDNA (anchor DNA) was used to immobilize the AuNP onto 174 nt ssDNA (template DNA). In the present study, two types of anchor DNA (anchor DNA-a and anchor DNA-t) were used. The other surface-bound DNA was the 3′-monothiol-modified 16 nt ssDNA (cover DNA), which served to induce the non-crosslinking assembly. The author designed two types of cover DNA (cover DNA-a and cover DNA-t) with sequences that differed only by a single nucleobase (A or T) at the solution-facing terminus. AuNP was modified with strictly one anchor DNA per particle (5 nm and 15 nm AuNPs) and then on average 9 cover DNA-t strands per particle (5 nm AuNP), 10 cover DNA-a strands per particle (5 nm AuNP), and 180 cover DNA-a strands per particle (15 nm AuNP) to produce an ssDNA–AuNP monomer. In this study, a pair of the monomers was prepared: one having anchor DNA-t and cover DNA-t and the other having anchor DNA-a and cover DNA-a. The former and latter particles are referred to as *T* and *A*, respectively. It is considered that the *T* and *A* particles nearly completely isotropic. This is because their colloidal stability was governed by one kind of cover DNA tethered uniformly to the particle surface in sharp contrast against Janus and patchy particles.

Then, the *T* and *A* particles were attached to template DNA through hybridization between anchor DNA and template DNA. The ssDNA–AuNP trimer was separated from the byproducts composed of the monomer, the monomer with the template, and the dimer by using agarose gel electrophoresis (Figure 2.3); the trimer was extracted from the small gel band.[24] As two examples, TEM images of trimers extracted from Figure 2.3a and Figure 2.3d were shown in Figure 2.5a and Figure 2.5b, respectively. The statistical analysis revealed that the number fraction of the trimer thus obtained was almost 90% (Table 2.1), albeit the total yield of the ssDNA–AuNP trimer based on the bare AuNP was less than 1%.

Subsequently, 16 nt ssDNA was added, whose sequence was complementary to cover DNA, to form DNA duplexes on the particle surface. The oligonucleotides complementary to cover DNA-a and cover DNA-t are termed complementary DNA-t and complementary DNA-a, respectively. The sequences of complementary DNA-t and complementary DNA-a differed only in terminal single base. The addition of complementary DNA-t or complementary DNA-a to an ssDNA–AuNP trimer with any particle composition resulted in the production of a trimer having fully matched dsDNA–AuNP (referred to as *F*) or terminal-mismatched dsDNA–AuNP (*M*) as a constituent particle (Figure 2.6).

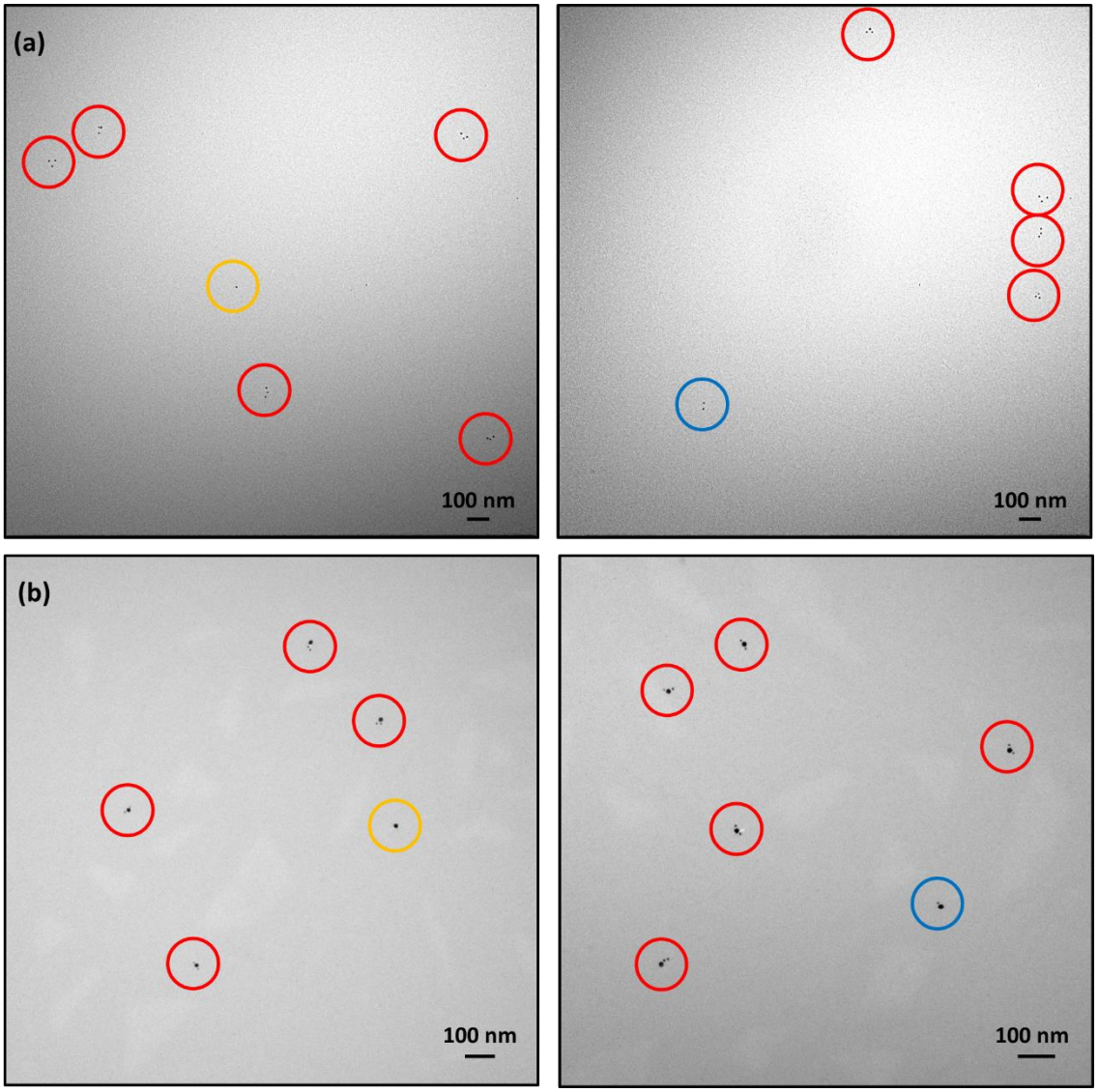

Figure 2.5 Representative TEM images used for estimating the particle-number distribution of (a) *T5-A5-T5* extracted from the band assigned to the trimer shown in Figure 2.3a and (b) *T5-A15-T5* extracted from the band assigned to the trimer shown in Figure 2.3d. The monomer, dimer, and trimer are highlighted with a yellow, blue, and red, respectively.

Table 2.1 Particle-number distribution of *T5-A5-T5* and *T5-A15-T5*.[a]

Code	Number fraction (%)			
	1 AuNP	2 AuNPs	**3 AuNPs**	>3 AuNPs
T5-A5-T5	1	7	**92**	0
T5-A15-T5	2	8	**90**	0

[a]The probability for *T5-A5-T5* was determined using the TEM images showing a total 5-nm AuNP number of 326. The probability for *T5-A15-T5*, which was defined on the basis of the central *A15*, was determined using the TEM images showing a total *A15* number of 111.

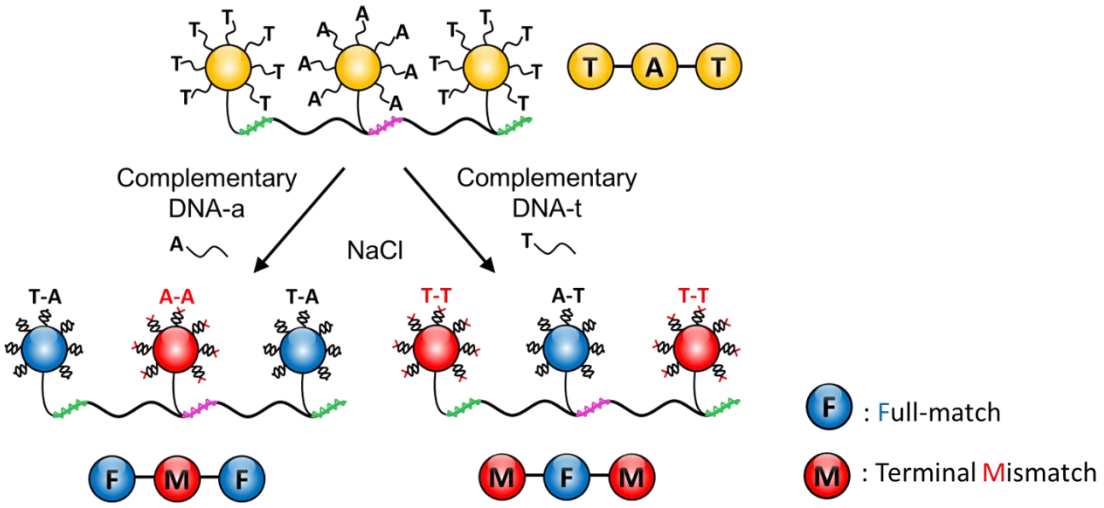

Figure 2.6 Schematics for preparation of AuNP trimers having fully matched dsDNA and terminal-mismatched dsDNA on the surface. As an example, two kinds of dsDNA–AuNP trimer are depicted, both of which are obtained from the precursory ssDNA–AuNP trimer composed of two peripheral AuNPs modified with cover DNA-t and a central AuNP modified with cover DNA-a (*T-A-T*). The addition of complementary DNA-a and complementary DNA-t to the dispersion of *T-A-T*s yields the dsDNA–AuNP trimers, *F-M-F* and *M-F-M*, respectively.

2.4.2 Directed Assembly of AuNP Trimers

As shown in Figure 2.7a, a trimer having one central *A* particle and two peripheral *T* particles was synthesized by using 5 nm AuNP (*T5-A5-T5*). Then, complementary DNA-a and complementary DNA-t were added to the *T5-A5-T5* dispersion to prepare *F5-M5-F5* and *M5-F5-M5*, respectively. An aliquot of the dispersion of *F5-M5-F5* and *M5-F5-M5* with 20 mM NaCl was dropped onto a TEM grid and dried in preparation for microscopic observation. During the drying of the sample solutions, the ionic strength was gradually augmented to induce the non-crosslinking assembly of *F5-M5-F5*s and *M5-F5-M5*s.

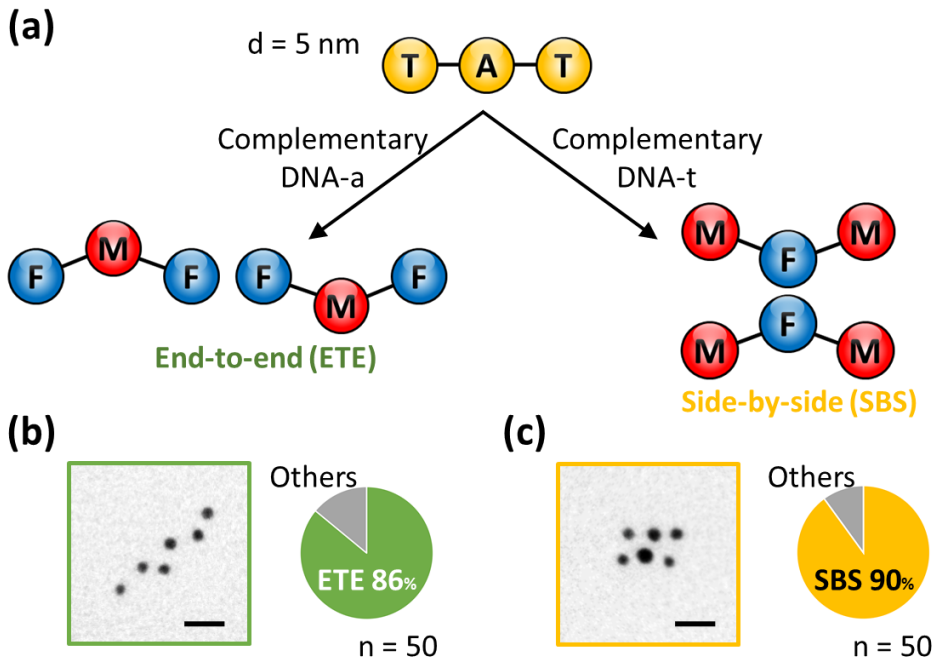

Figure 2.7 Directed assembly of *T5-A5-T5* in an end-to-end (ETE) and side-by-side (SBS) manner. (a) Schematics for preparation of *F5-M5-F5* and *M5-F5-M5* from *T5-A5-T5* for the ETE and SBS assembly, respectively. (b, c) The representative TEM images of *F5-M5-F5* (b) and *M5-F5-M5* (c). Scale bars are 20 nm. The number ratio of the ETE assembly (b) and the SBS assembly (c) is also depicted.

The initial NaCl concentration was determined such that formation of larger assemblies composed of more than two trimers was sufficiently suppressed for unambiguous discrimination of the assemblies. Only isolated trimers were observed with 4 mM NaCl (Figure 2.8a). On the other hand, the large assemblies were found with 50 mM NaCl (Figure 2.8b).

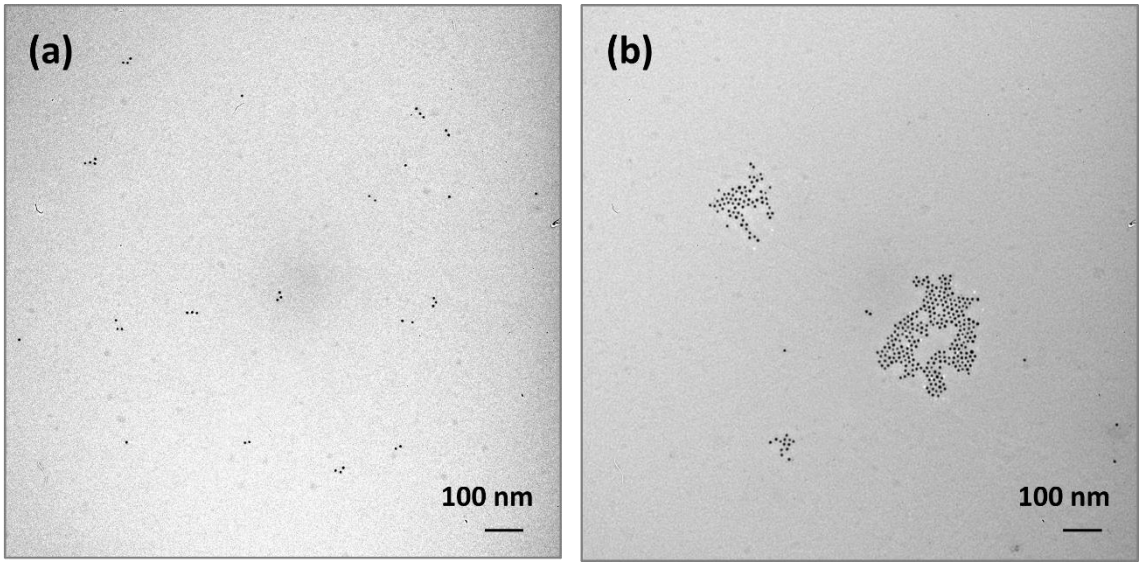

Figure 2.8 Representative field-of-view TEM images of *F5*-*M5*-*F5*s with (a) 4 mM NaCl and (b) 50 mM NaCl.

For *F5*-*M5*-*F5* with 20 mM NaCl, the assemblies observed were caused by attraction between peripheral *F5* particles in an end-to-end manner (Figures 2.7b and 2.9). A small number of cyclic assemblies were also found (Figure 2.9a). For *M5*-*F5*-*M5*, side-by-side assemblies were found due to attraction between central *F5* particles (Figures 2.7c and 2.10). The guidelines for the classification of the TEM images into the end-to-end and side-by-side configuration were as follows. (i) The assemblies composed of <5 AuNPs and >6 AuNPs were excluded from the image analysis. (ii) The selected assemblies (5 or

6 AuNPs) were categorized as end-to-end or side-by-side according to the morphology. (iii) The undirected assemblies were classified into "others". TEM statistical analysis revealed a high number ratio of the end-to-end and side-by-side assembly (Figure 2.7b, c). However, this classification cannot avoid ambiguity because the template DNA was unable to be identified with the conventional TEM analysis. For example, the observed assembly composed of 6 AuNPs was actually undistinguishable into two AuNP trimers or three AuNP dimers, even though the probability of two trimers was expected to be higher because the number ratio of ssDNA–AuNP trimer (*T5-A5-T5*) was 92%, whereas the ratio of the byproduct dimer was only 7% (Table 2.1).

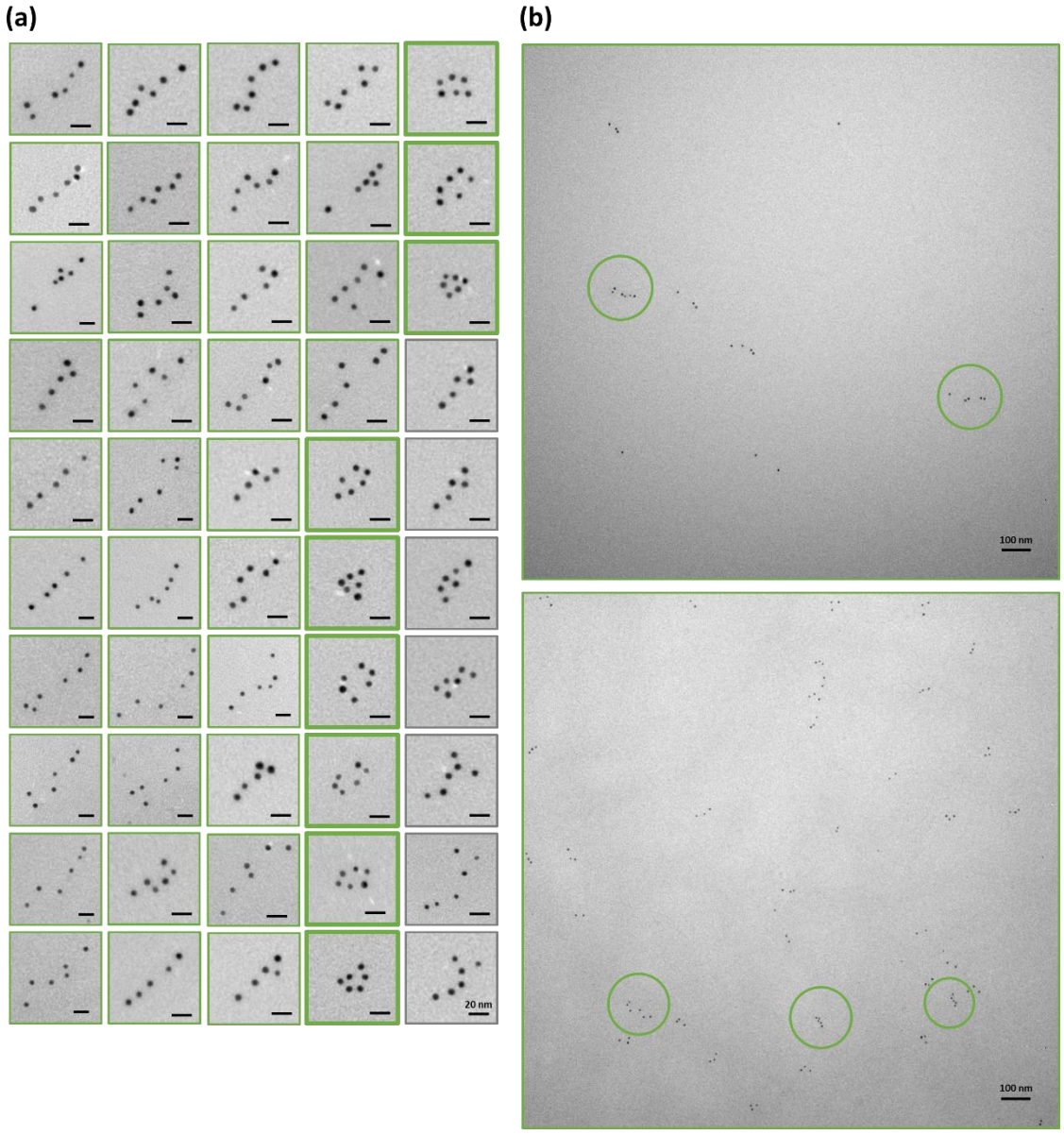

Figure 2.9 (a) All TEM images for the end-to-end assembly and the undirected assembly of *F5*-*M5*-*F5*s. Eight images for the cyclic assembly made by attraction at both ends are shown with a bold green frame. These cyclic assemblies were also classified into the end-to-end assembly. Seven images for the undirected assembly, which was classified into others, are depicted with a grey frame. (b) Representative field-of-view TEM images for the end-to-end assembly of *F5*-*M5*-*F5*s.

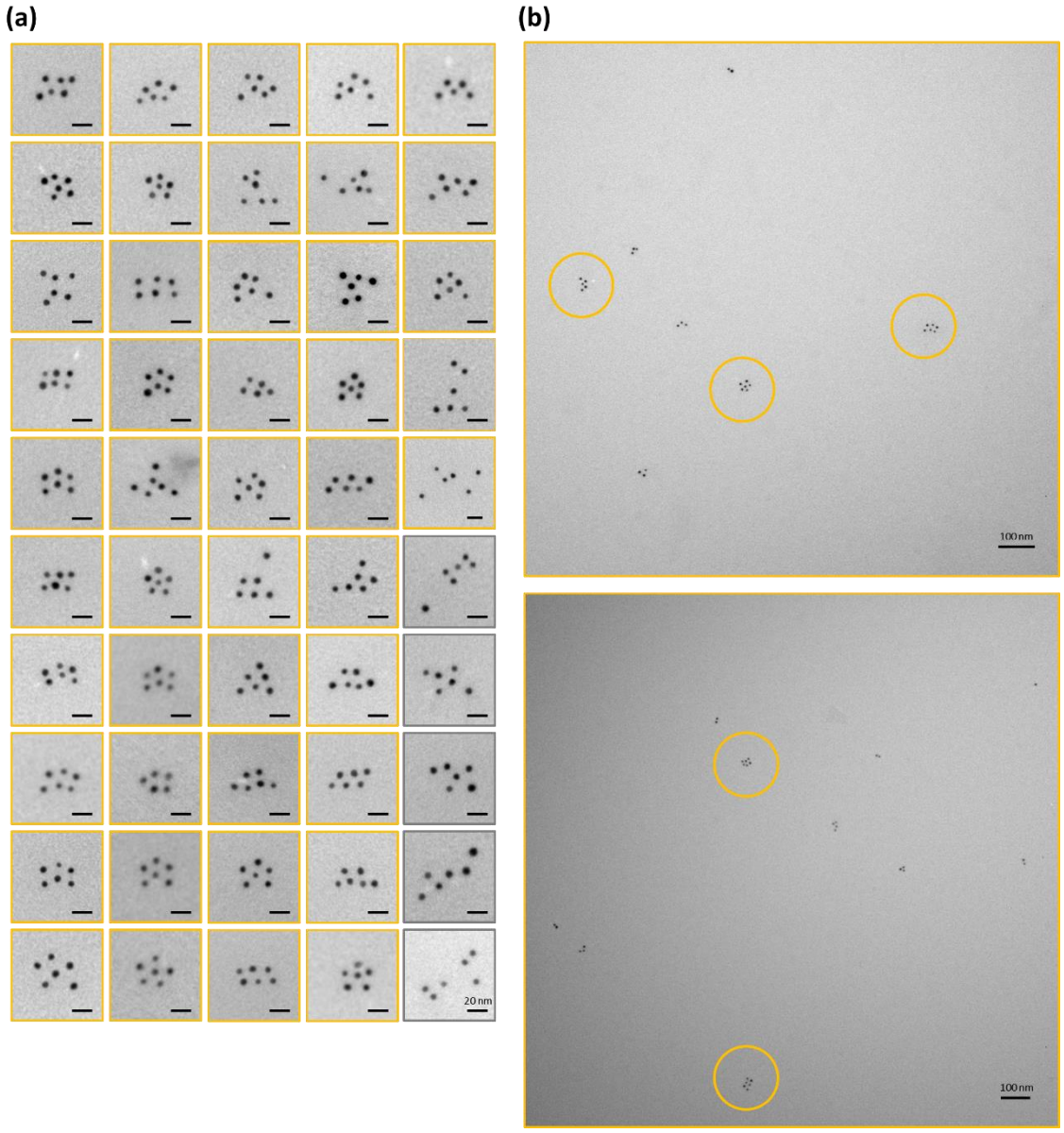

Figure 2.10 (a) All TEM images for the side-by-side assembly and the undirected assembly of *M5*-*F5*-*M5*s. Five images for the undirected assembly, which was classified into others, are depicted with a grey frame. (b) Representative field-of-view TEM images for the side-by-side assembly of *M5*-*F5*-*M5*s.

To compensate for the unavoidable ambiguity about characterization of each assembly, the author additionally made a careful comparison of different shapes of the assemblies in a quantitative manner. Specifically, circularity, the degree to which an object is round, was introduced to discuss the structural difference (Figure 2.11).[30]

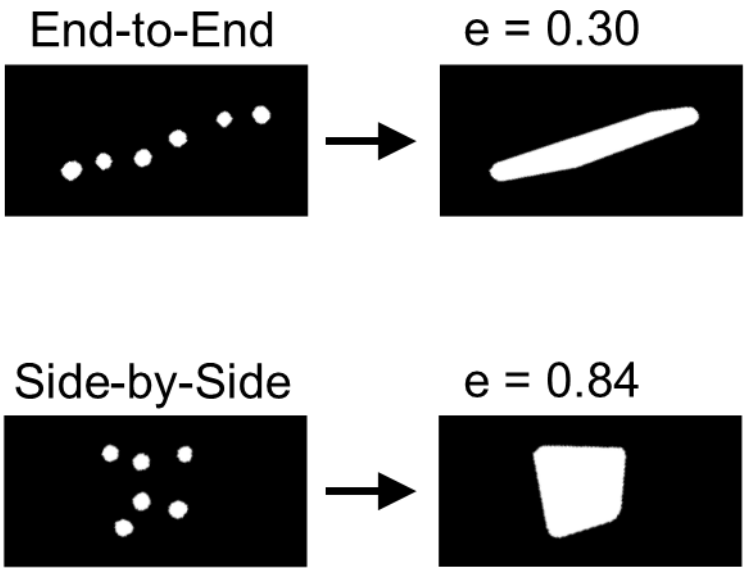

Figure 2.11 Determination of circularity of the TEM images (left) for the end-to-end and side-by-side assemblies of the AuNP trimers.

The circularity *e* is defined as follows:

$$e = 4\pi\,(\text{area})/(\text{perimeter})^2$$

Both the area and the perimeter length for each assembly image were determined with the image analysis software. The average circularity value for the assemblies of *F5-M5-F5*s (Figure 2.12a) was smaller than that of *M5-F5-M5*s (Figure 2.12b) with a *p*-value of less

than 0.001. This result indicated that *T5-A5-T5*s assembled into differently shaped structures when the complementary DNAs differing only in the terminal base were added. The author also calculated the particle number per 100 nm^2 (the particle density) by using the area described above and the number of the particles involved in the assembly (Figure 2.12c, d). The assembly of *M5-F5-M5*s was more densely packed than the assembly of *F5-M5-F5*s, even though the number of *F5* particles of *M5-F5-M5* was smaller than that of *F5-M5-F5*.

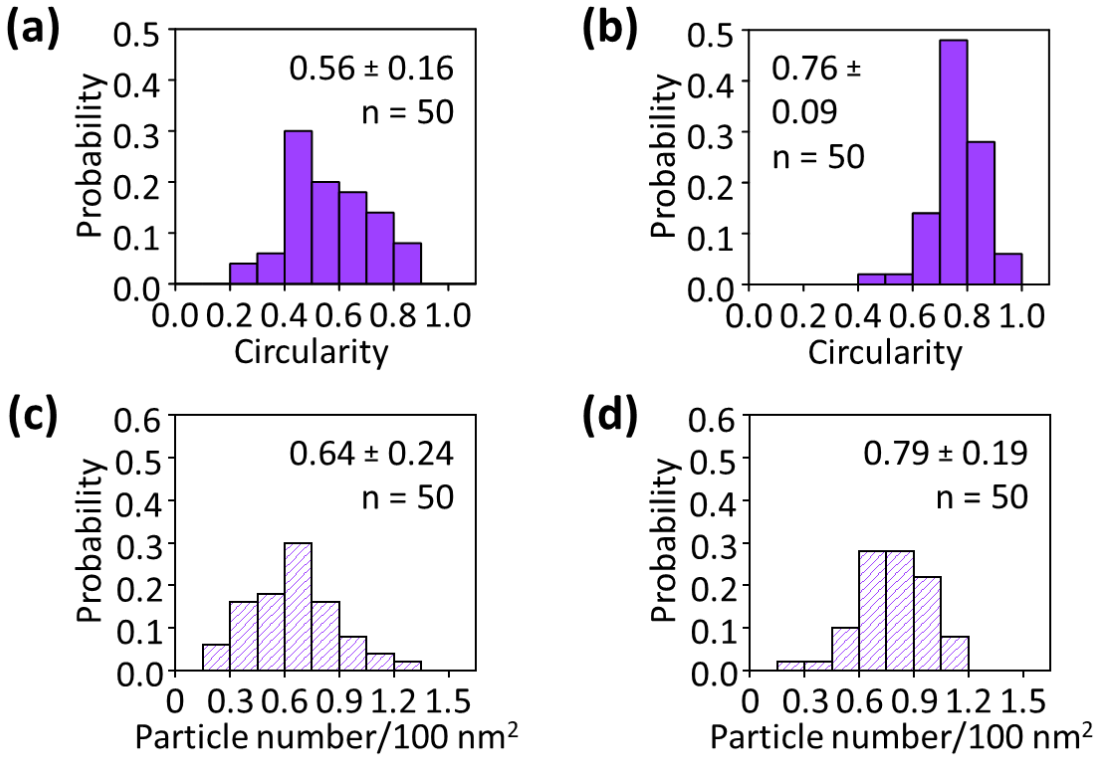

Figure 2.12 (a, b) The circularity distributions for the assembly of *F-M-F*s (a) and *M-F-M*s (b). (c, d) The particle density distributions for the assembly of *F-M-F*s (c) and *M-F-M*s (d).

Next, asymmetric *T5-A5-A5* was synthesized with the same method. Complementary DNA-a and complementary DNA-t were added to the trimer dispersion

to prepare *F5*-*M5*-*M5* and *M5*-*F5*-*F5*, respectively (Figure 2.13). For *F5*-*M5*-*M5*, the end-to-end assemblies were observed, which were caused by attraction between terminal *F5* particles (Figures 2.13b and 2.14). TEM statistical analysis revealed a high number ratio of the end-to-end assembly (Figure 2.13b). The author found the absence of cyclic assemblies and larger assemblies consisting of more than two trimers. For *M5*-*F5*-*F5*, the side-by-side assemblies emerged with a similar high ratio (Figures 2.13c and 2.15). The average circularity value for the assemblies of *F5*-*M5*-*M5*s (Figure 2.13d) was smaller than that of *M5*-*F5*-*F5*s (Figure 2.13e) with a *p*-value of less than 0.001. This result demonstrated that *T5*-*A5*-*A5*s also assembled into differently shaped structures with the complementary DNAs differing only in the terminal mononucleotide. The particle number per 100 nm^2 for the assemblies of *F5*-*M5*-*M5*s was smaller than that of *M5*-*F5*-*F5*s (Figure 2.13f, g); namely, the assemblies of *M5*-*F5*-*F5*s were more highly packed than those of *F5*-*M5*-*M5*s. In this case, the particle density was roughly proportional to the *F5* particle number.

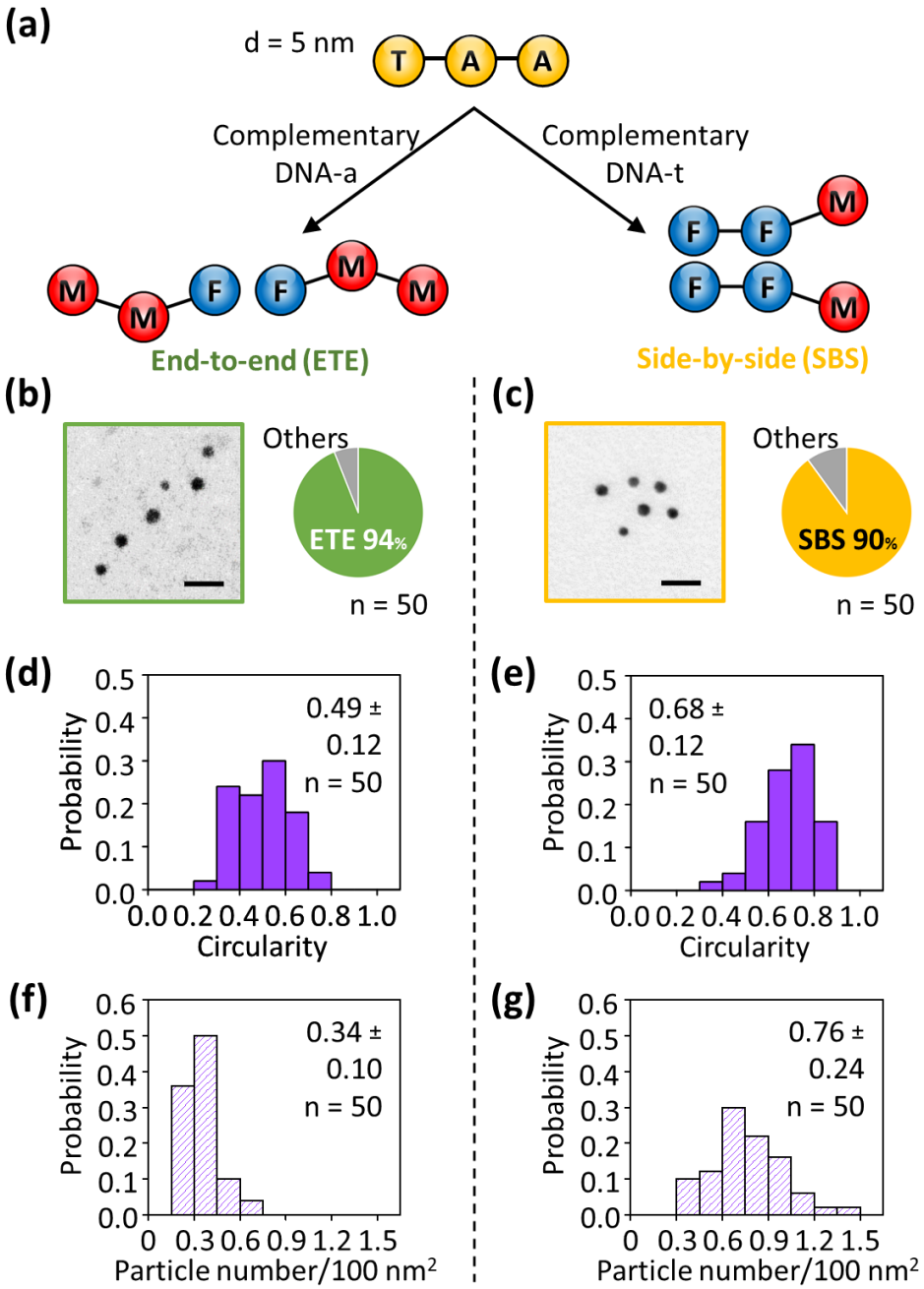

Figure 2.13 Directed assembly of *T5-A5-A5* in an end-to-end (ETE) and side-by-side (SBS) manner. (a) Schematics for preparation of *F5-M5-M5* and *M5-F5-F5* from *T5-A5-A5* for the ETE and SBS assembly, respectively. (b, c) The representative TEM images of *F5-M5-M5* (b) and *M5-F5-F5* (c). Scale bars are 20 nm. The number ratio of the ETE assembly (b) and the SBS assembly (c) is also depicted. (d, e) The circularity distributions for the assembly of *F5-M5-M5*s (d) and *M5-F5-F5*s (e). (f, g) The particle density distributions for the assembly of *F5-M5-M5*s (f) and *M5-F5-F5*s (g).

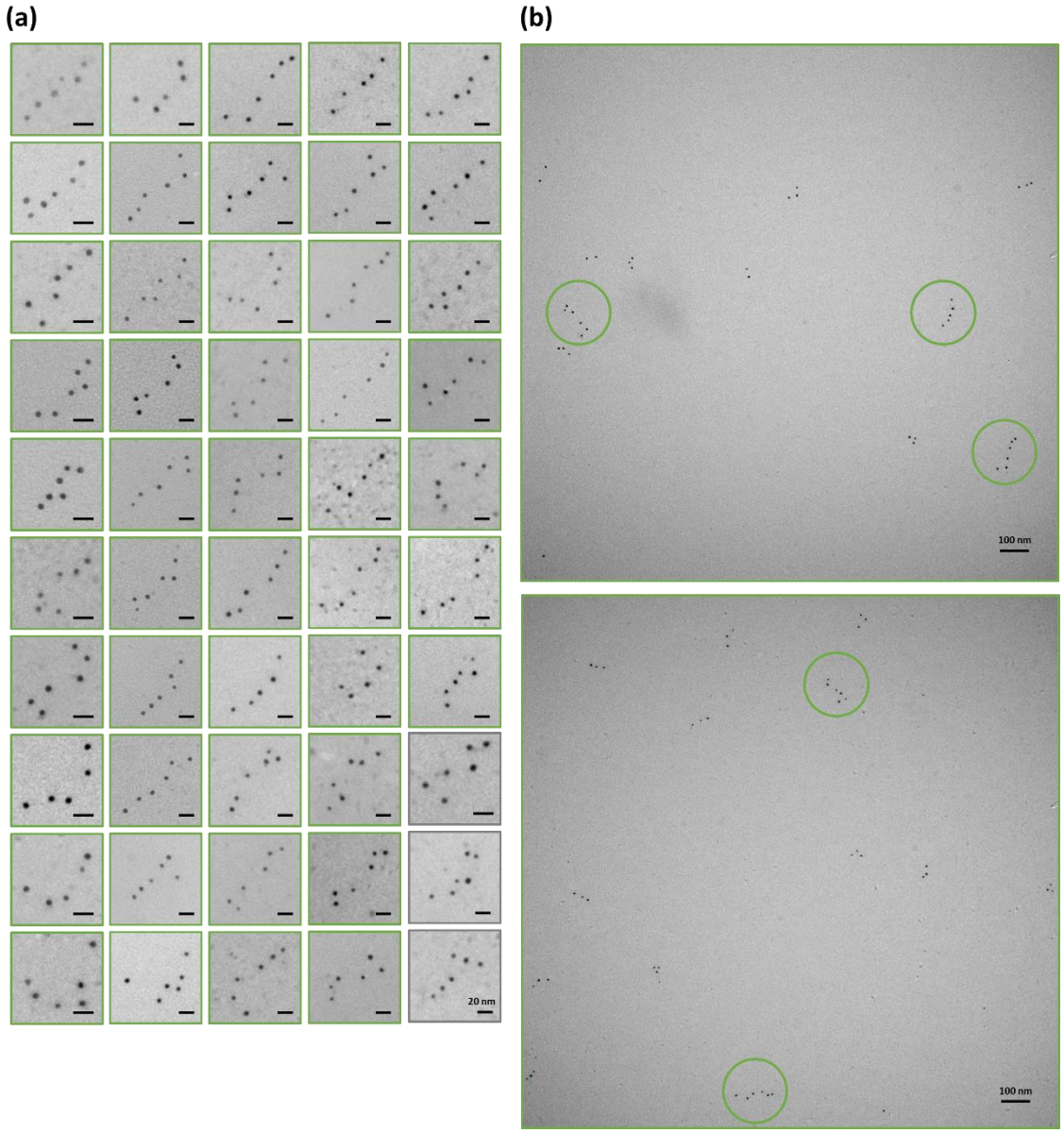

Figure 2.14 (a) All TEM images for the end-to-end assembly and the undirected assembly of *F5*-*M5*-*M5*s. Three images for the undirected assembly, which was classified into others, are depicted with a grey frame. (b) Representative field-of-view TEM images for the end-to-end assembly of *F5*-*M5*-*M5*s.

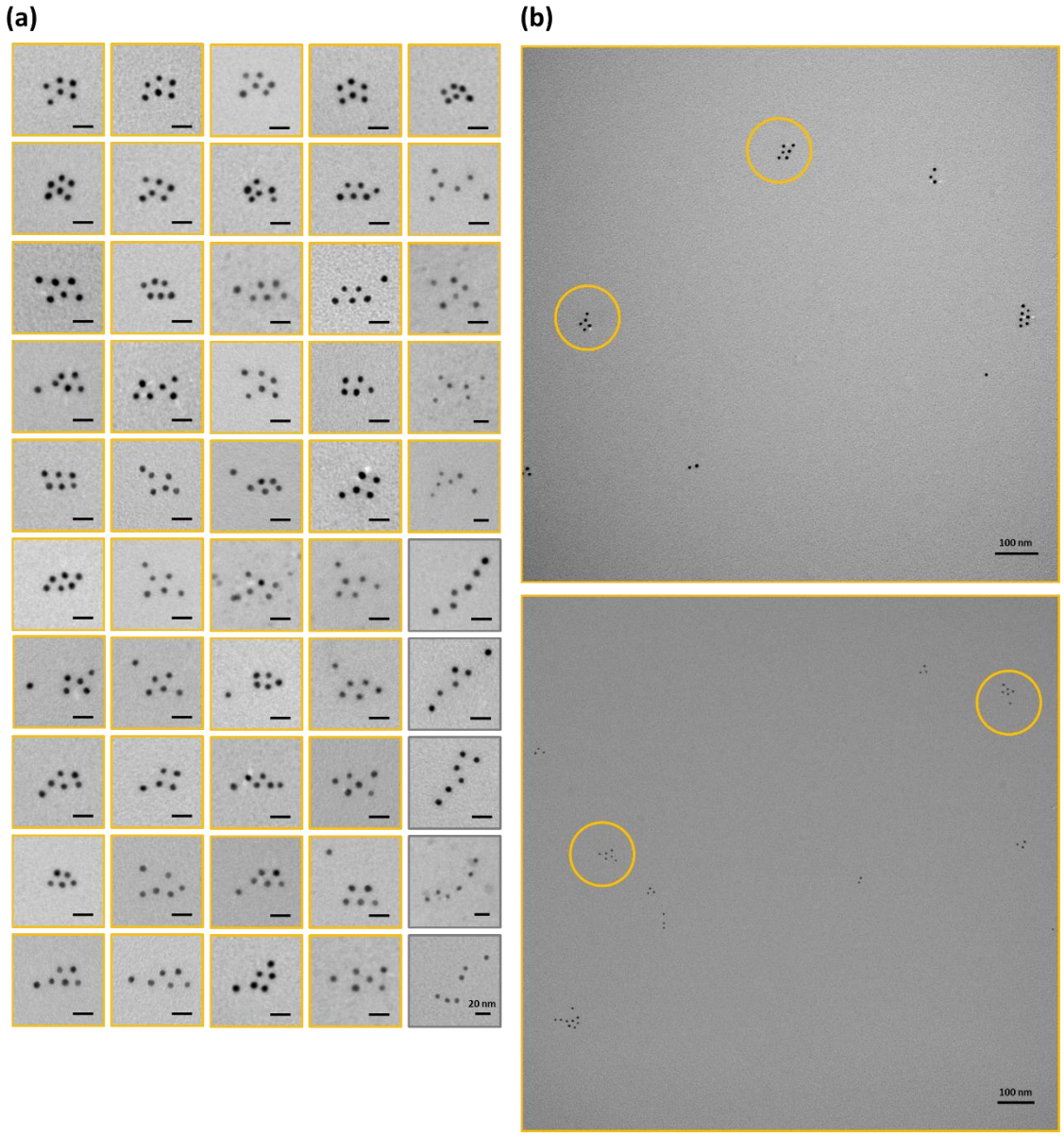

Figure 2.15 (a) All TEM images for the side-by-side assembly and the undirected assembly of *M5-F5-F5*s. Five images for the undirected assembly, which was classified into others, are depicted with a grey frame. (b) Representative field-of-view TEM images for the side-by-side assembly of *M5-F5-F5*s.

2.4.3 Basis of Anisotropic Structures

For comparison, the author also synthesized a homo-trimer *T5-T5-T5*, and then prepared *F5-F5-F5* and *M5-M5-M5* (Figure 2.16). As predicted, *F5-F5-F5*s assembled randomly (Figure 2.16b), while *M5-M5-M5*s dispersed stably (Figure 2.16c). The average circularity value of the random *F5-F5-F5* assemblies was determined to be 0.61 ± 0.18 (Figure 2.16d). The particle number per 100 nm^2 was also determined to be 0.84 ± 0.26 (Figure 2.16e). Comparisons of this homo-trimer with the preceding hetero-trimers allowed one to point out the following. (1) Substitution of central *M5* in *M5-M5-M5* with *F5* generated the side-by-side assembly. (2) Substitution of one terminal *M5* in *M5-M5-M5* with *F5* generated the end-to-end assembly. (3) Substitution of central *F5* in *F5-F5-F5* with *M5* made the transition from the undirected assembly to the end-to-end assembly. (4) Substitution of one terminal *F5* in *F5-F5-F5* with *M5* made the transition from the undirected assembly to the side-by-side assembly. Taken together, these results indicate that when the trimers were prepared by aligning the *F5* and *M5* particles in a strictly defined order, the resultant assembled structures were endowed with the anisotropy; namely, highly directed assemblies of the structurally isotropic particles were achieved in a programmed manner.

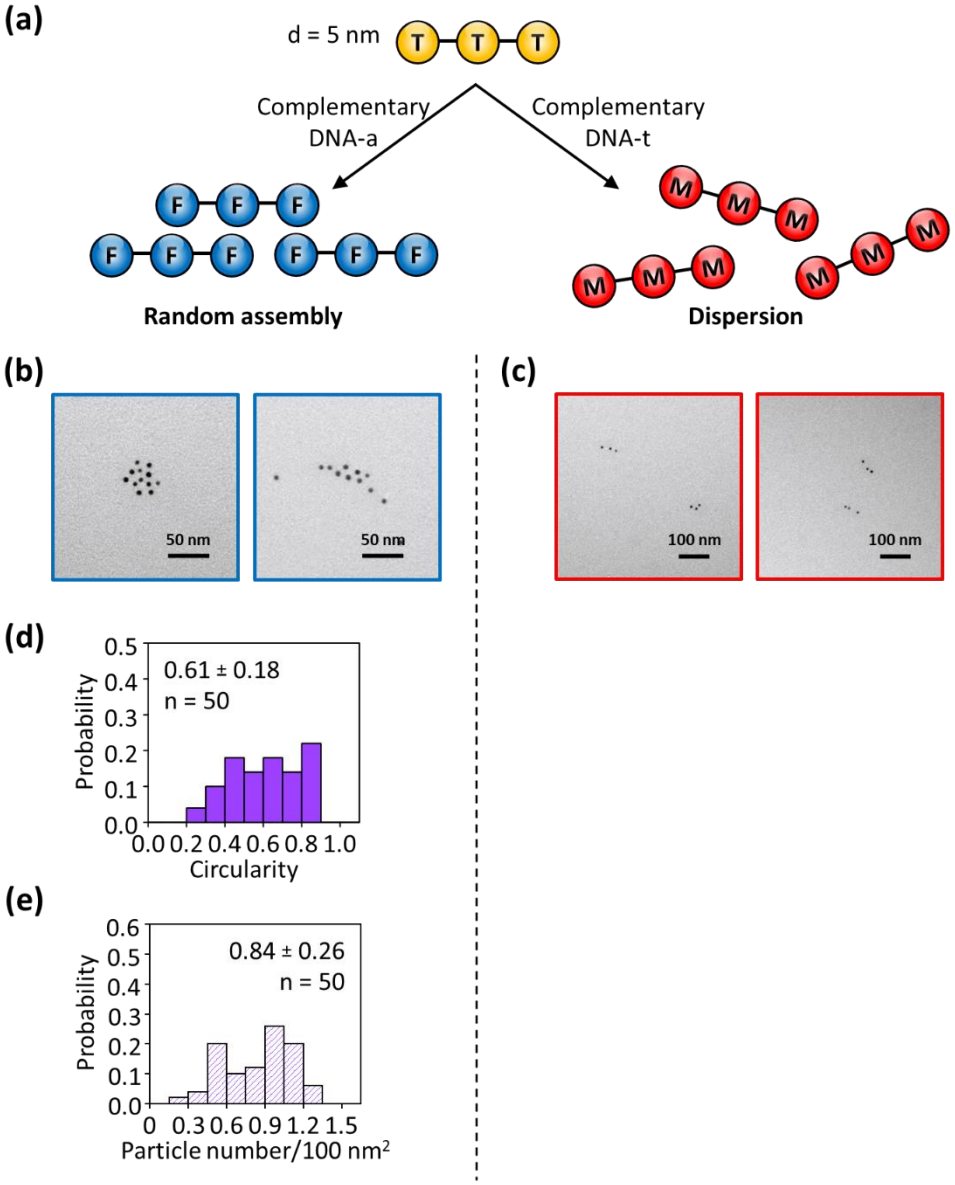

Figure 2.16 Random assembly and dispersion of *T5-T5-T5*s. (a) Schematics for preparation of *F5-F5-F5* and *M5-M5-M5* from *T5-T5-T5* for the random assembly and the dispersion, respectively. (b, c) The representative TEM images for the random assembly of *F5-F5-F5*s (b) and the dispersion of *M5-M5-M5*s (c). (d) The circularity distribution and (e) the particle density distribution for the *F5-F5-F5* assemblies. ± denotes the standard deviation.

The connection between the particles by DNA was essential for the anisotropic assembly. When no template DNA was added to a mixture of *F5* and *M5* with a given ratio, only isolated AuNPs were observed in the TEM images. A previous study demonstrated that region-selective DNA modification of circular-shaped ends and a side region of Au nanorod (15 nm × 45 nm) either with fully matched or terminal-mismatched dsDNA produced the non-crosslinked end-to-end or side-by-side assemblies of the Au nanorods.[31] The present results strongly suggested that the directed assemblies were also available with the AuNP trimers. Emphasis is placed on the technical advantage of the current approach; the modularity of *F5* and *M5* could allow one to design and fabricate a variety of anisotropic nanostructures.

The identity of the central particle (*F5* or *M5*) of the trimer controlled the structural anisotropy of the self-assembly. The circularity gradually increased in the following order: *M5-M5-F5* < *F5-M5-F5* < *F5-F5-M5* < *M5-F5-M5*. The circularity values for the trimers having the central *F5* were larger than those having the central *M5*. Figure 2.17 shows the relationship between the particle density and the circularity. The particle density for the assemblies of the trimers having the central *F* (*M5-F5-M5* and *F5-F5-M5*) with the side-by-side structure was as dense as that for the random assemblies of *F5-F5-F5*s, irrespective of the circularity value. In contrast, the particle density for those having the central *M5* (*F5-M5-F5* and *M5-M5-F5*) was augmented with increasing circularity. Therefore, the identity of the central particle determined the orientation of the trimer and the particle density. The importance of the central particle was presumably due to the fact that the mobility of the central particle was more restricted than that of the peripheral ones. For example, two *F5-M5-F5*s assembled into the end-to-end structure rather than the side-by-side structure. The side-by-side configuration made by attraction between the

peripheral *F5* particles should compel the central *M5* particles to exist in close proximity, thereby inducing the repulsion to impose substantial thermodynamic penalties to self-assembly. On the other hand, two *M5*-*F5*-*M5*s were able to assemble into the side-by-side structure, because the repulsion between the peripheral *M5* particles placed opposite to each other was avoidable due to greater flexibility.

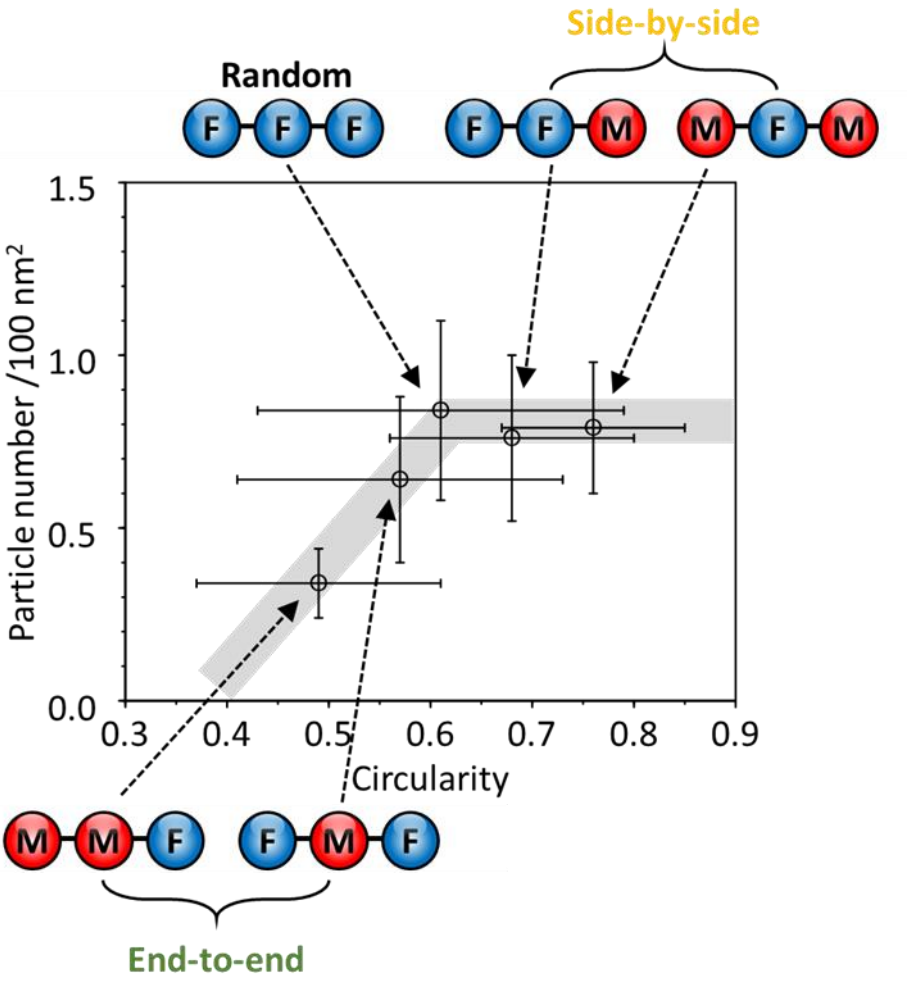

Figure 2.17 Relationship between the particle number per 100 nm^2 and the circularity for the AuNP trimer assemblies. The data shown in Figures 2.12, 2.13, and 2.16 are used. Gray bands are drawn as a guide to the eye.

2.4.4 Self-Assembly of Differently Sized Trimers

Based on this consideration, the author next synthesized the ssDNA–AuNP trimer consisting of a central large AuNP and peripheral small AuNPs (*T5-A15-T5*) (Figure 2.5b). Then, complementary DNA was added to prepare *F5-M15-F5* and *M5-F15-M5* (Figure 2.18a). TEM observation revealed that two *F5-M15-F5*s self-assembled into an anisotropic structure, which had the *F5* particle(s) between two *M15* particles (Figures 2.18b and 2.19). This structure is termed Interior. On the other hand, two *M5-F15-M5*s assembled into the inverted structure that contained the *F15* particles surrounded by the *M5* particles (Figures 2.18c and 2.20). The structure is referred to as Exterior. The guidelines for the classification of the TEM images into Interior and Exterior are described in Figure 2.21. Interior and Exterior were morphologically analogous to the end-to-end and side-by-side assembly, respectively. Interior essentially corresponded to the cyclic version of the end-to-end assembly (Figure 2.9a), whereas about 30% of Interior partially exhibited the linear end-to-end-like structure (Figure 2.19b).

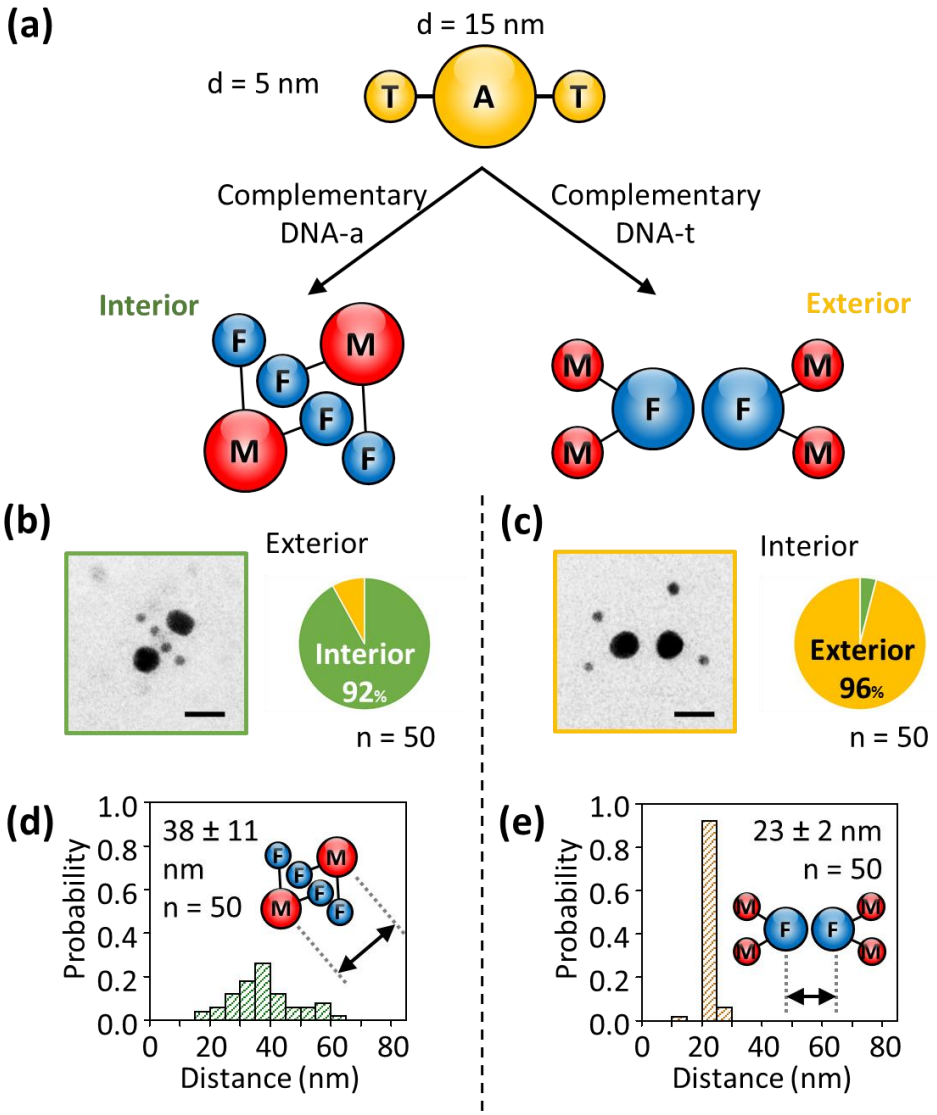

Figure 2.18 Directed assembly of trimers of dsDNA–AuNPs with a different diameter (*T5-A15-T5*). (a) Schematics for preparation of *F5-M15-F5* and *M5-F15-M5* for the assembly having 5 nm AuNPs between 15 nm AuNPs (Interior) and the assembly having 5 nm AuNPs around the 15 nm AuNPs (Exterior), respectively. (b, c) The representative TEM images of the assembly of *F5-M15-F5*s (b) and *M5-F15-M5*s (c). Scale bars are 20 nm. The number ratio of Interior and Exterior is also depicted. (d, e) Distributions of the center-to-center interparticle distance between the central 15 nm AuNPs for the assembly of *F5-M15-F5*s (d) and *M5-F15-M5*s (e).

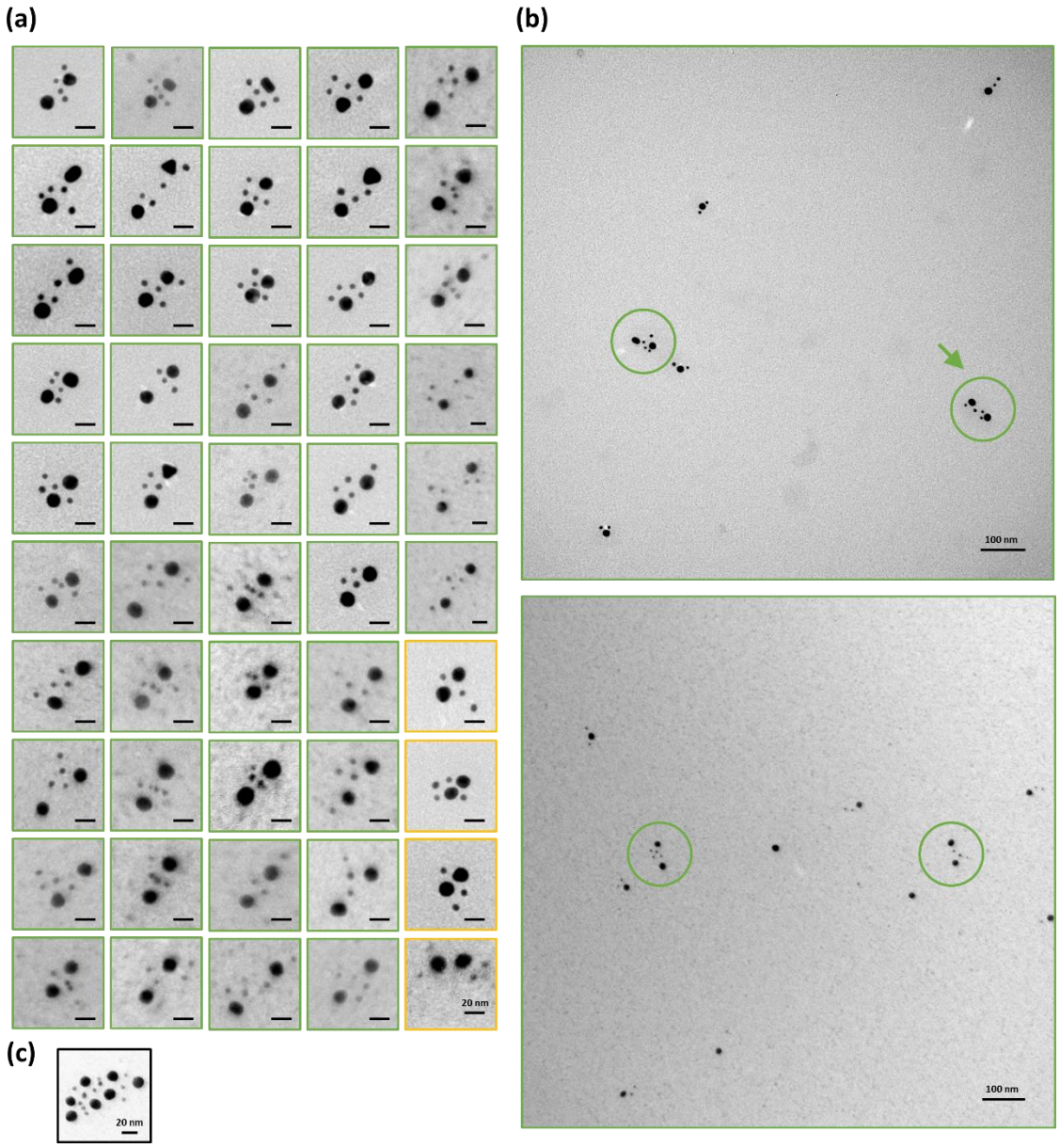

Figure 2.19 (a) All TEM images for Interior of *F5-M15-F5*s with a green frame. Four images for the unexpected Exterior are also depicted with a yellow frame. (b) Representative field-of-view TEM images for Interior of *F5-M15-F5*s. The Interior highlighted with a green arrow exhibited a partially linear end-to-end-like structure. (c) Representative TEM image for the minor oligomeric Interior-like assembly, which was excluded from the current analysis.

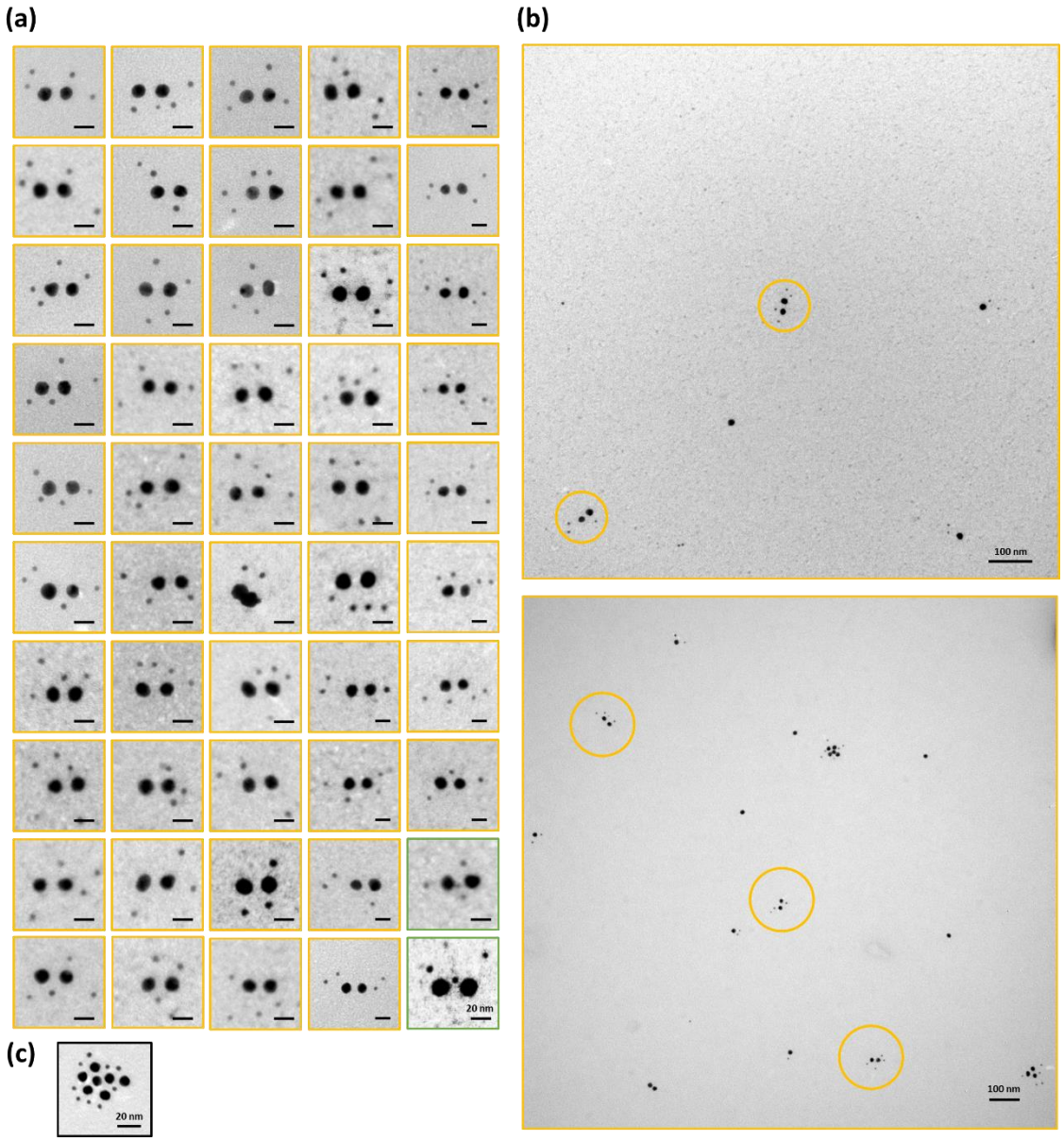

Figure 2.20 (a) All TEM images for Exterior of *M5-F15-M5*s with a yellow frame. Two images for the unexpected Interior are also depicted with a green frame. (b) Representative field-of-view TEM images for Exterior of *M5-F15-M5*s. (c) Representative TEM image for the minor oligomeric Exterior-like assembly, which was excluded from the current analysis.

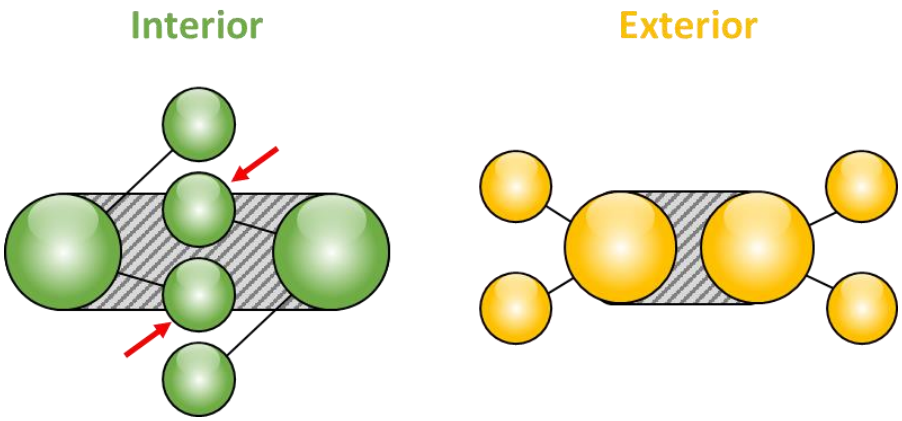

Figure 2.21 The guidelines for the classification of the TEM images into Interior and Exterior. (i) The assemblies perfectly composed of 6 AuNPs, along with those having two 15 nm AuNPs and three 5 nm AuNPs (namely, only one 5 nm AuNP dissociated), were used for the image analysis. (ii) The assemblies having at least one 5 nm AuNP (red arrows) in the grey area between the two 15 nm AuNPs were classified into Interior. (iii) The assemblies having no 5 nm AuNPs in the grey area were classified into Exterior.

TEM statistical analysis revealed that the number ratio of Interior of *F5-M15-F5*s and Exterior of *M5-F15-M5*s was extremely high (Figure 2.18b, c). A distinct difference in size between *F* and *M* for *F5-M15-F5* and *M5-F15-M5* enabled one to unambiguously discriminate between Interior and Exterior and thus perform detailed image analysis. Specifically, the attention was focused on the interparticle center-to-center distance between the central 15 nm AuNPs. It was found that the distance for Interior (Figure 2.18d) was 1.7 times longer than that for Exterior (Figure 2.18e). Further, it was confirmed that the observed value for Exterior (23 nm) was almost the same as the calculated one (25.9 nm) by using the contour length of the 16-base-pair-long B-form dsDNA and the AuNP diameter (Figure 2.22). The result was in line with the working hypothesis that the non-crosslinking assembly of the AuNP trimers was induced by the blunt-end stacking between the terminal base pairs of the surface-grafted dsDNA.[22,23]

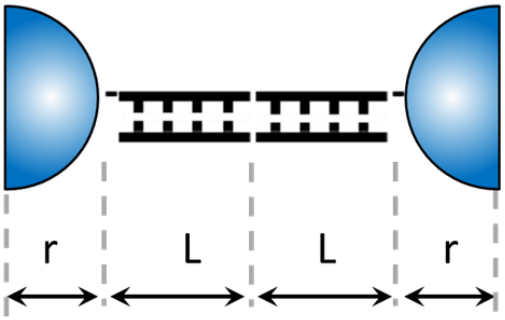

Figure 2.22 Schematic illustration for calculating the interparticle center-to-center distance between the central 15 nm AuNPs of Exterior. The contour length of B-form dsDNA (0.34 nm per 1 base pair, L = 5.44 nm) and a nominal diameter (2r = 15 nm) are used. For clarity, four peripheral 5 nm AuNPs are omitted from the schematic.

Finally, the author attempted to address the question as to whether the evaporation of the samples was required to produce the difference of the interparticle distance between the central 15 nm AuNPs for the *F5-M15-F5* assemblies and the *M5-F15-M5* assemblies. For this purpose, the surface plasmon scattering measurement was carried out without the sample drying under a dark-field microscope (Figures 2.23 and 2.24).[32,33] However, it was practically impossible to control the number of the trimers that composed the assembly in solution. It should be noted that the assembling number of the trimers in solution at high ionic strength for the dark-field microscopy was probably larger than that in the dried sample for the TEM analysis. Only the scattering light by large 15 nm AuNPs involved in the individual trimers and the trimer assemblies was detectable, owing to the limited sensitivity of the current system. Therefore, the author performed the surface plasmon scattering measurement in order to test the hypothesis that the plasmon coupling among the 15 nm AuNPs involved in the trimer assemblies in solution varied according to the type of the terminal nucleobase of the complementary DNA.

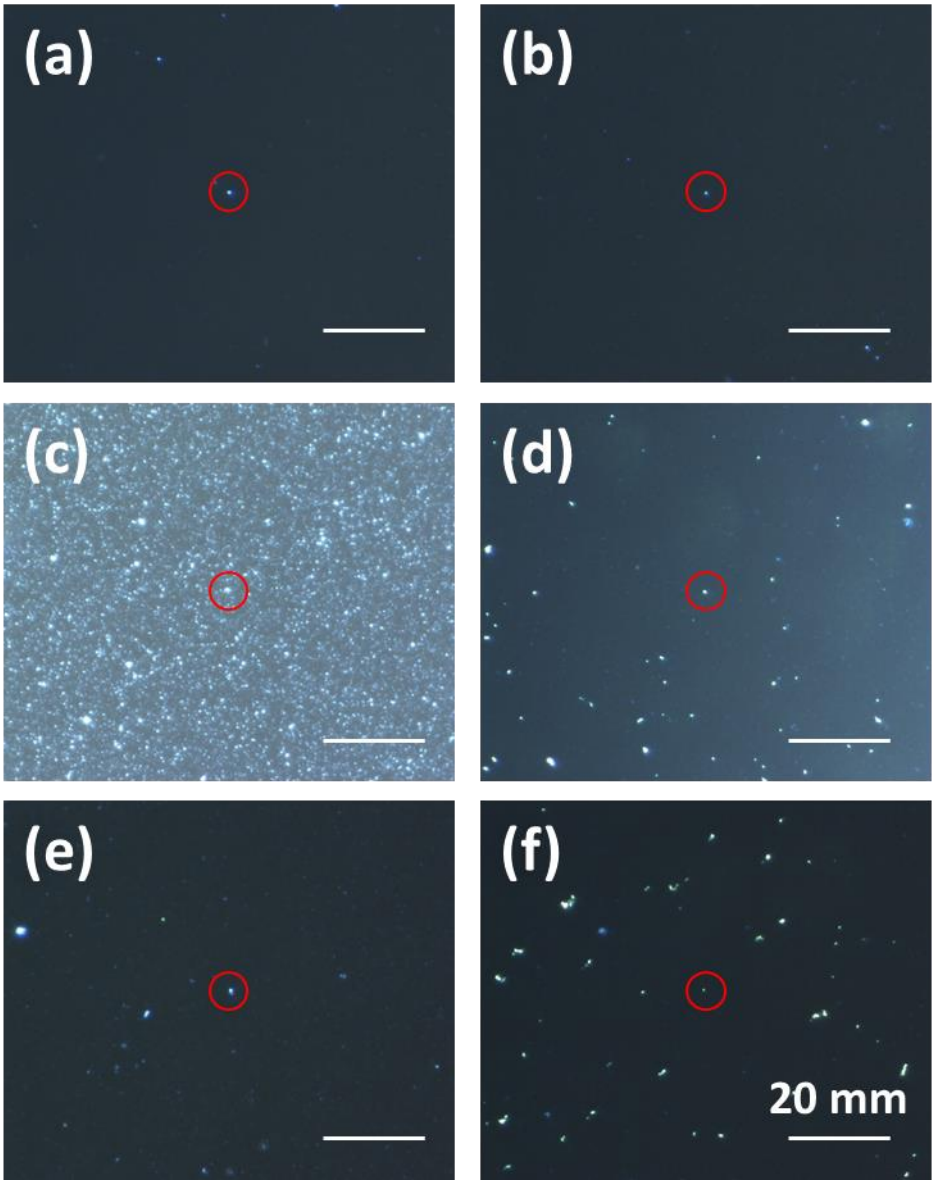

Figure 2.23 Representative dark-field scattering images for (a) *F5-M15-F5* with 0.2 M NaCl and (c) 1.5 M NaCl, (b) *M5-F15-M5* with 0.2 M NaCl and (d) 1.5 M NaCl, (e) *M15* with 1.5 M NaCl, and (f) *F15* with 1.5 M NaCl. The spots highlighted with a red circle were used to obtain the scattering spectra.

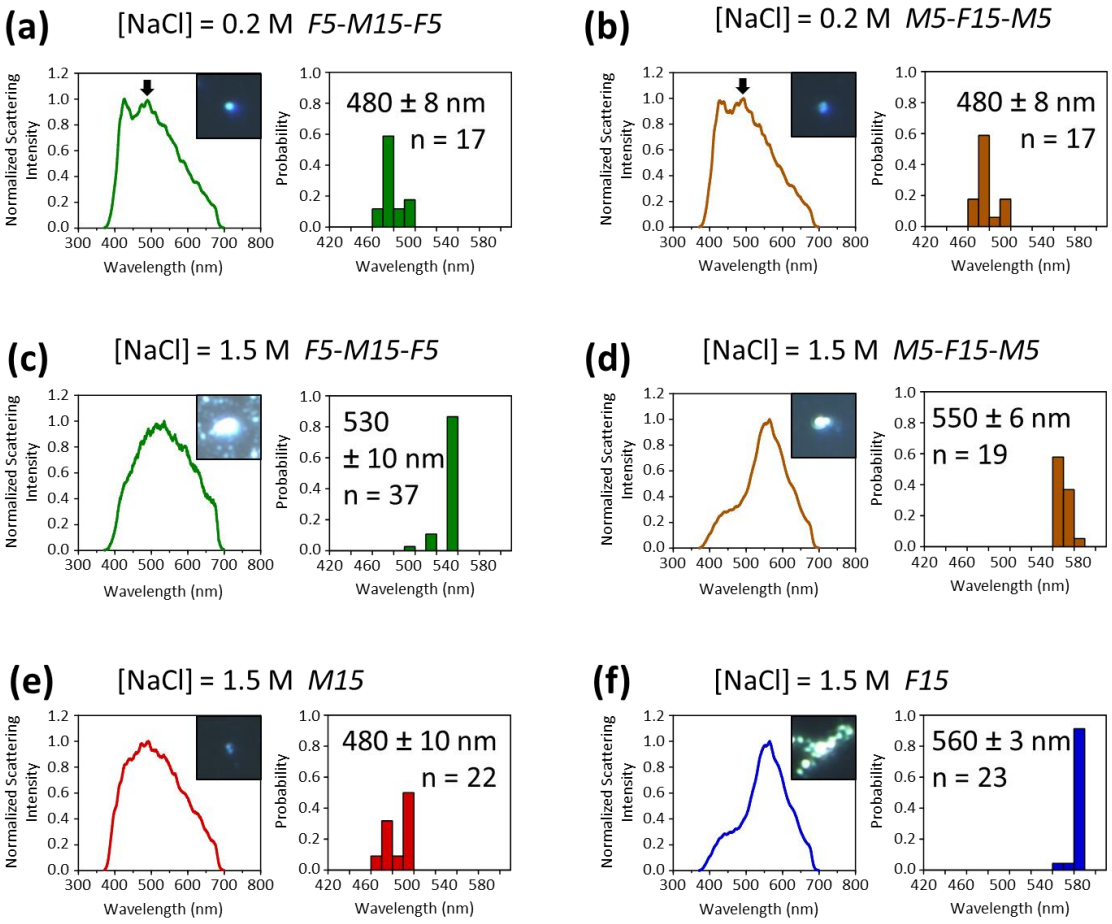

Figure 2.24 Dark-field scattering image analysis for (a) *F5-M15-F5* with 0.2 M NaCl and (c)1.5 M NaCl, (b) *M5-F15-M5* with 0.2 M NaCl and (d) 1.5 M NaCl, (e) *M15* with 1.5 M NaCl, and (f) *F15* with 1.5 M NaCl. Each panel is composed of two parts: a representative scattering spectrum (left), and a histogram of the plasmon resonance wavelength (right).

First, the NaCl concentration of the sample solutions was selected as 0.2 M. No remarkable difference was found between the spectra of *F5-M15-F5* and *M5-F15-M5* (Figure 2.24a, b). This result strongly suggested that their isolated states were almost identical. Next, the NaCl concentration was increased to 1.5 M to induce the non-crosslinking assembly. The author expected that *F5-M15-F5*s and *M5-F15-M5*s self-assembled into an oligomeric Interior-like structure as shown in Figure 2.19c and an oligomeric Exterior-like structure as shown in Figure 2.20c, respectively. For comparison, the scattering lights from the *F15* and *M15* particles alone were measured. The free *F15* particles were expected to form random assemblies in a non-crosslinking manner, while the free *M15* particles were expected to disperse stably. The scattering spectra were collected for the samples (Figure 2.24c–f), which were ordered according to the average resonance wavelength: *M15* < *F5-M15-F5* < *M5-F15*-M5 < *F15*. This result agreed with the TEM data, indicating that the distance between the central 15 nm AuNPs of Exterior was shorter than that of Interior (Figure 2.18d, e). It is thus strongly suggested that the sample drying was not responsible to make the difference in shape between the assemblies, which was indeed caused by the terminal single-base difference of the cover DNA.

2.5 Conclusions

In this chapter, the programmable anisotropic self-assemblies were constructed from trimers composed of two types of isotropic dsDNA–AuNP (*F* and *M*) that exhibited remarkably different colloidal stabilities caused by single-base difference. The observed anisotropic structures were simply deduced from the rule that an interparticle attractive force emerged only between the *F* particles, whereas no attraction occurred between the *M* particles, as well as between the *F* and *M* particles.[22,23] This rule was in line with the working hypothesis that interparticle attraction in the non-crosslinking assembly of dsDNA–AuNPs arose from the blunt-end stacking. The anisotropy was achieved by connecting different colloids in a strictly defined order by exploiting DNA hybridization. This modularity may potentially be harnessed to design and fabrication of a wide variety of anisotropic nanostructures. Furthermore, it would be of fundamental interest to explore similarities in behavior among the present metallic nanoparticle oligomers, amphiphilic small organic molecules, amphiphilic copolymers, and colloidal surfactants.[5,34] The increasing particle number and enhancing sequence diversity in the present particle chains could allow one to obtain various assemblies. Such an attempt would be promising for prospective use of the current methodology in the fabrication of functional materials, such as stimulus-responsive materials and optical devices.

2.6 References

1) Yu, L.; Shiraishi, S.; Wang, G.; Akiyama, Y.; Takarada, T.; Maeda, M. Connecting Nanoparticles with Different Colloidal Stability by DNA for Programmed Anisotropic Self-Assembly. *J. Phys. Chem. C.* **2019**, *123*, 15293–15300.

2) Jung, C. W.; Jalani, G.; Ko, J.; Choo, J.; Lim, D. W. Synthesis, Characterization, and Directional Binding of Anisotropic Biohybrid Microparticles for Multiplexed Biosensing. *Macromol. Rapid Commun.* **2014**, *35*, 56–65.

3) Yoshida, M.; Roh, K. H.; Mandal, S.; Bhaskar, S.; Lim, D.; Nandivada, H.; Deng, X.; Lahann, J. Structurally Controlled Bio-Hybrid Materials Based on Unidirectional Association of Anisotropic Microparticles with Human Endothelial Cells. *Adv. Mater.* **2009**, *21*, 4920–4925.

4) Nisisako, T.; Torii, T.; Takahashi, T.; Takizawa, Y. Synthesis of Monodisperse Bicolored Janus Particles with Electrical Anisotropy Using a Microfluidic Co-Flow System. *Adv. Mater.* **2006**, *18*, 1152–1156.

5) Kim, J.-W.; Lee, D.; Shum, H. C.; Weitz, D. A. Colloid Surfactants for Emulsion Stabilization. *Adv. Mater.* **2008**, *20*, 3239–3243.

6) Boles, M. A.; Engel, M.; Talapin, D. V. Self-Assembly of Colloidal Nanocrystals: From Intricate Structures to Functional Materials. *Chem. Rev.* **2016**, *116*, 11220–11289.

7) Du, J.; O′Reilly, R. K. Anisotropic Particles with Patchy, Multicompartment and Janus Architectures: Preparation and Application. *Chem. Soc. Rev.* **2011**, *40*, 2402–2416.

8) Zhang, K.; Jiang, M.; Chen, D. Self-Assembly of Particles—The Regulatory Role of Particle Flexibility. *Prog. Polym. Sci.* **2012**, *37*, 445–486.

9) Jiang, S.; Chen, Q.; Tripathy, M.; Luijten, E.; Schweizer, K. S.; Granick, S. Janus Particle Synthesis and Assembly. *Adv. Mater.* **2010**, *22*, 1060–1071.

10) Pang, X.; Wan, C.; Wang, M.; Lin, Z. Strictly Biphasic Soft and Hard Janus Structures: Synthesis, Properties, and Applications. *Angew. Chem., Int. Ed.* **2014**, *53*, 5524–5538.

11) Xu, X.; Rosi, N. L.; Wang, Y.; Huo, F.; Mirkin, C. A. Asymmetric Functionalization of Gold Nanoparticles with Oligonucleotides. *J. Am. Chem. Soc.* **2006**, *128*, 9286–9287.

12) Suzuki, K.; Hosokawa, K.; Maeda, M. Controlling the Number and Positions of Oligonucleotides on Gold Nanoparticle Surfaces. *J. Am. Chem. Soc.* **2009**, *131*, 7518–7519.

13) Maye, M. M.; Nykypanchuk, D.; Cuisinier, M.; van der Lelie, D.; Gang, O. Stepwise Surface Encoding for High-Throughput Assembly of Nanoclusters. *Nat. Mater.* **2009**, *8*, 388–391.

14) Li, Z.; Cheng, E.; Huang, W.; Zhang, T.; Yang, Z.; Liu, D.; Tang, Z. Improving the Yield of Mono-DNA-Functionalized Gold Nanoparticles through Dual Steric Hindrance. *J. Am. Chem. Soc*. **2011**, *133*, 15284–15287.

15) Zhang, T.; Dong, Y.; Sun, Y.; Chen, P.; Yang, Y.; Zhou, C.; Xu, L.; Yang, Z.; Liu, D. DNA Bimodified Gold Nanoparticles. *Langmuir* **2012**, *28*, 1966–1970.

16) Tan, L. H.; Xing, H.; Chen, H.; Lu, Y. Facile and Efficient Preparation of Anisotropic DNA-Functionalized Gold Nanoparticles and Their Regioselective Assembly. *J. Am. Chem. Soc*. **2013**, *135*, 17675–17678.

17) Edwardson, T. G. W.; Lau, K. L.; Bousmail, D.; Serpell, C. J.; Sleiman, H. F. Transfer of Molecular Recognition Information from DNA Nanostructures to Gold Nanoparticles. *Nat. Chem.* **2016**, *8*, 162–170.

18) Zhu, G.; Xu, Z.; Yang, Y.; Dai, X.; Yan, L.-T. Hierarchical Crystals Formed from DNA-Functionalized Janus Nanoparticles. *ACS Nano* **2018**, *12*, 9467–9475.

19) Chen, G.; Gibson, K. J.; Liu, D.; Rees, H. C.; Lee, J.-H.; Xia, W.; Lin, R.; Xin, H. L.; Gang, O.; Weizmann, Y. Regioselective Surface Encoding of Nanoparticles for Programmable Self-Assembly. *Nat. Mater.* **2019**, *18*, 169–174.

20) Sato, K.; Hosokawa, K.; Maeda, M. Rapid Aggregation of Gold Nanoparticles Induced by Non-Cross-Linking DNA Hybridization. *J. Am. Chem. Soc.* **2003**, *125*, 8102–8103.

21) Akiyama, Y.; Shikagawa, H.; Kanayama, N.; Takarada, T.; Maeda, M. DNA Dangling-End-Induced Colloidal Stabilization of Gold Nanoparticles for Colorimetric Single-Nucleotide Polymorphism Genotyping. *Chem. - Eur. J.* **2014**, *20*, 17420–17425.

22) Kanayama, N.; Sekine, T.; Ozasa, K.; Kishi, S.; Nyu, T.; Hayashi, T.; Maeda, M. Terminal-Specific Interaction between Double-Stranded DNA Layers: Colloidal Dispersion Behavior and Surface Force. *Langmuir* **2016**, *32*, 13296–13304.

23) Sekine, T.; Kanayama, N.; Ozasa, K.; Nyu, T.; Hayashi, T.; Maeda, M. Stochastic Binding Process of Blunt-End Stacking of DNA Molecules Observed by Atomic Force Microscopy. *Langmuir* **2018**, *34*, 15078–15083.

24) Akiyama, Y.; Shikagawa, H.; Kanayama, N.; Takarada, T.; Maeda, M., Modulation of Interparticle Distance in Discrete Gold Nanoparticle Dimers and Trimers by DNA Single-Base Pairing. *Small* **2015**, *11*, 3153–3161.

25) Wang, G.; Yu, L.; Akiyama, Y.; Takarada, T.; Maeda, M. Reversible Shrinkage of DNA-Functionalized Gold Nanoparticle Assemblies Revealed by Surface Plasmon Resonance. *Biotechnol. J.* **2018**, *13*, e1800090.

26) Shiraishi, S.; Yu, L.; Akiyama, Y.; Wang, G.; Kikitsu, T.; Miyamura, K.; Takarada, T.; Maeda, M. Folding of Nanoparticle Chains into 2D Arrays: Structural Change of DNA-Functionalized Gold Nanoparticle Assemblies. *Adv. Mater. Interfaces* **2018**, *5*, 1800189.

27) Mirkin, C. A.; Letsinger, R. L.; Mucic, R. C.; Storhoff, J. J. A DNA-Based Method for Rationally Assembling Nanoparticles into Macroscopic Materials. *Nature* **1996**, *382*, 607-609.

28) Alivisatos, A. P.; Johnsson, K. P.; Peng, X.; Wilson, T. E.; Loweth, C. J.; Bruchez Jr, M. P.; Schultz, P. G. Organization of 'Nanocrystal Molecules' Using DNA. *Nature* **1996**, *382*, 609–611.

29) Sato, K.; Hosokawa, K.; Maeda, M. Non-Cross-Linking Gold Nanoparticle Aggregation as a Detection Method for Single-Base Substitutions. *Nucleic Acids Res.* **2005**, *33*, e4.

30) Ferreira, T.; Rasband, W. *Image J. User Guide*. *IJ. 1.46r*; Natl. Inst. Health: Bethesda, MD, 2012.

31) Wang, G.; Akiyama, Y.; Kanayama, N.; Takarada, T.; Maeda, M. Directed Assembly of Gold Nanorods by Terminal-Base Pairing of Surface-Grafted DNA. *Small* **2017**, *13*, 1702137.

32) Bu, T.; Zako, T.; Fujita, M.; Maeda, M. Detection of DNA Induced Gold Nanoparticle Aggregation with Dark Field Imaging. *Chem. Commun.* **2013**, *49*, 7531–7533.

33) Wang, G.; Bu, T.; Zako, T.; Watanabe-Tamaki, R.; Tanaka, T.; Maeda, M. Dark Field Microscopic Analysis of Discrete Au Nanostructures: Understanding the Correlation of Scattering with Stoichiometry. *Chem. Phys. Lett.* **2017**, *684*, 310–315.

34) Chen, D.; Amstad, E.; Zhao, C.-X.; Cai, L.; Fan, J.; Chen, Q.; Hai, M.; Koehler, S.; Zhang, H.; Liang, F.; Yang, Z.; Weitz, D. A. Biocompatible Amphiphilic Hydrogel–Solid Dimer Particles as Colloidal Surfactants. *ACS Nano* **2017**, *11*, 11978–11985.

Chapter 3

DNA-Guided Formation of 2D AuNP Arrays

3.1 Abstract

Nanoparticle arrays exhibit collective physical and chemical properties, which are potentially applicable to various nanodevices, such as data storage media and biosensors. This chapter described a spontaneous method of constructing 2D nanoparticle arrays from precursory 1D chains of DNA-modified nanoparticles.[1] The single-stranded DNA-modified gold nanoparticles were hybridized to a long repetitive single-stranded DNA synthesized with rolling circle amplification to produce the precursory nanoparticle chains. Transmission electron microscopy revealed that the chains of fully matched double-stranded DNA-modified gold nanoparticles underwent shrinkage and folding during evaporation to afford the 2D nanoparticle arrays. By contrast, the terminal-mismatched double-stranded DNA-modified gold nanoparticle chains maintained the linear shape. Noticeably, the chains of long double-stranded DNA-modified gold nanoparticles with short interparticle spacing formed the nanoparticle arrays with anisotropic interparticle spacing. The present approach could be useful for readily aligning nanoparticles on the substrate surface.

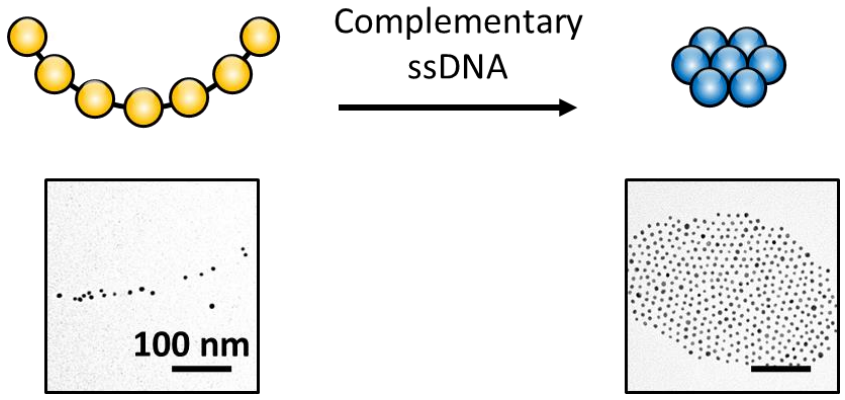

3.2 Introduction

Ordered assemblies of metal nanoparticles (NPs) exhibit collective physical and chemical properties, which are different from those of individual NPs and bulk materials. Various 1D, 2D and 3D NP assemblies have been built with an eye toward practical application.[2–7] To prepare well-defined NP assemblies, Watson–Crick base pairing in nucleic acids is extremely helpful.[8–13] For example, hybridization of NPs modified with single-stranded DNA (ssDNA–NPs) to a long repetitive ssDNA, which is synthesized using rolling circle amplification (RCA), readily affords 1D chains.[14–21] As for 2D assemblies, the preceding works have exploited crystallization of ssDNA–NPs,[22,23] self-organization at air-liquid interfaces[24,25] or supported lipid bilayers,[26,27] linkage through duplex formation,[28–33] and deposition at DNA origami nanostructures.[34–42] In general, 2D NP arrays have been applied to various nanodevices, including data storage media, solar cells and biosensors, all of which generally require a simpler production process.

Chapter 3 describes a method of constructing 2D NP arrays from precursory 1D chains of ssDNA–AuNPs.[1] The structural change was induced by spontaneous assembling behaviour of fully matched double-stranded (ds) DNA–AuNPs in a non-crosslinking manner.[43,44] As expected, no structural change took place when the dsDNA–AuNPs had terminal mismatches. The ssDNA–AuNPs were able to stably disperse even at high ionic strength, due to electrostatic and steric repulsion caused by surface-grafted ssDNAs. However, when complementary ssDNA was added to form a duplex on the AuNP surface, the resultant dsDNA–AuNPs were rapidly aggregated. By contrast, the dsDNA–AuNPs having a single-base mismatch[43,44] or a single-base overhang[45,46] at the outermost surface were stably dispersed under the same conditions. In general, the

colloidal stability is determined by the balance between the interparticle attractive and repulsive forces. In this case, the attraction could originate from terminal π–π stacking interaction.[47,48] The emergence of this force between dsDNA termini was reported for various molecular assemblies, such as DNA liquid crystals[49] and DNA origami nanostructures.[50] On the other hand, the repulsion could occur due to micro-Brownian fraying motion of unpaired terminal nucleobases.[51–53] This motion is referred to as terminal "breathing," which is a transient and local fluctuation induced by reversible breaking of hydrogen bonds and base stacking.[54]

A previous study demonstrated that non-crosslinked aggregates of dsDNA–AuNPs exhibited lower thermodynamic stability than the crosslinked aggregates; however, the rate of non-crosslinking aggregation was faster than the crosslinking counterpart under optimal conditions.[55] More importantly, non-crosslinking aggregation exhibits an outstanding sensitivity to a single-base difference. Therefore, the author herein adopt a strategy of preparing a precursory AuNP chain in a crosslinking manner and then inducing its structural change in a non-crosslinking fashion.[56]

3.3 Experimental Section

3.3.1 General

All reagents were purchased from Wako Pure Chemical unless otherwise specified. Citric acid-coated AuNPs with a nominal diameter of 5 nm and 15 nm were obtained from BBI Solutions. Bis(*p*-sulfonatophenyl)phenylphosphine (BSPP) dihydrate dipotassium salt was purchased from Strem Chemicals. Tris-borate-EDTA (TBE) buffer was obtained from Nippon Gene. Ultra-pure water (>18 MΩ cm) was prepared using a Milli-Q pure

water purification system (Millipore) and was sterilized for all experiments. Agarose (L03) was obtained from Takara Bio. All chemically synthesized DNA strands were purchased from Tsukuba Oligo Service and Eurofins Genomics. The DNA sequences used in this study were as follows.

Anchor DNA (35 nt):

5′-CAGCTCCAACTACCACTTTTCGCAACAATAACTGA-3′-DTT

Extender DNA (94 nt):

5′-GTGGTAGTTGGAGCTG-T_{78}-3′

Remover DNA (94 nt):

5′-A_{78}-CAGCTCCAACTACCAC-3′

Cover DNA-t (16 nt):

5′-TCGCAACAATAACTGA-3′-SH

Complementary DNA-a (16 nt):

5′-TCAGTTATTGTTGCGA-3′

Complementary DNA-t (16 nt):

5′-TCAGTTATTGTTGCGT-3′

Template DNA for RCA (precursory circular DNA, 74 nt):

5′-pCAGCTCCAACTACCAC-A_{52}-GAACAT-3′

Primer DNA for RCA (22 nt):

5′-GTGGTAGTTGGAGCTGATGTTC-3′

Extended complementary DNA (45 nt):

3′-TATGCAGTAGGATCTAATGGCTGGTAACGAGCGTTGTTATTGACT-5′

Auxiliary DNA (29 nt):

5′-ATACGTCATCCTAGATTACCGACCATTGC-3′

Extended complementary DNA (25 nt):

3′-CTGGTAACGAGCGTTGTTATTGACT-5′

Auxiliary DNA (9 nt):

5′-GACCATTGC-3′

3.3.2 Synthesis of ssDNA–AuNP Monomers

The AuNP was functionalized with two kinds of ssDNA (anchor DNA and cover DNA) by using the procedure described in **2.3.2**.[56] Briefly, the AuNP stabilized with BSPP was functionalized with anchor DNA through Au–S bond formation. The anchor-DNA–AuNP was purified by agarose gel electrophoresis. After electrophoretic extraction from the corresponding gel pieces, the anchor-DNA–AuNP was further modified with cover DNA. The average number of cover DNAs on the AuNP surface was determined using the method reported elsewhere.[56]

3.3.3 Synthesis of Template DNA by RCA

The template DNA with a repetitive sequence was synthesized by RCA according to the method described in the literature.[15] To prepare the circular DNA, 0.01 μM template DNA for RCA (74 nt) and 1 μM primer DNA for RCA (22 nt) in 50 mM Tris-HCl buffer (pH 7.5) including 10 mM $MgCl_2$, 10 mM dithiothreitol, and 1 mM ATP was incubated at 65ºC for 5 min, slowly cooled down to 37ºC. After adding T4 DNA ligase (13 U/μL), the reaction solution was further incubated at 25ºC for 90 min. Aliquots of the ligation reaction solutions (20 μL) were used for RCA. The RCA reaction solutions (100 μL) contained 50 mM Tris-HCl, 10 mM $MgCl_2$, 10 mM $(NH_4)_2SO_4$, 4 mM dithiothreitol,

200 μg/mL bovine serum albumin, 6.3 mM dNTP, and 0.1 U/μL ϕ29 DNA polymerase. The RCA reaction solutions were incubated at 30ºC for 3 h, and then inactivated at 65ºC for 10 min.

3.3.4 Construction of Precursory AuNP Chains

A mixture (10 μL) of ssDNA–AuNP (600 nM for 5 nm AuNP or 15 nM for 15 nm AuNP) and the RCA product (2.2 nM for 5 nm AuNP or 56 pM for 15 nm AuNP) was allowed to stand at room temperature overnight before incubation at 60ºC for 10 min. After adding an aqueous solution of NaCl (50 mM and 90 μL), the resultant mixture was centrifuged at 8,000 × *g* for 5 min (5 nm AuNP) or 5,000 rpm for 3 min (15 nm AuNP) at 4ºC, followed by removal of the supernatant (90 μL) and addition of an aqueous solution of NaCl (50 mM and 10 μL). The final concentrations of ssDNA–AuNP (5 or 15 nm), template DNA (the RCA product), and NaCl were 30 nM/110 pM/50 mM (for 5 nm AuNP) or 750 pM/2.8 pM/50 mM (for 15 nm AuNP), respectively.

3.3.5 UV-vis Spectroscopy

A dispersion of the ssDNA–AuNP chain (30 nM of 5 nm AuNP) in Tris-HCl buffer containing 50 mM or 1000 mM NaCl was mixed with an aqueous solution of the 16 nt complementary ssDNA or the terminal-mismatched ssDNA (20 equivalents of the total amount of the surface-grafted ssDNA in the AuNP chain). After incubation at room temperature for 10 min to allow DNA hybridization, an aliquot of this dispersion (198 μL) was added to a 1 mL-tube containing 1% w/v Tween 20 (2 μL). After incubation at room temperature for 30 min, extinction spectra were obtained with a Cary 50 UV-vis spectrophotometer (Varian). The concentration was calculated by Lambert-Beer's Law.

3.3.6 Transmission Electron Microscopy (TEM)

An elastic-carbon-coated copper grid (ELS-C10) from Okenshoji was previously hydrophilized under UV/ozone treatment. A dispersion (2 μL) of the precursory AuNP chain was mixed with complementary DNA and dropped onto the grid. After incubation at room temperature for 1.5 min, an aqueous solution of NaCl (25 mM and 10 μL) was further dropped onto the sample on the grid. The excess solution was removed by blotting with a dry Kim Wipe. Then, the dispersion was dried under a vacuum for 3 min. The measurements were performed on a JEM 1230 TEM (JEOL) operated at an accelerating voltage of 80 kV. The interparticle center-to-center distance between the adjacent AuNPs was evaluated using image analysis software (Particle Analyzer ver. 3.5; NSST).

3.4 Results and Discussion

3.4.1 Design and Preparation of AuNP Chains

An AuNP chain was constructed by hybridizing ssDNA–AuNP to an RCA product (template DNA). Initially, 5 nm AuNPs were modified with 35 nt anchor DNA (precisely one strand per particle), and then with 16 nt cover DNA (approximately 5 strands per particle), according to the reported procedure (Figure 3.1a).[56] Next, a long, repetitive ssDNA consisting of a 16 nt AuNP-binding site and 58 nt spacer was synthesized using RCA (Figure 3.1b). Finally, the anchor DNA of AuNPs was hybridized to the AuNP-binding site of template DNA to yield the AuNP chain (Figure 3.1c). Transmission electron microscopy (TEM) revealed that the AuNPs were linearly aligned (Figure 3.2a). In the absence of template DNA, only isolated AuNPs were observed (Figure 3.3a). 1D chain structure was also observed in an aqueous solution with liquid-phase TEM (Figure

3.4).[57,58]

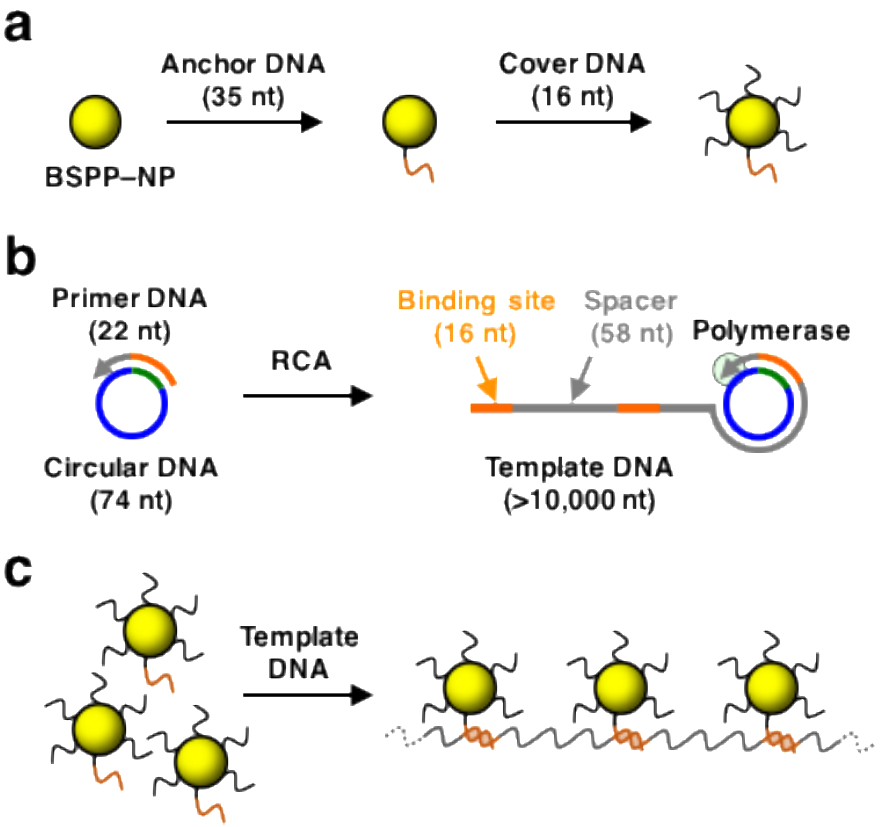

Figure 3.1 Schematics for preparation of precursory 1D chains of ssDNA–AuNPs. (a) Conjugation of anchor DNA and cover DNA to a bis(*p*-sulfonatophenyl)phenylphosphine (BSPP)-stabilized AuNP through Au–S bond formation. (b) Synthesis of a long repetitive ssDNA (template DNA) using RCA. (c) Hybridization of the ssDNA–AuNPs to the template DNA to produce the 1D AuNP chain.

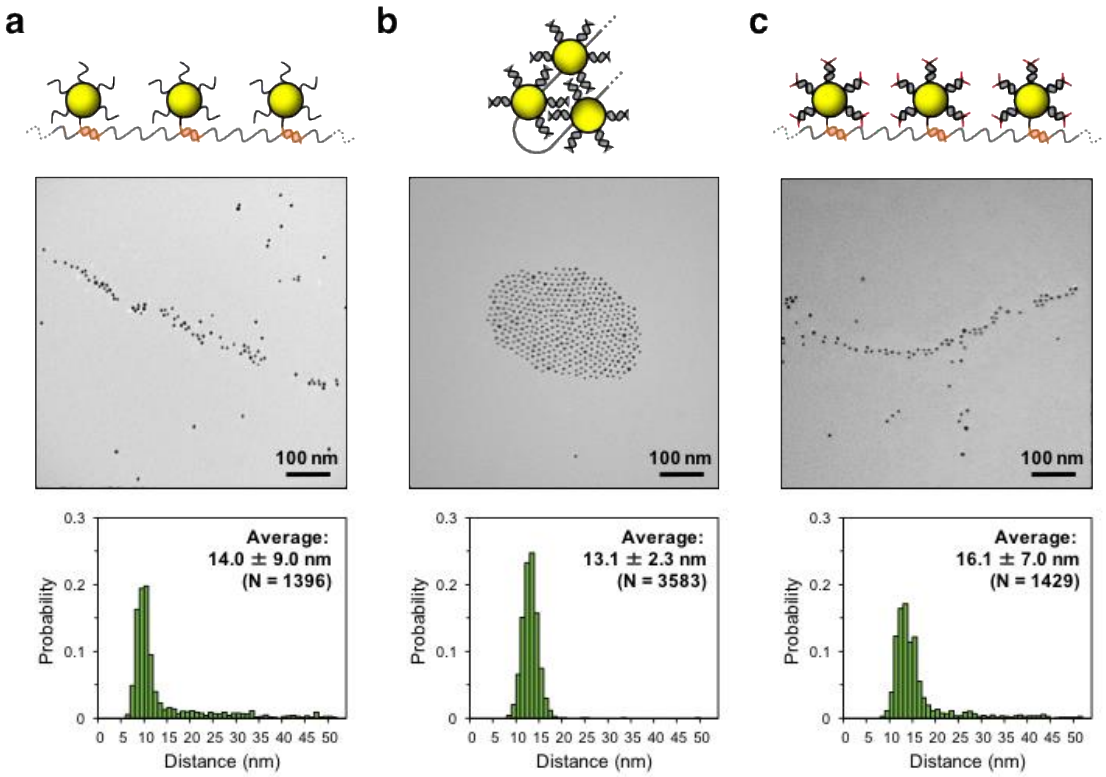

Figure 3.2 Schematics, representative TEM images, and distributions of interparticle center-to-center distances of (a) the ssDNA–AuNP assembly, (b) the fully matched dsDNA–AuNP assembly, and (c) the terminal-mismatched dsDNA–AuNP assembly. AuNPs with a nominal diameter of 5 nm were used.

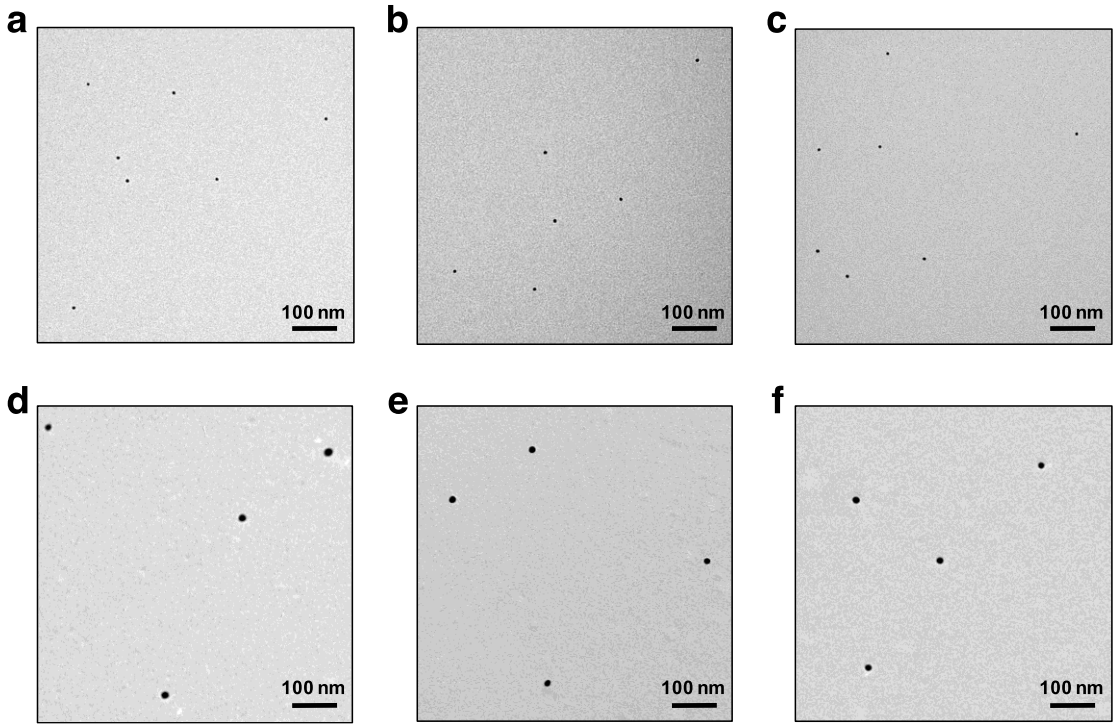

Figure 3.3 Representative TEM images of (a,d) the ssDNA–AuNPs, (b,e) the fully matched dsDNA–AuNPs, and (c,f) the terminal-mismatched dsDNA–AuNPs without the template DNA. AuNPs with a nominal diameter of (a–c) 5 nm or (d–f) 15 nm were used.

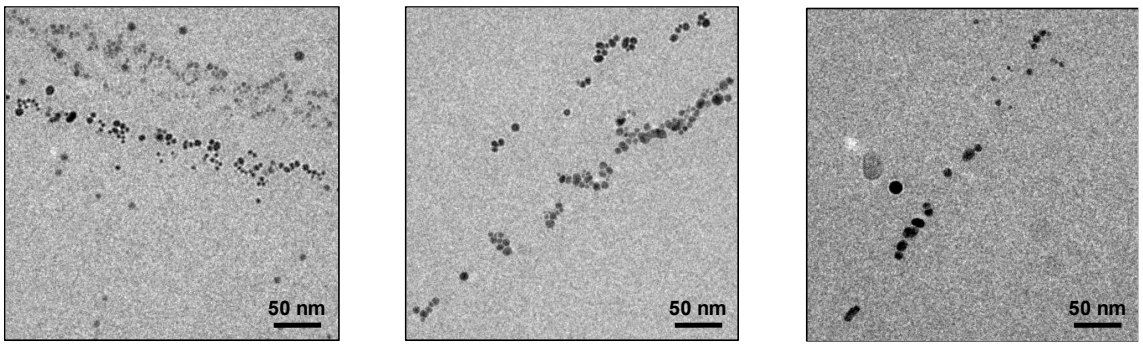

Figure 3.4 Representative liquid-phase TEM images of the ssDNA–AuNP assembly. AuNPs with a nominal diameter of 5 nm were used. Liquid-phase TEM analysis was conducted on a JEM 2100F TEM (JEOL).

Prior to constructing 2D AuNP arrays on a substrate surface, the behavior of the AuNP chains in an aqueous solution at high ionic strength was investigated. dsDNA–AuNP chains were prepared by adding a 16 nt ssDNA complementary to the cover DNA to form a fully matched duplex on the AuNP surface. When the NaCl concentration of the AuNP chain dispersion was increased from 50 mM to 1000 mM, small red-shifting of the surface plasmon band from 515 nm to 528 nm was observed due to the interparticle plasmon coupling (Figure 3.5b). As expected, no shifting was found for the AuNP chain without the complementary ssDNA (Figure 3.5a) or with the terminal-mismatched ssDNA (Figure 3.5c). In addition, no shifting was also achieved for the fully matched dsDNA–AuNPs alone without the template ssDNA under the same conditions (Figure 3.5d), suggesting that the small red-shifting of the dsDNA-AuNP chain was not caused by the non-crosslinking aggregation of free dsDNA-AuNPs that were undesirably involved in the AuNP chain dispersion. These results indicate that the fully matched dsDNA–AuNP chains obviously yet slightly undergo the shrinkage and/or aggregation in aqueous solutions in a non-crosslinking manner.

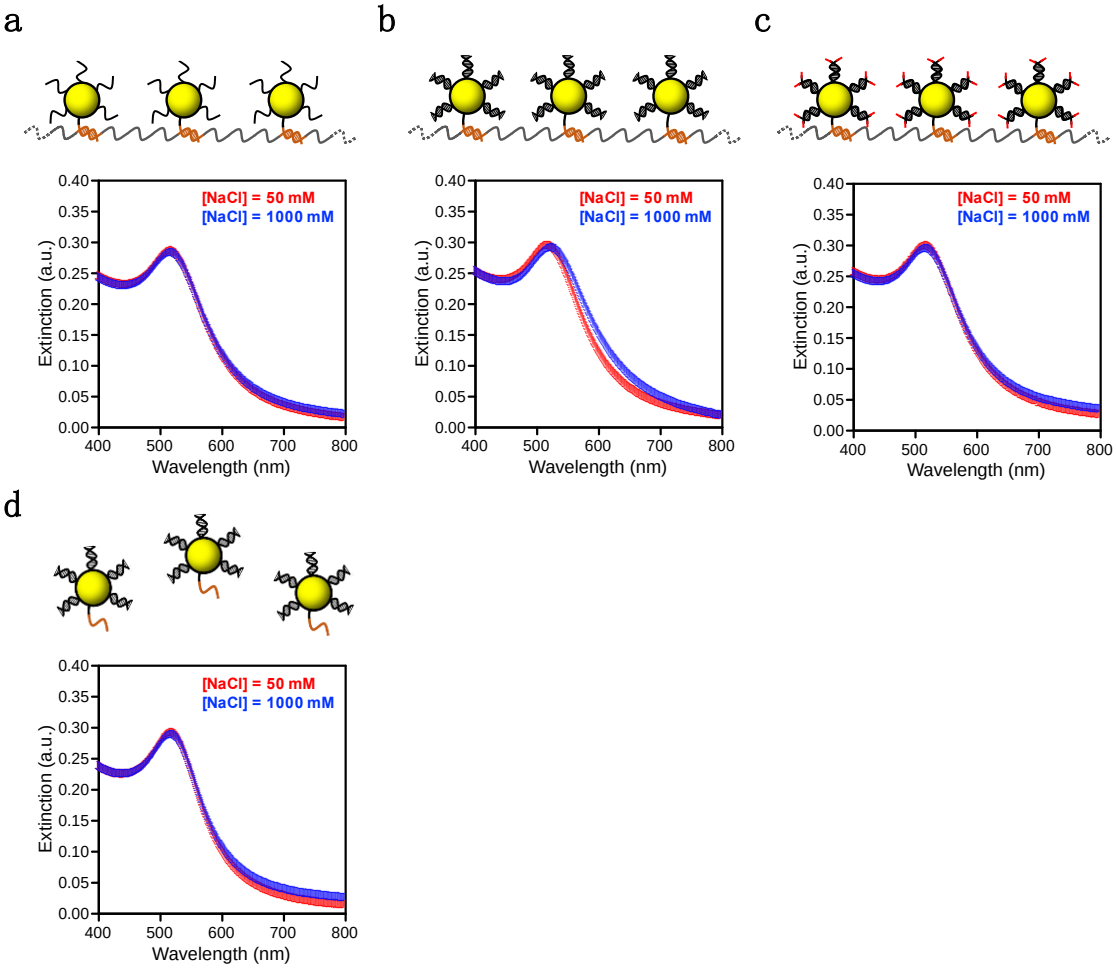

Figure 3.5 Schematics and extinction spectra for (a) the ssDNA–AuNP assembly, (b) the fully matched dsDNA–AuNP assembly, (c) the terminal-mismatched dsDNA–AuNP assembly, and (d) the fully matched dsDNA–AuNPs alone without template ssDNA in the presence of 50 mM (red) or 1000 mM NaCl (blue). AuNPs with a nominal diameter of 5 nm were used.

3.4.2 Structural Changes of AuNP Chains

Then, the author tried to enhance the structural changes of the AuNP chain on a substrate surface by evaporating the disperse medium. When the complementary ssDNA was added to the dispersion of the ssDNA–AuNP chains, TEM observation revealed that the fully matched dsDNA–AuNP chains had shrunk and folded to exhibit an island-like 2D array structure (Figure 3.2b). By sharp contrast, when a terminal-mismatched 16 nt ssDNA was added, the structural change of the terminal-mismatched dsDNA–AuNP chains was strongly inhibited; the 1D chains were still observed (Figure 3.2c). A statistical analysis using several TEM images determined the interparticle center-to-center distance between adjacent AuNPs in the island-like 2D structure to be 13.1 ± 2.3 nm (Figure 3.2b). Both the averaged value and its standard deviation were smaller than those of the precursory AuNP chain (Figure 3.2a) and the terminal-mismatched dsDNA–AuNP chain (Figure 3.2c). Because the persistence length of ssDNA is estimated to be 1.5–3 nm in the presence of 25–2000 mM NaCl,[59] the strain force induced by folding of the template ssDNA could be small enough to afford the AuNP arrays with the interparticle distance of 13 nm. The TEM images also indicated that the single island-like 2D structure was composed of 150 AuNPs on average. Because the single precursory 1D chain consisted of approximately >100 AuNPs, it was suggested that the single island-like 2D arrays were mostly constructed from the single precursory 1D chain. A similar structural change of the 1D chain of ssDNA–AuNPs with a nominal diameter of 15 nm was also confirmed (Figure 3.6).

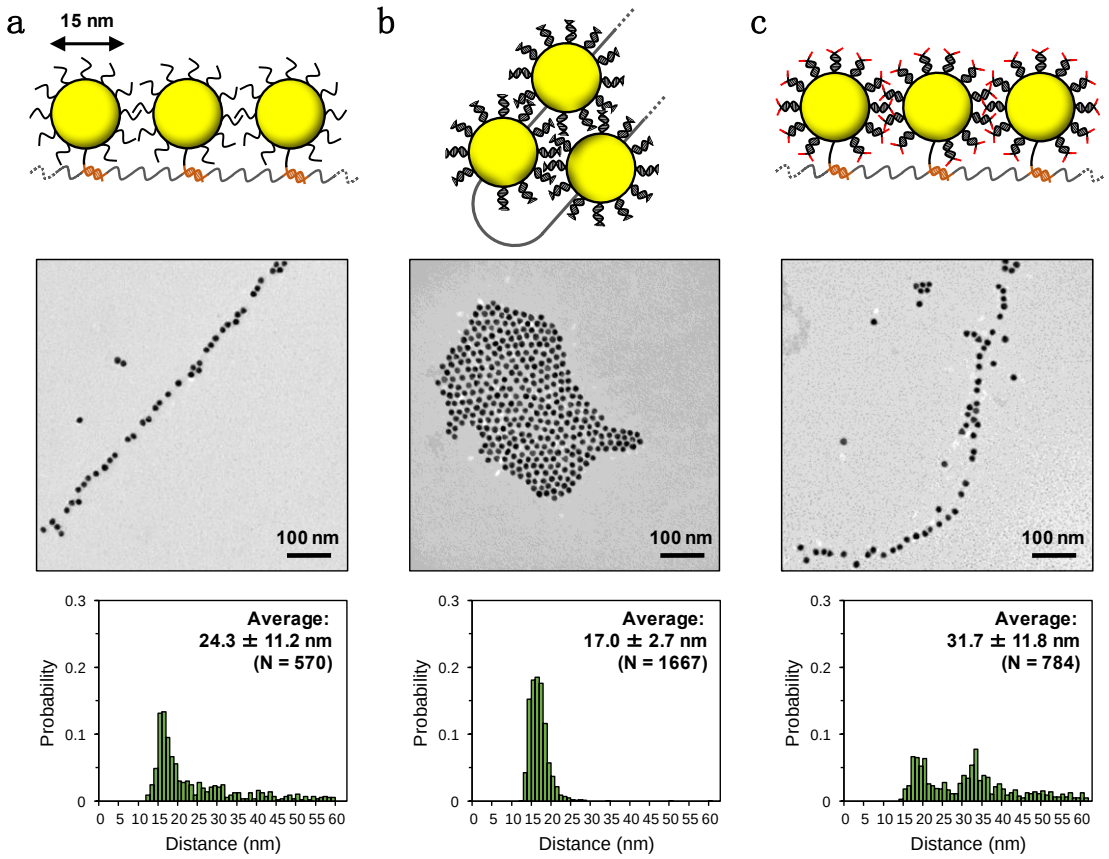

Figure 3.6 Schematics, representative TEM images, and distributions of interparticle center-to-center distances of (a) the ssDNA–AuNP assembly, (b) the fully matched dsDNA–AuNP assembly, and (c) the terminal-mismatched dsDNA–AuNP assembly. AuNPs with a nominal diameter of 15 nm were used.

3.4.3 Proposed Mechanism for Structural Change

Figure 3.7a shows the proposed mechanism for formation of the island-like monolayer 2D structure. Initially, the sample solution is concentrated by evaporation of the disperse medium (water), which is accompanied by an increase of the ionic strength. Subsequently, the precursory 1D AuNP chains, which disperse in an aqueous buffer solution, are accumulated at air-liquid interface to form a monolayer.[23] The non-crosslinking aggregation is then induced among the fully matched dsDNA–AuNPs

involved in the chains. Both the terminal π–π stacking interaction and the capillary force emerging during the evaporation give rise to the shrinkage and folding of the AuNP chain on the TEM grid, thereby producing the island-like 2D AuNP array. By contrast, the interparticle repulsion caused by the fraying motion of the unpaired nucleobases of the terminal-mismatched dsDNA–AuNPs strongly inhibit the shrinkage and folding (Figure 3.7b). As a result, the 1D chain structure is observed for the terminal-mismatched dsDNA–AuNP assembly.

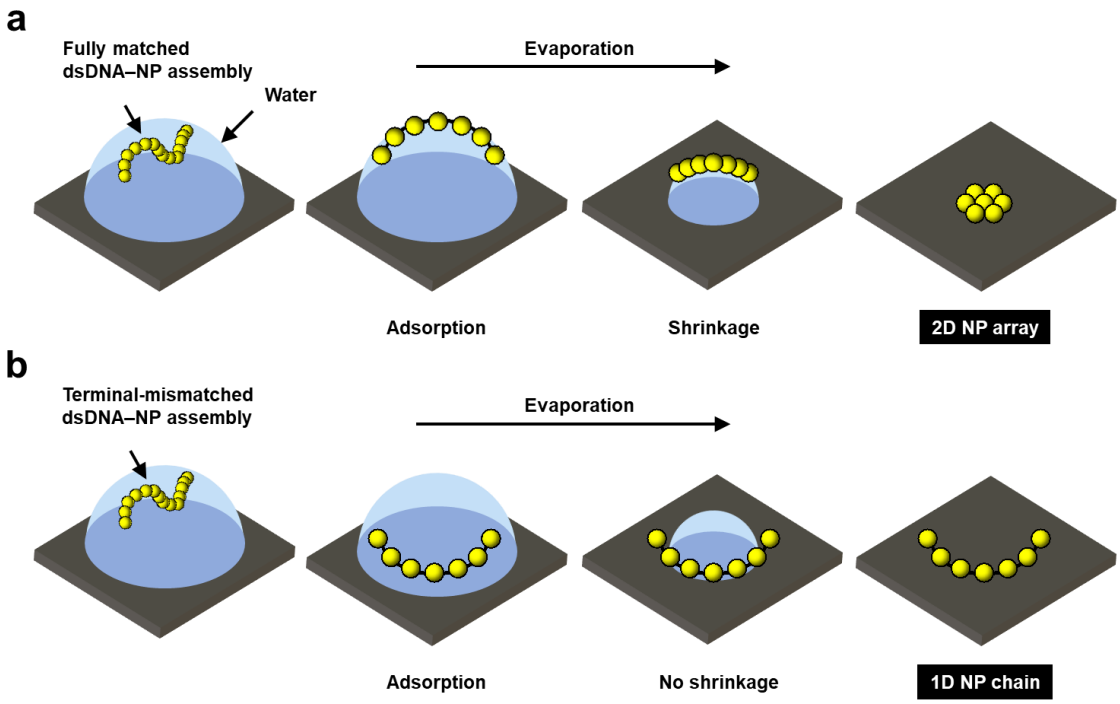

Figure 3.7 Schematic illustrations for formation of (a) the 2D array of the fully matched dsDNA–AuNPs and (b) the 1D chain of the terminal-mismatched dsDNA–AuNPs after evaporation on the TEM microgrid.

The following two experimental results were consistent with the proposed

mechanism. First, a gradual change was observed from the linear structure to the island-like structure by increasing the number of the complementary ssDNAs from 2 to 20 equivalents, compared to the total number of cover DNAs. The increase in the number of DNA duplexes on the AuNP surface caused the gradual change from the linear structure with 0 equivalent (Figure 3.2a), through the bundle structure with 2 equivalents (Figure 3.8a), to the elliptical island-like structure with 8 equivalents (Figure 3.8b) and finally the circular island-like structure with 12 equivalents (Figure 3.2b) and 20 equivalents (Figure 3.8c). These results suggest that the interparticle attractive forces were augmented by increasing the number of DNA duplexes on the AuNP surface. Second, the interparticle distance of the island-like 2D AuNP array was almost independent of the length of the spacer involved in the precursory 1D AuNP chain. Similar island-like 2D AuNP arrays with an interparticle distance of approximately 10 nm were constructed from the 1D AuNP chains having a 28 nt to 150 nt spacer (Figure 3.9). Moreover, the fully matched dsDNA–AuNPs alone without the template DNA were unable to self-assemble into the island-like 2D structure (Figure 3.3b). Therefore, the linkage between the adjacent AuNPs was necessary for the present structural change.

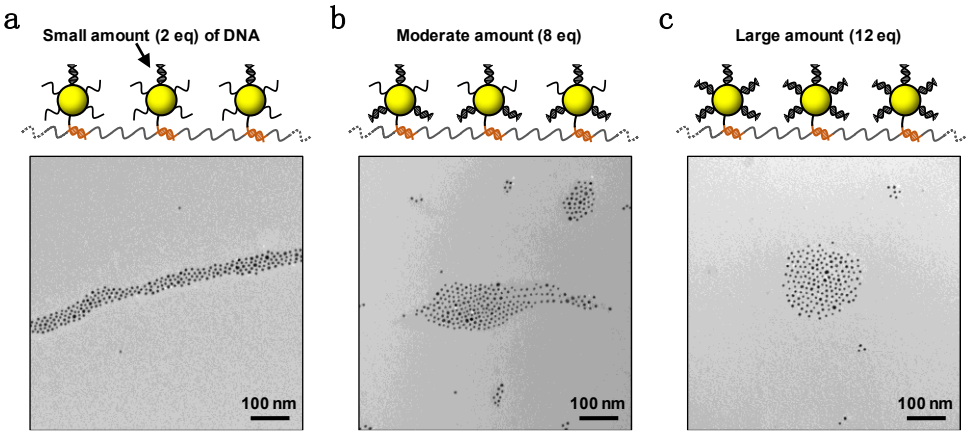

Figure 3.8 Schematics and representative TEM images of the DNA–AuNP assemblies with (a) 2, (b) 8, and (c) 12 equivalents of the complementary DNA.

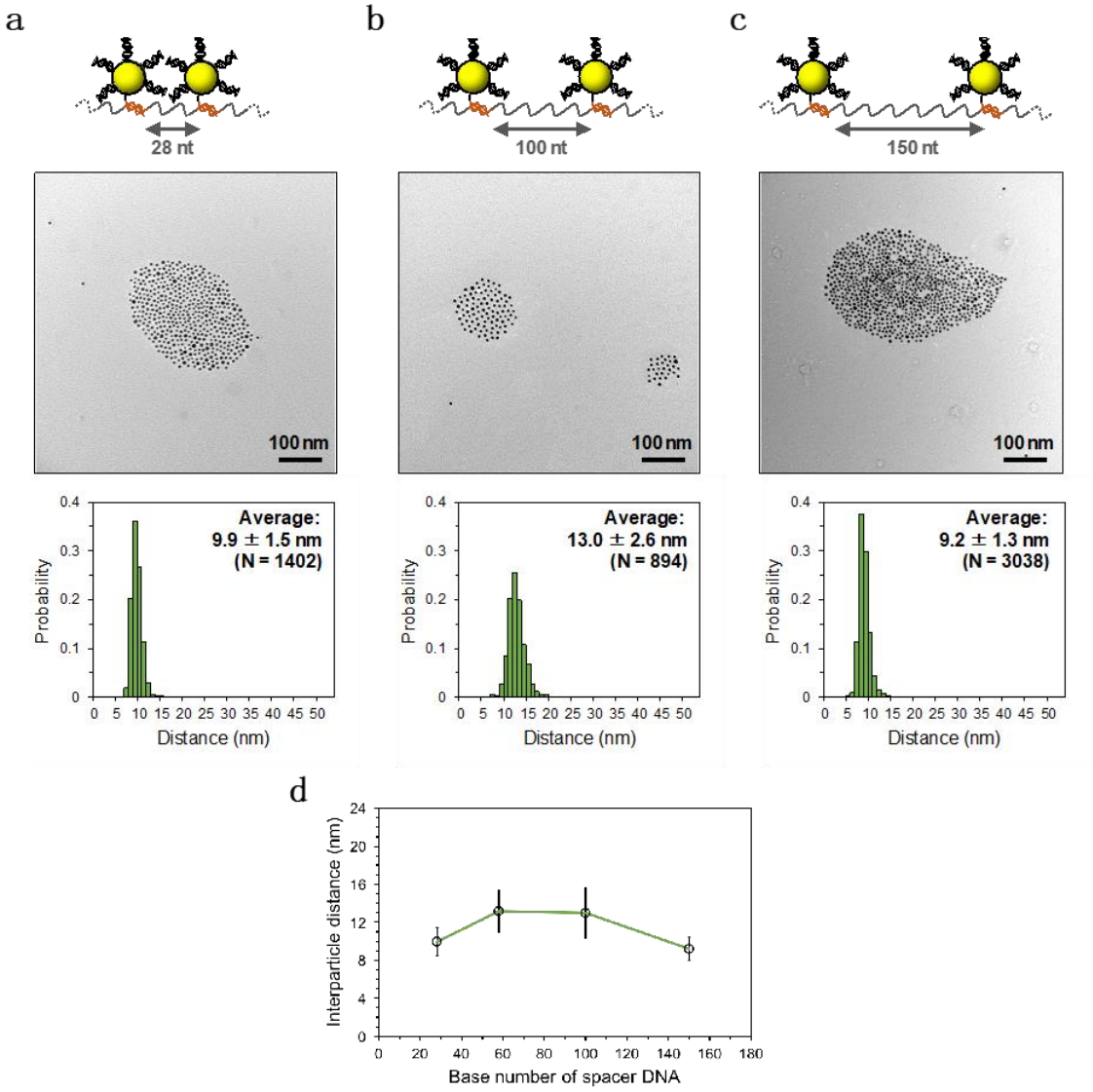

Figure 3.9 (a-c) Schematics, representative TEM images, and distributions of interparticle center-to-center distances of the dsDNA–AuNP assemblies having spacers of various lengths: (a) 28 nt, (b) 100 nt, and (c) 150 nt. (d) The averaged interparticle center-to-center distance as a function of the base number of the spacer.

3.4.4 Construction of 2D Arrays with Anisotropic Interparticle Spacing

Finally, the author extended the length of the surface-bound dsDNA. As shown in Figure 3.10a, a singly nicked 45 bp dsDNA on the AuNP surface was prepared. An island-like structure was observed with unique anisotropic interparticle spacing. TEM images showed long and short interparticle center-to-center spacing of 30.3 ± 2.5 nm and 10.2 ± 3.0 nm, respectively (Figure 3.11). The maximum value of the interparticle center-to-center distance within the 1D AuNP chain was roughly considered as the contour length of the 58 nt ssDNA spacer (25 nm). This value was smaller than twice the value of the contour length of the 45 bp B-form dsDNA with the AuNP diameter (35 nm). Therefore, the adjacent AuNPs connected by the template DNA should not be allowed to shrink in a non-crosslinking manner. Instead, direct attachment between bare AuNP surfaces could energetically be more favorable. Consequently, the 45 bp surface-bound dsDNA was expelled from a space between two adjacent AuNPs to undergo terminal π–π stacking interaction with another 45 bp dsDNA on a more remote AuNP (Figure 3.10a).

This working hypothesis is supported by the following experimental results. First, when the spacer length was increased from 58 nt to 100 nt, the anisotropic spacing disappeared completely (Figure 3.10b). The maximum value of the interparticle center-to-center distance within the precursory 1D AuNP chain could be treated in a similar manner as the contour length of the 100 nt ssDNA spacer (43 nm). This value was larger than twice the value of the contour length of 45 bp dsDNA with the AuNP diameter (35 nm). Therefore, the adjacent AuNPs could undergo non-crosslinking shrinkage so that the precursory 1D AuNP chain was folded into a 2D array structure with isotropic interparticle spacing. Second, when the length of surface-bound dsDNA was decreased from 45 bp to 25 bp, the anisotropic interparticle spacing was also dissipated (Figure

3.10c). The maximum value of the interparticle center-to-center distance within the precursory 1D AuNP chain was considered as the contour length of the 58 nt spacer (25 nm), which was larger than twice the value of the contour length of 25 bp dsDNA with the AuNP diameter (22 nm). The adjacent AuNPs were allowed to experience the non-crosslinking shrinkage so that the precursory 1D AuNP chain was folded into a 2D array structure with isotropic interparticle spacing. Third, the precursory 1D chain of the DNA–AuNPs having a 29 nt overhang at the outermost surface exhibited a linear structure under the same conditions (Figure 3.10d). This result demonstrated that the terminal base-pairing located at the outermost AuNP surface was required for construction of the 2D AuNP array, thereby indicating that the structural change took place in a non-crosslinking fashion. However, the proximity effect obtained by connecting AuNPs was indispensable to the non-crosslinking assembly in the current non-equilibrium open system; the 2D AuNP array was not achieved in the absence of the template DNA (Figure 3.10e).

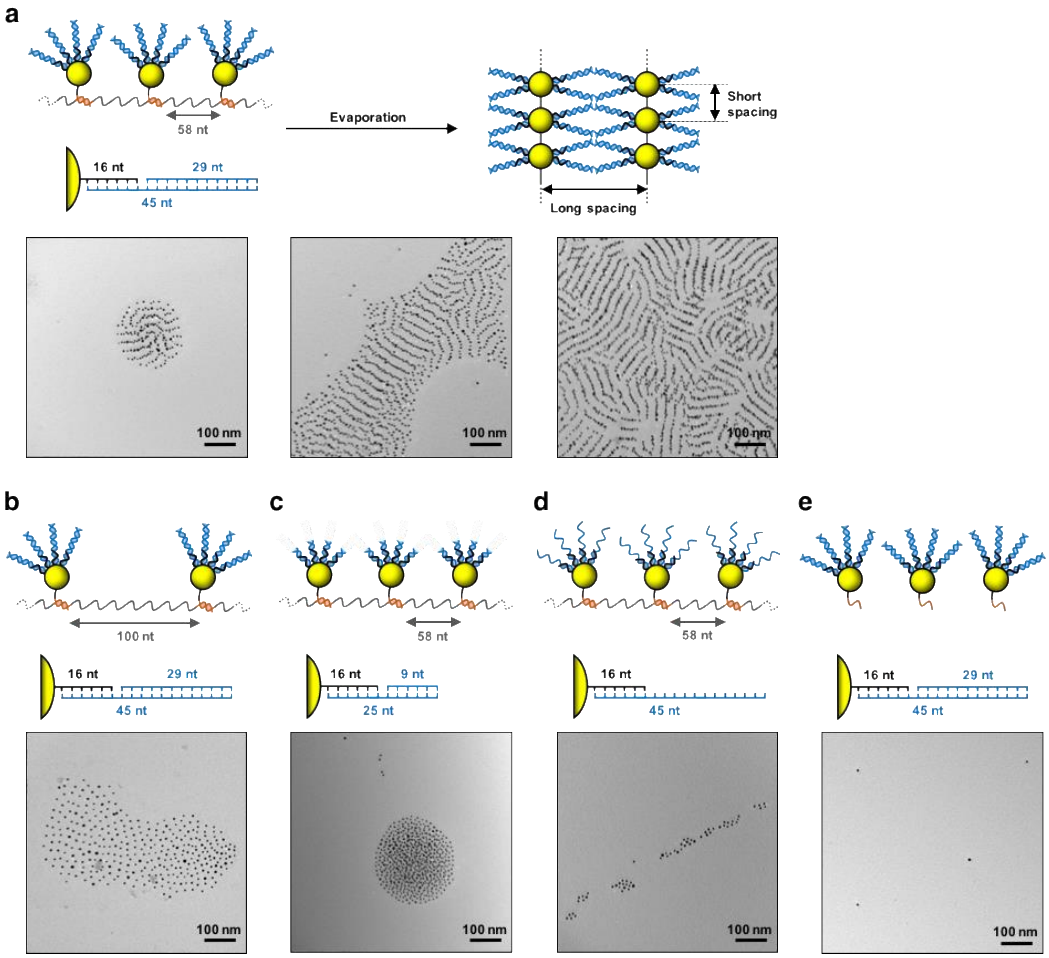

Figure 3.10 Schematics and representative TEM images for the dsDNA–AuNP assemblies having (a) 45 bp surface-grafted dsDNA and 58 nt spacer, (b) 45 bp dsDNA and 100 nt spacer, (c) 25 bp dsDNA and 58 nt spacer, and (d) 29 nt-protruded 16 bp dsDNA and 58 nt spacer, and (e) 45 bp dsDNA without the template DNA. AuNPs with a nominal diameter of 5 nm were used.

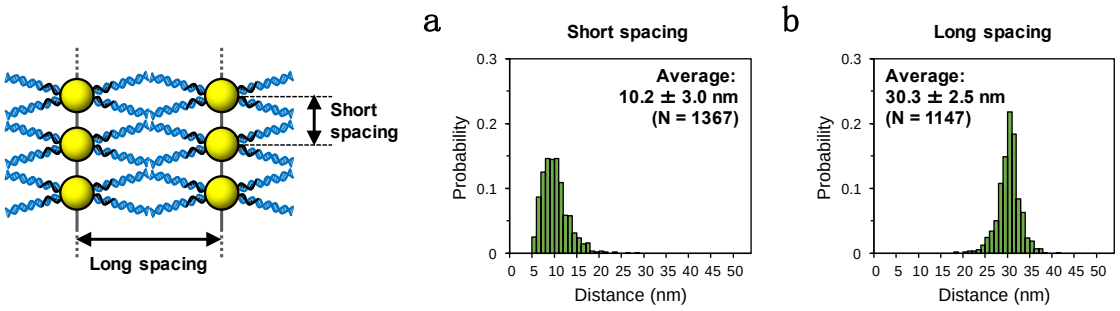

Figure 3.11 Distributions of interparticle center-to-center (a) short and (b) long spacing for the dsDNA–AuNP assemblies having 45 bp surface-grafted dsDNA and 58 nt spacer.

3.5 Conclusions

In this chapter, the 1D chains of fully matched dsDNA–AuNPs adsorbed onto the substrate surface underwent drastic structural change to afford the 2D AuNP arrays. Further, it was demonstrated that AuNPs with isotropic surface modification could self-assemble to form an island-like structure with anisotropic interparticle spacing, when the free motion of the isotropic AuNPs was spatially restricted by the interparticle linkage. It should be emphasized that the formation of 2D AuNP arrays was strongly inhibited when terminal single-base mismatch existed at the outermost surface of the dsDNA–AuNPs in the precursory 1D chains. The current method of preparing 2D NP arrays from precursory 1D NP chains could be an alternative approach to readily align various NPs on 2D substrates, which would be potentially applicable to various nanodevices, including solar cells, biosensors, and stimulus-responsive materials.

3.6 References

1) Shiraishi, S.; Yu, L.; Akiyama, Y.; Wang, G.; Kikitsu, T.; Miyamura, K.; Takarada, T.; Maeda, M. Folding of Nanoparticle Chains into 2D Arrays: Structural Change of DNA-Functionalized Gold Nanoparticle Assemblies. *Adv. Mater. Interfaces* **2018**, *5*, 1800189.

2) Grzelczak, M.; Vermant, J.; Furst, E. M.; Liz-Marzan, L. M. Directed Self-Assembly of Nanoparticles. *ACS Nano* **2010**, *4*, 3591–3605.

3) Nie, Z.; Petukhova, A.; Kumacheva, E. Properties and Emerging Applications of Self-Assembled Structures Made from Inorganic Nanoparticles. *Nat. Nanotechnol.* **2010**, *5*, 15–25.

4) Xu, L.; Ma, W.; Wang, L.; Xu, C.; Kuang, H.; Kotov, N. A. Nanoparticle Assemblies: Dimensional Transformation of Nanomaterials and Scalability. *Chem. Soc. Rev.* **2013**, *42*, 3114–3126.

5) Xi, C.; Marina, P. F.; Xia, H.; Wang, D. Directed Self-Assembly of Gold Nanoparticles into Plasmonic Chains. *Soft Matter* **2015**, *11*, 4562–4571.

6) Boles, M. A.; Engel, M.; Talapin, D. V. Self-Assembly of Colloidal Nanocrystals: From Intricate Structure to Functional Materials. *Chem. Rev.* **2016**, *116*, 11220–11289.

7) Lu, C.; Tang, Z. Advanced Inorganic Nanoarchitectures from Oriented Self-Assembly. *Adv. Mater.* **2016**, *28*, 1096–1108.

8) Komiyama, M.; Yoshimoto, K.; Sisido, M.; Ariga, K. Chemistry Can Make Strict and Fuzzy Controls for Bio-Systems: DNA Nanoarchitectonics and Cell-Macromolecular Nanoarchitectonics. *Bull. Chem. Soc. Jpn.* **2017**, *90*, 967–1004.

9) Tan, S. J.; Campolongo, M. J.; Luo, D.; Cheng, W. Building Plasmonic Nanostructures with DNA. *Nat. Nanotechnol.* **2011**, *6*, 268–276.

10) Kumar A.; Hwang, J.-H.; Kumar, S.; Nam, J.-M. Tuning and Assembling Metal Nanostructures with DNA. *Chem. Commun.* **2013**, *49*, 2597–2609.

11) Barrow, S. J.; Funston, A. M.; Wei, X.; Mulvaney, P. DNA-Directed Self-Assembly and Optical Properties of Discrete 1D, 2D and 3D Plasmonic Structures. *Nano Today* **2013**, *8*, 138–167.

12) Tan, L. H.; Xing, H.; Lu, Y. DNA as a Powerful Tool for Morphology Control, Spatial Positioning, and Dynamic Assembly of Nanoparticles. *Acc. Chem. Res.* **2014**, *47*, 1881–1890.

13) Lan, X.; Wang, Q. DNA-Programmed Self-Assembly of Photonic Nanoarchitectures. *NPG Asia Mater.* **2014**, *6*, e97.

14) Deng, Z.; Tian, Y.; Lee, S.-H.; Ribbe, A. E.; Mao, C. DNA-Encoded Self-Assembly of Gold Nanoparticles into One-Dimensional Arrays. *Angew. Chem., Int. Ed.* **2005**, *44*, 3582–3585.

15) Beyer, S.; Nickels, P.; Simmel, F. C. Periodic DNA Nanotemplates Synthesized by Rolling Circle Amplification. *Nano Lett.* **2005**, *5*, 719–722.

16) Zhao, W.; Gao, Y.; Kandadai, S. A.; Brook, M. A.; Li, Y. DNA Polymerization on Gold Nanoparticles through Rolling Circle Amplification: Towards Novel Scaffolds for Three-Dimensional Periodic Nanoassemblies. *Angew. Chem., Int. Ed.* **2006**, *45*, 2409–2413.

17) Cheglakov, Z.; Weizmann, Y.; Braunschweig, A. B.; Wilner, O. I.; Willner, I. Increasing the Complexity of Periodic Protein Nanostructures by the Rolling-Circle-Amplified Synthesis of Aptamers. *Angew. Chem., Int. Ed.* **2008**, *47*, 126–130.

18) Li, J.; Deng, T.; Chu, X.; Yang, R.; Jiang, J.; Shen, G.; Yu, R. Rolling Circle Amplification Combined with Gold Nanoparticle Aggregates for Highly Sensitive Identification of Single-Nucleotide Polymorphisms. *Anal. Chem.* **2010**, *82*, 2811–2816.

19) Ali, M. M.; Kanda, P.; Aguirre, S. D.; Li, Y. Modulation of DNA-Modified Gold-Nanoparticle Stability in Salt with Concatemeric Single-Stranded DNAs for Colorimetric Bioassay Development. *Chem. - Eur. J.* **2011**, *17*, 2052–2056.

20) Russell, C.; Welch, K.; Jarvius, J.; Cai, Y.; Brucas, R.; Nikolajeff, F.; Svedlindh, P.; Nilsson, M. Gold Nanowire Based Electrical DNA Detection Using Rolling Circle Amplification. *ACS Nano* **2014**, *8*, 1147–1153.

21) Lau, K. L.; Hamblin, G. D.; Sleiman, H. F. Gold Nanoparticle 3D-DNA Building Blocks: High Purity Preparation and Use for Modular Access to Nanoparticle Assemblies. *Small* **2014**, *10*, 660–666.

22) Cheng, W.; Campolongo, M. J.; Cha, J. J.; Tan, S. J.; Umbach, C. C.; Muller, D. A.; Luo, D. Free-Standing Nanoparticle Superlattice Sheets Controlled by DNA. *Nat. Mater.* **2009**, *8*, 519–525.

23) Tan, S. J.; Kahn, J. S.; Derrien, T. L.; Campolongo, M. J.; Zhao, M.; Smilgies, D. M.; Luo, D. Crystallization of DNA-Capped Gold Nanoparticles in High-Concentration, Divalent Salt Environments. *Angew. Chem., Int. Ed.* **2014**, *53*, 1316–1319.

24) Srivastava, S.; Nykypanchuk, D.; Fukuto, M.; Gang, O. Tunable Nanoparticle Arrays at Charged Interfaces. *ACS Nano* **2014**, *8*, 9857–9866.

25) Srivastava, S.; Nykypanchuk, D.; Fukuto, M.; Halverson, J. D.; Tkachenko, A. V.; Yager, K. G.; Gang, O. Two-Dimensional DNA-Programmable Assembly of Nanoparticles at Liquid Interfaces. *J. Am. Chem. Soc.* **2014**, *136*, 8323–8332.

26) Isogai, T.; Piednoir, A.; Akada, E.; Akahoshi, Y.; Tero, R.; Harada, S.; Ujihara, T.; Tagawa, M. Forming Two-Dimensional Structure of DNA-Functionalized Au Nanoparticles via Lipid Diffusion in Supported Lipid Bilayers. *J. Cryst. Growth* **2014**, *401*, 494–498.

27) Isogai, T.; Akada, E.; Nakada, S.; Yoshida, N.; Tero, R.; Harada, S.; Ujihara, T.; Tagawa, M. Effect of Magnesium Ion Concentration on Two-Dimensional Structure of DNA-Functionalized Nanoparticles on Supported Lipid Bilayer. *Jpn. J. Appl. Phys.* **2016**, *55*, 03DF11.

28) Ohya, Y.; Miyoshi, N.; Hashizume, M.; Tamaki, T.; Uehara, T.; Shingubara, S.; Kuzuya, A. Formation of 1D and 2D Gold Nanoparticle Arrays by Divalent DNA–Gold Nanoparticle Conjugates. *Small* **2012**, *8*, 2335–2340.

29) Estephan, Z. G.; Qian, Z.; Lee, D.; Crocker, J. C.; Park, S. J. Responsive Multidomain Free-Standing Films of Gold Nanoparticles Assembled by DNA-Directed Layer-by-Layer Approach. *Nano Lett.* **2013**, *13*, 4449–4455.

30) Myers, B. D.; Lin, Q. Y.; Wu, H.; Luijten, E.; Mirkin, C. A.; Dravid, V. P. Size-Selective Nanoparticle Assembly on Substrates by DNA Density Patterning. *ACS Nano* **2016**, *10*, 5679–5686.

31) Shen, J.; Luan, B.; Pei, H.; Yang, Z.; Zuo, X.; Liu, G.; Shi, J.; Wang, L.; Zhou, R.; Cheng, W.; Fan, C. Humidity-Responsive Single-Nanoparticle-Layer Plasmonic Films. *Adv. Mater.* **2017**, *29*, 1606796.

32) Shim, T. S.; Estephan, Z. G.; Qian, Z.; Prosser, J. H.; Lee, S. Y.; Chenoweth, D. M.; Lee, D.; Park, S. J.; Crocker, J. C. Shape Changing Thin Films Powered by DNA Hybridization. *Nat. Nanotechnol.* **2017**, *12*, 41–47.

33) Ma, W.; Sun, M.; Fu, P.; Li, S.; Xu, L.; Kuang, H.; Xu, C. A Chiral-Nanoassemblies-Enabled Strategy for Simultaneously Profiling Surface Glycoprotein and MicroRNA in Living Cells. *Adv. Mater.* **2017**, *29*, 1703410.

34) Pinto, Y. Y.; Le, J. D.; Seeman, N. C.; Musier-Forsyth, K.; Taton, T. A.; Kiehl, R. A. Sequence-Encoded Self-Assembly of Multiple-Nanocomponent Arrays by 2D DNA Scaffolding. *Nano Lett.* **2005**, *5*, 2399–2402.

35) Sharma, J.; Chhabra, R.; Liu, Y.; Ke, Y.; Yan, H. DNA-Templated Self-Assembly of Two-Dimensional and Periodical Gold Nanoparticle Arrays. *Angew. Chem., Int. Ed.* **2006**, *45*, 730–735.

36) Zhang, J.; Liu, Y.; Ke, Y.; Yan, H. Periodic Square-Like Gold Nanoparticle Arrays Templated by Self-Assembled 2D DNA Nanogrids on a Surface. *Nano Lett.* **2006**, *6*, 248–251.

37) Zheng, J.; Constantinou, P. E.; Micheel, C.; Alivisatos, A. P.; Kiehl, R. A.; Seeman, N. C. Two-Dimensional Nanoparticle Arrays Show the Organizational Power of Robust DNA Motifs. *Nano Lett.* **2006**, *6*, 1502–1504.

38) Hung, A. M.; Micheel, C. M.; Bozano, L. D.; Osterbur, L. W.; Wallraff, G. M.; Cha, J. N. Large-Area Spatially Ordered Arrays of Gold Nanoparticles Directed by Lithographically Confined DNA Origami. *Nat. Nanotechnol.* **2010**, *5*, 121–126.

39) He, Y.; Ye, T.; Ribbe, A. E.; Mao, C. DNA-Templated Fabrication of Two-Dimensional Metallic Nanostructures by Thermal Evaporation Coating. *J. Am. Chem. Soc.* **2011**, *133*, 1742–1744.

40) Schreiber, R.; Santiago, I.; Ardavan, A.; Turberfield, A. J. Ordering Gold Nanoparticles with DNA Origami Nanoflowers. *ACS Nano* **2016**, *10*, 7303–7306.

41) Wang, P.; Gaitanaros, S.; Lee, S.; Bathe, M.; Shih, W. M.; Ke, Y. Programming Self-Assembly of DNA Origami Honeycomb Two-Dimensional Lattices and Plasmonic Metamaterials. *J. Am. Chem. Soc.* **2016**, *138*, 7733–7740.

42) Liu, W.; Halverson, J.; Tian, Y.; Tkachenko, A. V.; Gang, O. Self-Organized Architectures from Assorted DNA-Framed Nanoparticles. *Nat. Chem.* **2016**, *8*, 867–873.

43) Maeda, M. Sequence-Specific Aggregation Behavior of DNA-Carrying Colloidal Nanoparticles Prepared from Poly(*N*-isopropylacrylamide)-*graft*-Oligodeoxyribonucleotide. *Polym. J.* **2006**, *38*, 1099–1104.

44) Sato, K.; Hosokawa, K.; Maeda, M. Rapid Aggregation of Gold Nanoparticles Induced by Non-Cross-Linking DNA Hybridization. *J. Am. Chem. Soc.* **2003**, *125*, 8102–8103.

45) Akiyama, Y.; Shikagawa, H.; Kanayama, N.; Takarada, T.; Maeda, M. DNA Dangling-End-Induced Colloidal Stabilization of Gold Nanoparticles for Colorimetric Single-Nucleotide Polymorphism Genotyping. *Chem. - Eur. J.* **2014**, *20*, 17420–17425.

46) Wang, G.; Akiyama, Y.; Takarada, T.; Maeda, M. Rapid Non-Crosslinking Aggregation of DNA-Functionalized Gold Nanorods and Nanotriangles for Colorimetric Single-Nucleotide Discrimination. *Chem. - Eur. J.* **2016**, *22*, 258–263.

47) Sato, Y.; Hosokawa, K.; Maeda, M. Detection of Non-Cross-Linking Interaction between DNA-Modified Gold Nanoparticles and a DNA-Modified Flat Gold Surface Using Surface Plasmon Resonance Imaging on a Microchip. *Colloids Surf. B* **2008**, *62*, 71–76.

48) Kanayama, N.; Sekine, T.; Ozasa, K.; Kishi, S.; Nyu, T.; Hayashi, T.; Maeda, M. Terminal-Specific Interaction between Double-Stranded DNA Layers: Colloidal Dispersion Behavior and Surface Force. *Langmuir* **2016**, *32*, 13296–13304.

49) Nakata, M.; Zanchetta. G.; Chapman, B. D.; Jones, C. D.; Cross, O. C.; Pindak, R.; Bellini, T.; Clark, N. A. End-to-End Stacking and Liquid Crystal Condensation of 6- to 20-Base Pair DNA Duplexes. *Science* **2007**, *318*, 1276–1279.

50) Kilchherr, F.; Wachauf, C.; Pelz, B.; Rief, M.; Zacharias, M.; Dietz, H. Single-Molecule Dissection of Stacking Forces in DNA. *Science* **2016**, *353*, aaf5508.

51) Kanayama, N.; Takarada, T.; Maeda, M. Rapid Naked-Eye Detection of Mercury Ions Based on Non-Crosslinking Aggregation of Double-Stranded DNA-Carrying Gold Nanoparticles. *Chem. Commun.* **2011**, *47*, 2077–2079.

52) Kanayama, N.; Takarada, T.; Fujita, M.; Maeda, M. DNA Terminal Breathing Regulated by Metal Ions for Colloidal Logic Gates. *Chem. - Eur. J.* **2013**, *19*, 10794–10798.

53) Wang, G.; Akiyama, Y.; Kanayama, N.; Takarada, T.; Maeda, M. Directed Assembly of Gold Nanorods by Terminal-Base Pairing of Surface-Grafted DNA. *Small* **2017**, *13*, 1702137.

54) Andreatta, D.; Sen, S.; Lustres, J. L. P.; Kovalenko, S. A.; Ernsting, N. P.; Murphy, C. J.; Coleman, R. S.; Berg, M. A. Ultrafast Dynamics in DNA: "Fraying" at the End of the Helix. *J. Am. Chem. Soc.* **2006**, *128*, 6885–6892.

55) Wang, G.; Akiyama, Y.; Shiraishi, S.; Kanayama, N.; Takarada, T.; Maeda, M. Cross-Linking Versus Non-Cross-Linking Aggregation of Gold Nanoparticles Induced by DNA Hybridization: A Comparison of the Rapidity of Solution Color Change. *Bioconjugate Chem.* **2017**, *28*, 270–277.

56) Akiyama, Y.; Shikagawa, H.; Kanayama, N.; Takarada, T.; Maeda, M. Modulation of Interparticle Distance in Discrete Gold Nanoparticle Dimers and Trimers by DNA Single-Base Pairing. *Small* **2015**, *11*, 3153–3161.

57) Keskin, S.; Besztejan, S.; Kassier, G.; Manz, S.; Bucker, R.; Riekeberg, S.; Trieu, H. K.; Rentmeister, A.; Miller, R. J. Visualization of Multimerization and Self-Assembly of DNA-Functionalized Gold Nanoparticles Using In-Liquid Transmission Electron Microscopy. *J. Phys. Chem. Lett.* **2015**, *6*, 4487–4492.

58) Lin, G.; Chee, S. W.; Raj, S.; Kral, P.; Mirsaidov, U. Linker-Mediated Self-Assembly Dynamics of Charged Nanoparticles. *ACS Nano* **2016**, *10*, 7443–7450.

59) Murphy, M. C.; Rasnik, I.; Cheng, W.; Lohman, T. M.; Ha, T. Probing Single-Stranded DNA Conformational Flexibility Using Fluorescence Spectroscopy. *Biophys. J.* **2004**, *86*, 2530–2537.

Chapter 4

Conclusion and Outlook

Conclusion and Outlook

This thesis has dealt with self-organization of nanoparticles with a main focus on the facile controlling of the assembled structure. Although isotropic and homogeneous nanoparticle assemblies have intensively been studied thus far, the works concerning anisotropic assemblies have been relatively limited. In the present work, the author has tried to develop a novel methodology to produce anisotropic structures from isotropic nanoparticles; namely, gold nanospheres were successfully assembled into anisotropic 2D structures by employing DNA. All anisotropic structures obtained in this study were simply deduced from the rule that an interparticle attractive force emerged only between the fully matched double-stranded DNA-modified nanoparticles. This rule was in line with the working hypothesis that interparticle attraction in the non-crosslinking assembly of fully matched double-stranded DNA-modified nanoparticles arose from the blunt-end stacking. The methodology was composed of two steps. Initially, 1D assemblies were fabricated as a precursor by crosslinking the gold nanoparticles with a single-stranded DNA through DNA hybridization. Then, the nanoparticle oligomers/chains thus prepared were self-organized to provide anisotropic 2D structures through the non-crosslinking assembly. It is imperative to note that this methodology exhibited extremely high selectivity, which was stimulated by only a single nucleotide substitution. Such local structural changes led to entirely opposite colloidal behaviors, which were expected to be useful for device fabrication.

However, there are several challenges that need to be overcome for future practical applications. First, various types of nanoparticle should be applied to the current methodology. DNA modification techniques have already been developed for various

metallic nanoparticles, such as silver, platinum, and palladium, as well as quantum dots. Meanwhile, it has already been strongly suggested that the non-crosslinking aggregation/assembly took place irrespective of the composition of particle core. Therefore, it is highly expected to fabricate binary and ternary 2D nanoparticle arrays by using the present method. Second, the present methodology should be improved to work in an aqueous phase for generating anisotropic 3D structures. This extension would also be useful for eliminating the interference of capillary force during evaporation. The author believes that these two improvements will be harnessed to fabrication of various advanced nanodevices on the basis of the current methodology.

Bibliography

List of Publications

1. Shota Shiraishi, Li Yu, Yoshitsugu Akiyama, Guoqing Wang, Tomoka Kikitsu, Kazuo Miyamura, Tohru Takarada, and Mizuo Maeda, "Folding of Nanoparticle Chains into 2D Arrays: Structural Change of DNA-Functionalized Gold Nanoparticle Assemblies", *Advanced Materials Interfaces* **2018**, *5*, 1800189.

2. Guoqing Wang, Li Yu, Yoshitsugu Akiyama, Tohru Takarada, and Mizuo Maeda, "Reversible Shrinkage of DNA-Functionalized Gold Nanoparticle Assemblies Revealed by Surface Plasmon Resonance", *Biotechnology Journal* **2018**, *13*, 1800090.

3. Li Yu, Shota Shiraishi, Guoqing Wang, Yoshitsugu Akiyama, Tohru Takarada, and Mizuo Maeda, "Connecting Nanoparticles with Different Colloidal Stability by DNA for Programmed Anisotropic Self-Assembly", *The Journal of Physical Chemistry C* **2019**, *123*, 15293–15300.

List of Presentations

1. Li Yu, Shota Shiraishi, Guoqing Wang, Yoshitsugu Akiyama, Tohru Takarada, and Mizuo Maeda, "Self-Organization of DNA-Functionalized Nanoparticle Assemblies with a Beads-on-a-String Structure", The 27th Biopolymer Symposium, Tokyo, Japan. (July 2017)

2. Li Yu, Shota Shiraishi, Guoqing Wang, Yoshitsugu Akiyama, Tohru Takarada, and Mizuo Maeda, "Structural Conversion of DNA-Modified Gold Nanoparticle Assemblies by Non-Crosslinking Aggregation", The 15th International Conference on Advanced Materials (IUMRS-ICAM 2017), Kyoto, Japan. (August 2017)

3. Li Yu, Shota Shiraishi, Guoqing Wang, Yoshitsugu Akiyama, Tohru Takarada, and Mizuo Maeda, "Diversity of Aggregated Structures of Heterogeneous DNA-

Functionalized Gold Nanoparticle Assemblies", The 66th Symposium on Macromolecules, Ehime, Japan. (September 2017)

4. Li Yu, Shota Shiraishi, Guoqing Wang, Yoshitsugu Akiyama, Tohru Takarada, and Mizuo Maeda, "Self-Organization of DNA-Modified Gold Nanoparticle Oligomers", CEMS International Symposium on Supramolecular Chemistry and Functional Materials (CEMSupra) 2018, Tokyo, Japan. (January 2018)

5. Li Yu, Shota Shiraishi, Guoqing Wang, Yoshitsugu Akiyama, Tohru Takarada, and Mizuo Maeda, "Directed Association of DNA-Functionalized Gold Nanoparticle Oligomers", The 98th CSJ Annual Meeting, Funabashi, Japan. (March 2018)

6. Li Yu, Tzung-Ying Yang, Guoqing Wang, Yoshitsugu Akiyama, Tohru Takarada, and Mizuo Maeda, "Directed Assembly of Nanoparticle Oligomers by DNA", The 28th Biopolymer Symposium, Tokyo, Japan. (July 2018)

7. Li Yu, Tzung-Ying Yang, Yoshitsugu Akiyama, Tohru Takarada, and Mizuo Maeda, "Directed Association of DNA-Functionalized Nanoparticle Assemblies", The 67th Symposium on Macromolecules, Sapporo, Japan. (September 2018)

8. Li Yu, Tzung-Ying Yang, Yoshitsugu Akiyama, Tohru Takarada, and Mizuo Maeda, "Selective 2D Arrangement of DNA-Modified Gold Nanoparticles with Different Sizes", The 68th SPSJ Annual Meeting, Osaka, Japan. (May 2019)

Award

1. SPSJ Annual Meeting Poster Award (May 2019)
   "Selective 2D Arrangement of DNA-Modified Gold Nanoparticles with Different Sizes"